TECHNISCHE UNIVERSITÄT MÜNCHEN

Lehrstuhl für Numerische Mechanik

Three-dimensional Homogenized Constrained Mixture Model of Anisotropic Vascular Growth and Remodeling

Fabian Albert Bräu

Vollständiger Abdruck der von der Fakultät für Maschinenwesen der Technischen Universität München zur Erlangung des akademischen Grades eines

Doktor-Ingenieurs (Dr.-Ing.)

genehmigten Dissertation.

Vorsitzender:	Prof. Phaedon-Stelios Koutsourelakis, Ph.D.
Prüfer der Dissertation:	
	1. Prof. Dr.-Ing. Christian Cyron
	2. Prof. Dr.-Ing. Wolfgang A. Wall
	3. Assoc. Prof. Alessio Gizzi, Ph.D.

Die Dissertation wurde am 23.04.2019 bei der Technischen Universität München eingereicht und durch die Fakultät für Maschinenwesen am 19.09.2019 angenommen.

Abstract

Abdominal aortic aneurysms are a focal and permanent dilation of the arterial wall. In over 80% of the cases, rupturing of an aneurysm leads to immediate death. Assessing the rupture risk of abdominal aortic aneurysms is a challenging task. In everyday common clinical practice, the maximum diameter criterion is used. However, this criterion only accounts for the current state of the aneurysm and does not include any information about its further development. In order to assess the future development of abdominal aortic aneurysms, mathematical models for growth and remodeling in soft biological tissues have attracted increasing interest over the last two decades.

Kinematic growth models are one major approach to model soft tissue growth and remodeling. Because of their conceptual simplicity and computational efficiency, they are applied to many different types of biomaterials. However, they are purely phenomenological models with no micromechanical information. To overcome this limitation, multi-network constrained mixture models have been developed, which are based on a realistic micromechanical model. Nevertheless, these models are not widely used because they are mathematically highly complex and computationally expensive. Recently, homogenized constrained mixture models have been introduced to combine the advantages of both kinematic growth and multi-network constrained mixture models. However, these suffer, so far, still from two problems: First, they are limited to two dimensions. Second, homogenized constrained mixture models – along with kinematic growth and multi-network constrained mixture models – still face the problem of being reliant on a largely heuristic definition of the growth anisotropy. This thesis aims to overcome the two major problems described above.

To this end, in paper A (see Chapter 4), the homogenized constrained mixture model is further developed to model volumetric growth in three dimensions. To exemplify the application of three dimensional homogenized constrained mixture models, the enlargement of an idealized fusiform abdominal aortic aneurysm over 15 years is studied. Growth and remodeling is triggered by a prescribed loss of elastin. Depending on the rate of mass production of collagen and smooth muscle, the blood vessel can, on the one hand, attain – after a period of adaptation – a new stable state or, on the other hand, the damage to the elastin layer can result in an unbounded dilatation of the vessel. Additionally, the growth response of a simple model aorta due to a sudden and permanent increase in blood pressure is studied. For a specific rate of mass production of collagen and smooth muscle and assuming anisotropic volumetric growth in the thickness direction, the growth model developed in this thesis can reproduce experimental observations. Furthermore, it is presented that isotropic volumetric growth models have some difficulties in reproducing the physiological growth response of the aorta. Therefore, the incorporation of anisotropic growth is necessary to reproduce experimental findings. However, three-dimensional homogenized constrained mixture models – along with kinematic growth and multi-network constrained mixture models – still rely on heuristic assumptions regarding the anisotropy of growth.

For this reason, in paper B (see Chapter 5), a new theory is developed to determine from fundamental micromechanical considerations the anisotropy of the changes in tissue geometry resulting from volumetric growth in soft biological tissues. It is shown that anisotropic tissue stiffness and the mechanism of tensional homeostasis induce a natural growth anisotropy. In most of the previous works, volumetric growth is captured by an inelastic (growth) part of the deformation

gradient which is often defined based on purely heuristic assumptions. In this paper, volumetric growth is modeled by a mass production term, a special penalty-type strain energy function, and a relaxation process by tensional homeostasis without the need for any additional heuristic assumptions or quantities (such as ad hoc defined growth tensors). As a rule of thumb, the resulting natural induced growth anisotropy makes differential tissue volume elements dilate mainly in the direction(s) of lowest stiffness. Furthermore, it is demonstrated that this model can reproduce experimentally observed growth behavior in a host of different soft biological tissues.
Three-dimensional homogenized constrained mixture models as introduced in this thesis are, in combination with the newly developed anisotropic growth theory, an efficient, reliable, and universal tool to model growth and remodeling processes in various kinds of soft biological tissues.

Zusammenfassung

Bauchaortenaneurysmen stellen eine lokale und dauerhafte Erweiterung der Arterienwand dar. Eine Ruptur des Aneurysmas führt in über 80% der Fälle zum sofortigen Tod. Die Abschätzung der Rupturwahrscheinlichkeit von Bauchaortenaneurysmen stellt eine schwierige Aufgabe dar. Im klinischen Alltag wird sehr häufig der Durchmesser als Entscheidungsgrundlage verwendet. Dieses Kriterium basiert jedoch nur auf dem aktuellen Zustand des Aneurysmas und berücksichtigt keinerlei Informationen über die weitere Entwicklung. Um die zukünftige Entwicklung von Bauchaortenaneurysmen zu bestimmen, sind in den letzten zwei Jahrzehnten mathematische Modelle, die Wachstums- und Umbauprozesse in biologischen Weichgeweben simulieren, immer populärer geworden.
Kinematische Wachstumsmodelle stellen einen grundlegenden Ansatz zur Modellierung von Wachstums- und Umbauprozessen in Weichgeweben dar. Aufgrund ihres einfachen Konzepts und ihrer numerischen Effizienz kommen sie bei vielen verschiedenen Arten von Biomaterialien zum Einsatz. Allerdings handelt es sich um rein phänomenologische Modelle ohne Informationen über die Mikroebene. Zur Überwindung dieser Einschränkung wurden *Multi-Network Constrained-Mixture-Models* entwickelt, die auf einer realistischen Modellierung der Mikroebene basieren. Jedoch sind diese Modelle mathematisch sehr komplex und rechenintensiv und daher nicht weit verbreitet. Vor Kurzem wurden homogenisierte *Constrained-Mixture-Models* eingeführt, um die Vorteile der kinematischen Wachstumsmodelle und der *Multi-Network Constrained-Mixture-Models* zu vereinen. Allerdings weisen diese Modelle bislang immer noch zwei Probleme auf: Erstens sind sie auf zwei Dimensionen beschränkt. Zweitens stehen homogenisierte *Constrained-Mixture-Models* – wie auch kinematische Wachstumsmodelle und *Multi-Network Constrained-Mixture-Models* – immer noch vor dem Problem, dass sie auf einer weitgehend heuristischen Definition der Wachstumsanisotropie beruhen. Das Ziel dieser Arbeit ist es, die zwei oben beschriebenen grundlegenden Probleme zu beseitigen.
Zu diesem Zweck wird in Artikel A (siehe Kapitel 4) das homogenisierte *Constrained-Mixture-Model* weiterentwickelt, um volumetrische Wachstumsprozesse in drei Dimensionen zu modellieren. Um die Anwendung von dreidimensionalen homogenisierten *Constrained-Mixture-Model* zu veranschaulichen, wird die Aufweitung eines idealisiertem fusiformen Bauchaortenaneurysmas in einem Zeitraum von 15 Jahren untersucht. Wachstums- und Umbauprozesse werden durch einen vorgeschriebenen Abbau von Elastin ausgelöst. In Abhängigkeit der Geschwindigkeit des Massenzuwachses von Kollagen und glattem Muskel kann das Blutgefäß einerseits – nach einiger Zeit der Anpassung – einen neuen stabilen Zustand einnehmen, oder andererseits der Elastinschaden zu einer unbegrenzten Aufweitung des Gefäßes führen. Zusätzlich wird das Wachstumsverhalten, aufgrund eines plötzlichen und permanenten Anstieg des Blutdrucks, in einer einfachen Modellaorta untersucht. Für eine bestimmte Geschwindigkeit des Massenzuwachses von Kollagen und glattem Muskel und unter der Annahme von anisotropen Wachstum in Dickenrichtung, kann das in dieser Arbeit entwickelte Wachstumsmodell die experimentellen Beobachtungen reproduzieren. Des Weiteren wird gezeigt, dass isotrope volumetrische Wachstumsmodelle Schwierigkeiten haben, das physiologische Wachstumsverhalten von Arterien nachzubilden. Um Versuchsergebnisse zu reproduzieren ist daher ein anisotropes Wachstumsverhalten notwendig. In Bezug auf die Wachstumsanisotropie beruhen dreidimensionale homogenisierte *Constrained-Mixture-Models* – wie auch kinematische Wachstumsmod-

elle und *Multi-Network Constrained-Mixture-Models* – allerdings immer noch auf heuristischen Annahmen.
Daher wird in Artikel B (siehe Kapitel 5) eine neue Theorie entwickelt, um die anisotrope Änderung der Gewebegeometrie, die sich aus Volumenwachstum in biologischen Weichgeweben ergibt, aus grundlegenden mikromechanischen Überlegungen heraus zu berechnen. Es wird gezeigt, dass eine anisotrope Gewebesteifigkeit und der Mechanismus der Spannungshomäostase eine natürliche Wachstumsanisotropie herbeiführen. In den meisten früheren Arbeiten wird volumetrisches Wachstum mit Hilfe eines inelastischen (Wachstums-) Anteils des Deformationsgradienten erfasst, der häufig auf Grundlage rein heuristischer Annahmen definiert wird. In diesem Artikel wird volumetrisches Wachstum mit einem Term für die Massenproduktion, einen Strafterm in der Verzerrungsenergiefunktion und einer Relaxation durch die Spannungshomäostase modelliert, wodurch keine zusätzlichen heuristischen Annahmen getroffen oder mathematische Größen festgelegt werden müssen (wie z. B. einen vordefinierten Wachstumstensor). Als Faustregel gilt, dass diese natürliche Anisotropie differenzielle Gewebevolumenelemente hauptsächlich in die Richtung(en) mit der geringsten Steifigkeit dehnt. Darüber hinaus wird dargelegt, dass dieses Modell das Wachstumsverhalten, das experimentell in einer Vielzahl biologischer Weichgewebe beobachtet wird, nachbilden kann.
Dreidimensionale homogenisierte *Constrained-Mixture-Models*, wie sie in dieser Arbeit eingeführt werden, sind, in Kombination mit der neu entwickelten Theorie der Wachstumsanisotropie, ein effizientes, zuverlässiges und universell einsetzbares Werkzeug zur Modellierung von Wachstums- und Umbauprozessen in zahlreichen biologischen Weichgeweben.

Contents

1 Introduction **1**

2 Nonlinear Solid Mechanics **3**
2.1 Kinematics . . . 3
2.2 The Concept of Stress . . . 6
2.3 Constitutive Laws . . . 7
2.4 Balance Equations . . . 9
2.5 Initial Boundary Value Problem . . . 11

3 Mathematical Models of Growth and Remodeling **13**
3.1 Kinematic Growth Model . . . 13
3.2 Multi-Network Constrained Mixture Model . . . 15
3.3 Homogenized Constrained Mixture Model . . . 17
3.3.1 General Idea . . . 17
3.3.2 Mass Production . . . 18
3.3.3 Remodeling . . . 18
3.3.4 Growth . . . 21

4 Paper A **23**

5 Paper B **25**

6 Discussion **27**

Bibliography **31**

A Full Text: Paper A **37**

B Full Text: Paper B **59**

1 Introduction

Cardiovascular diseases are the number one cause of death worldwide [59]. Abdominal aortic aneurysms (AAAs) form part of this group. They are permanent, focal, and abnormal dilations of the infrarenal aorta by more than 50%. Prevalence of AAAs is 4% – 8% for men but significantly lower at 0.5% – 1.5% for women over the age of 65 [11]. The rupturing of an aneurysm is a life-threatening event with a mortality rate of over 80% [27]. Prophylactic surgery can help to overcome the risk of rupture, with 30-day-mortality ranging between 0.6% and 5.8% for open repair and 1.7% for endovascular aortic repair [20, 25].
Until now, in everyday clinical practice, the maximum diameter criterion is most commonly used to assess the rupture risk of AAAs. Surgery is performed if the maximum diameter exceeds 5.5 cm [42]. However, in 10% - 15% of the cases, AAAs rupture below the well-accepted diameter criterion [9, 56]. Over the last few years, more accurate computational techniques have been developed [15, 38], which essentially rely on risk indices comparing the wall stress in aneurysms to some admissible value, which may take into account criteria such as vessel dilation, gender and familial history. This course of action is similar to the common practice in structural engineering. However, there are doubts on whether it provides optimal results in complex biomechanical systems especially on the clinically relevant time scale of several months or years, where ongoing growth and remodeling and biochemical degradation processes in the aneurysm wall will significantly influence the risk of rupture.
At the moment, growth of aneurysms is taken into account clinically – if at all – only in certain cases and in a very ad-hoc manner based on estimated expansion rates where sufficient data from continuous monitoring of patients are available [47]. Therefore, modeling growth and remodeling processes in the aneurysm wall is an important step towards a predictive patient-specific risk assessment method.
The adaptation of biological tissues to its mechanical environment has already been observed a long time ago. In 1892, Julius Wolff postulated that bone in a healthy person or animal will adapt to the loads it is subjected to [58]. A similar behavior for soft biological tissues was postulated by Henry Gassett Davis in 1867. He stated "... soft tissue, when put under even a moderate degree of tension ... will elongate by the addition of new material, on the contrary, when ... soft tissues remain uninterruptedly in a loose or lax state, they will gradually shorten, as the effete material is removed ..." [10]. This comes down to two central postulates:

1. There exists a preferred stress/strain state, also called the homeostatic state
2. Perturbation of the homeostatic state causes a proportional inelastic deformation and change of mass (growth)

Examples range from atrophy (that is, loss of tissue mass) in disused tendons [43], thickening of the lamina cribrosa in early glaucoma [24], load-driven remodeling in tissue engineered heart valves [37], skin growth in pediatric scalp reconstruction [60], to the thickening of the aortic

wall due to chronic hypertension [2, 41].
These two laws can be considered landmarks on the way to modern mechanobiology, that is, the study of the biological response of cells to an altered mechanical environment [30]. Over the last two decades, this field has attracted increasing interest. Nowadays, the importance of mechano-regulated biological growth and remodeling is acknowledged in many different research fields. In-depth knowledge of these processes could help to better understand the geometric evolution of living organisms during morphogenesis as well as the mechanobiological adaptation processes in adult tissue. Large efforts have been undertaken to better understand growth and remodeling especially for aneurysmatic or hypertensive blood vessels [13, 22, 23, 35, 51]. From the late 1970s on, mathematical models of growth and remodeling have been developed to give further insights into these complex mechanisms. There is a broad consensus that growth and remodeling of vascular tissue is largely directed by mechanical stress and/or strain mainly in the collagen fibers, albeit the precise governing equations remains controversial [14, 34, 57]. Moreover, the kinematic growth models introduced by Rodriguez et al. [49] which are widely used for vascular growth and remodeling neglect various physiological details on the microscale, the importance of which seems indisputable in the light of experimental and clinical observations. In addition to that, they also suffer from a comparatively poor theoretical foundation. So far, growth and remodeling models are based on several rather heuristic mathematical assumptions, emphasizing the need for a more rigorous mathematical foundation. To overcome these limitations, Humphrey et al. [31] developed the multi-network constrained mixture models, which are based on a realistic micromechanical foundation. However, these models suffer from their mathematical complexity and computational inefficiency. Recently, Cyron et al. [8] introduced the homogenized constrained mixture models, in order to combine the advantages of both kinematic growth and multi-network constrained mixture models. Nevertheless, so far, these models are limited to two-dimensional continua and – along with kinematic growth and multi-network constrained mixture models – are still facing the problem that they rely on a largely heuristic definition of the growth anisotropy.
Therefore, the main objective of this thesis is to overcome the above described shortcomings of current models of vascular growth and remodeling by the development of microscopically informed, mathematically more rigorous, and computationally more efficient models based on the mathematical and mechanical foundations given in [8]. Specifically, this thesis introduces

A) a three-dimensional growth and remodeling approach based on the homogenized constrained mixture model and

B) a rather natural way to determine the anisotropic changes of the tissue geometry resulting from volumetric growth in a host of different soft biological tissues.

This is understood as an important step towards quantitative and truly predictive models of vascular growth and remodeling as urgently needed in many fields ranging from tissue engineering to rupture risk assessment of aneurysms.

2 Nonlinear Solid Mechanics

Soft biological tissue mechanics is often associated with large deformations. Therefore, it is best addressed within the mathematical framework of nonlinear continuum mechanics. Here, a brief introduction to nonlinear continuum mechanics is given. For a more detailed description, the reader is referred to the corresponding literature, e.g. Bonet and Wood [3], Holzapfel [28], and Truesdell and Noll [52].
In this thesis, the trace of a second order tensor is denoted by $\mathrm{tr}(\cdot)$. The symbol $\otimes$ represents a tensor product and for a double dot product, the symbol $:$ is used.

2.1 Kinematics

Motion of Continuum Bodies

In this thesis, we will denote the reference or material configuration by $\mathcal{B}_0 \subset \mathbb{R}^3$ with the boundary $\partial\mathcal{B}_0$. It is mapped at time $t \geq 0$ to the current or spatial configuration $\mathcal{B}(t)$ with the boundary $\partial\mathcal{B}(t)$ (see Figure 2.1). Without loss of generality, we assume that the initial configuration $\mathcal{B}(t=0)$ coincides with the reference configuration $\mathcal{B}_0$. A point in the material configuration is represented by the position vector $\boldsymbol{X}$ and in the spatial configuration by the vector $\boldsymbol{x}$, respectively. The continuous and sufficiently smooth mapping between these two configurations at a specific time t is described by:

$$\varphi_t : \mathcal{B}_0 \to \mathcal{B}(t),\ \boldsymbol{X} \mapsto \boldsymbol{x} = \varphi_t(\boldsymbol{X}, t)\,. \tag{2.1}$$

For each spatial point $\boldsymbol{x}$, a unique inverse mapping $\boldsymbol{X} = \varphi_t^{-1}(\boldsymbol{x}, t)$ exists to ensure, from a physical point of view, that the body does not penetrate itself nor are there any other singularities. Throughout the thesis, a total Lagrangian formulation is used, whereby all kinematic relations and derived quantities are described with respect to the material points $\boldsymbol{X}$, of the reference configuration $\mathcal{B}_0$. Therefore, the material displacement field $\boldsymbol{u}$ (see again Figure 2.1), which is a function of the referential position $\boldsymbol{X}$ and the time t, results in

$$\boldsymbol{u}(\boldsymbol{X}, t) = \boldsymbol{x}(\boldsymbol{X}, t) - \boldsymbol{X}. \tag{2.2}$$

Deformation Gradient

In addition to the description of the motion of a body which, in general, also includes rigid body motions, the characterization of the deformation of a body (i.e. change of shape) is crucial in nonlinear continuum mechanics. The primary measure for the change of shape of a body is the deformation gradient

$$\boldsymbol{F}(\boldsymbol{X}, t) = \frac{\partial \boldsymbol{x}(\boldsymbol{X}, t)}{\partial \boldsymbol{X}} = \boldsymbol{I} + \frac{\partial \boldsymbol{u}(\boldsymbol{X}, t)}{\partial \boldsymbol{X}} \tag{2.3}$$

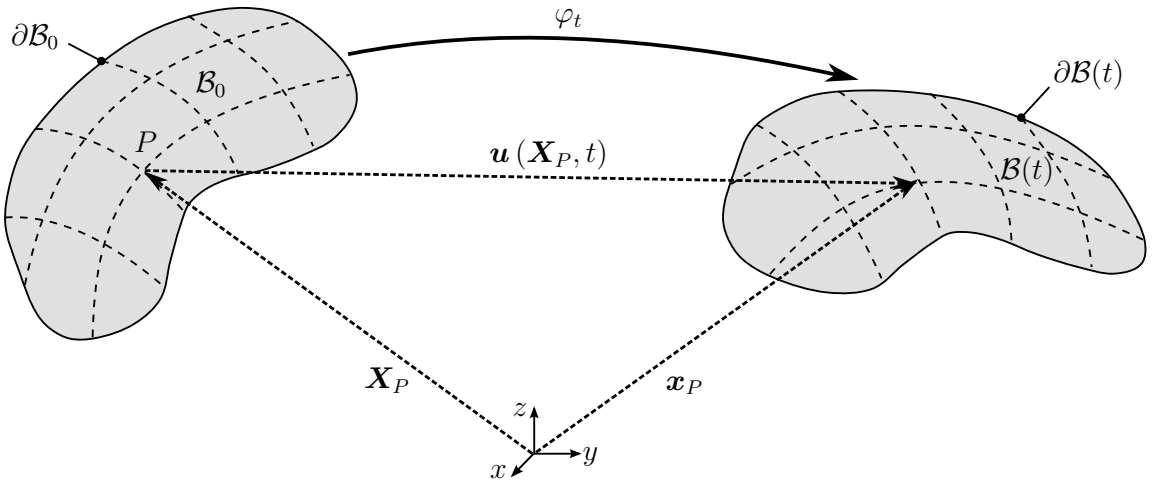

Figure 2.1: Deformation φ_t of a body from the reference configuration $\mathcal{B}_0$ to its current configuration $\mathcal{B}(t)$. The point P with reference position vector $\boldsymbol{X}_P$ is mapped to its displaced position vector $\boldsymbol{x}_P$ (image adapted from Sebastian L. Fuchs under Creative Commons license) [6].

where $\boldsymbol{I}$ is the second order identity tensor. The deformation gradient $\boldsymbol{F}$ is a two-point tensor with the first base vector in the displaced configuration and the second in the referential configuration. An important property of the deformation gradient that results from its definition is the mapping of an infinitesimal referential line element (vector) $\mathrm{d}\boldsymbol{X}$ to the corresponding line element in the current configuration $\mathrm{d}\boldsymbol{x}$ by

$$\mathrm{d}\boldsymbol{x} = \boldsymbol{F}\mathrm{d}\boldsymbol{X}. \tag{2.4}$$

In addition to that, an oriented infinitesimal surface element in the referential configuration $\mathrm{d}\boldsymbol{A} = \mathrm{d}A\boldsymbol{N}$ with the unit vector $\boldsymbol{N}$ normal to the surface and $\mathrm{d}A$ the surface area is mapped to the current configuration by using Nanson's formula

$$\mathrm{d}\boldsymbol{a} = J\boldsymbol{F}^{-T}\mathrm{d}\boldsymbol{A} \tag{2.5}$$

where $J = \det(\boldsymbol{F})$ denotes the Jacobian determinant of the mapping φ_t. Finally, infinitesimal referential volume elements $\mathrm{d}V$ are transformed to the current configuration by

$$\mathrm{d}v = \det(\boldsymbol{F})\ \mathrm{d}V = J\ \mathrm{d}V \tag{2.6}$$

where $\mathrm{d}v$ represents the infinitesimal volume element in the spatial configuration.
As mentioned above, the deformation gradient is an important auxiliary quantity to measure the deformation. However, it is not suitable to describe the local deformation of a body since it also includes rigid body rotation. Therefore, the deformation gradient $\boldsymbol{F}$ is multiplicatively split into a rotation and a stretch part (also known as polar decomposition):

$$\boldsymbol{F} = \boldsymbol{R}\boldsymbol{U} = \boldsymbol{v}\boldsymbol{R}. \tag{2.7}$$

The unique rotation tensor $\boldsymbol{R} \in SO(3)$ is an orthonormal tensor with $\boldsymbol{R}^{-1} = \boldsymbol{R}^T$ and $\det(\boldsymbol{R}) = 1$. The right and left stretch tensor $\boldsymbol{U}$ and $\boldsymbol{v}$ are symmetric and positive definite tensors that are independent of any rigid body motion. Therefore, they form the basis of objective strain measures.

Strain Measures

An important kinematic quantity for measuring the stretch of a body is the right Cauchy-Green tensor

$$\boldsymbol{C} = \boldsymbol{F}^T\boldsymbol{F} = \boldsymbol{U}^T\boldsymbol{R}^T\boldsymbol{R}\boldsymbol{U} = \boldsymbol{U}^T\boldsymbol{U} = \boldsymbol{U}^2. \tag{2.8}$$

In contrast to the deformation gradient which is a two-point tensor, the right Cauchy-Green tensor is solely defined in the reference configuration and a well-suited quantity to describe the internal state of a body. Its three principal invariants are defined as follows:

$$I_1 = \operatorname{tr}\boldsymbol{C}, \tag{2.9}$$

$$I_2 = \frac{1}{2}\left((\operatorname{tr}\boldsymbol{C})^2 - \operatorname{tr}\left(\boldsymbol{C}^2\right)\right), \tag{2.10}$$

$$I_3 = \det\boldsymbol{C}. \tag{2.11}$$

With the help of the right Cauchy-Green tensor a real strain measure, namely the Green-Lagrange strain, can be defined:

$$\boldsymbol{E} = \frac{1}{2}\left(\boldsymbol{F}^T\boldsymbol{F} - \boldsymbol{I}\right) = \frac{1}{2}\left(\boldsymbol{C} - \boldsymbol{I}\right) \tag{2.12}$$

In contrast to the right Cauchy-Green tensor, the Green-Lagrange strain yields a zero tensor in the presence of only rigid body motions. It is, like the right Cauchy-Green tensor, a symmetric tensor and exclusively defined in the reference configuration.
For some materials, especially when modeling biological soft tissues, it can be beneficial to split the deformation gradient into a volumetric and an isochoric part

$$\boldsymbol{F} = \left(J^{\frac{1}{3}}\boldsymbol{I}\right)\bar{\boldsymbol{F}}, \tag{2.13}$$

where $J^{\frac{1}{3}}\boldsymbol{I}$ represents the volume-changing (volumetric), shape-preserving part and $\bar{\boldsymbol{F}} = J^{-\frac{1}{3}}\boldsymbol{F}$ the volume-preserving (isochoric), shape-changing part. Subsequently, the isochoric or modified right Cauchy-Green tensor is given by

$$\bar{\boldsymbol{C}} = J^{-\frac{2}{3}}\boldsymbol{C} = \bar{\boldsymbol{F}}^T\bar{\boldsymbol{F}} \tag{2.14}$$

and its invariants by

$$\bar{I}_1 = J^{-\frac{2}{3}}I_1, \tag{2.15}$$

$$\bar{I}_2 = J^{-\frac{4}{3}}I_2, \tag{2.16}$$

$$\bar{I}_3 = 1. \tag{2.17}$$

Most soft biological tissues are composed of a matrix material (often called ground substance) and one or more fiber families. These fiber materials can be modeled with the help of two additional pseudo-invariants. Assuming the fibers are aligned with the unit direction vector $\boldsymbol{a}_0$ in reference configuration, the pseudo-invariants result in

$$I_4 = \boldsymbol{C} : (\boldsymbol{a}_0 \otimes \boldsymbol{a}_0) = \lambda^2 \text{ and} \tag{2.18}$$

$$I_5 = \boldsymbol{C}^2 : (\boldsymbol{a}_0 \otimes \boldsymbol{a}_0), \tag{2.19}$$

where λ is the stretch in fiber direction. Interactions between different fiber families can be modeled by additional pseudo-invariants. In this thesis, these interactions are neglected and therefore not further discussed here. Interested readers are referred to [28].
In transient problems, additional kinematic quantities are needed, e.g., the first and second total time derivative of the displacement field. The velocity $\boldsymbol{V}$ and the acceleration field $\boldsymbol{A}$ for a fixed material position $\boldsymbol{X}$ are given by

$$\boldsymbol{V}(\boldsymbol{X},t) = \dot{\boldsymbol{u}}(\boldsymbol{X},t) = \left.\frac{\partial \varphi_t(\boldsymbol{X},t)}{\partial t}\right|_{\boldsymbol{X}} \tag{2.20}$$

and

$$\boldsymbol{A}(\boldsymbol{X},t) = \dot{\boldsymbol{V}}(\boldsymbol{X},t) = \ddot{\boldsymbol{u}}(\boldsymbol{X},t) = \left.\frac{\partial^2 \varphi_t(\boldsymbol{X},t)}{\partial t^2}\right|_{\boldsymbol{X}} . \tag{2.21}$$

where the superscripts $\dot{(\cdot)}$ and $\ddot{(\cdot)}$ denote the first and second derivatives with respect to the time at a fixed reference point $\boldsymbol{X}$. In addition to that, one can define the material and spatial velocity gradient $\dot{\boldsymbol{F}}$ and $\boldsymbol{L}$

$$\mathrm{Grad}(\boldsymbol{V}) = \frac{\partial}{\partial \boldsymbol{X}}\frac{\partial \boldsymbol{x}}{\partial t} = \dot{\boldsymbol{F}} \ , \tag{2.22}$$

$$\mathrm{grad}(\boldsymbol{V}) = \frac{\partial}{\partial \boldsymbol{x}}\frac{\partial \boldsymbol{u}}{\partial t} = \dot{\boldsymbol{F}}\boldsymbol{F}^{-1} =: \boldsymbol{l}. \tag{2.23}$$

$\mathrm{Grad}(\cdot)$ and $\mathrm{grad}(\cdot)$ are the gradient operators w.r.t. the material position vector $\boldsymbol{X}$ and the current position vector $\boldsymbol{x}$, respectively. The spatial velocity gradient $\boldsymbol{l}$ can be further split into its symmetric part, the rate of deformation $\boldsymbol{d}$, and its skew symmetric part, the spin $\boldsymbol{w}$:

$$\boldsymbol{d} = \frac{1}{2}(\boldsymbol{l} + \boldsymbol{l}^T) \ , \tag{2.24}$$

$$\boldsymbol{w} = \frac{1}{2}(\boldsymbol{l} - \boldsymbol{l}^T) \ . \tag{2.25}$$

Finally, the time derivative of the right Cauchy-Green tensor (2.8) and the Green-Lagrange strain (2.12) are given by

$$\dot{\boldsymbol{C}} = 2\dot{\boldsymbol{E}} = \dot{\boldsymbol{F}}^T\boldsymbol{F} + \boldsymbol{F}^T\dot{\boldsymbol{F}} \ . \tag{2.26}$$

2.2 The Concept of Stress

Assume that we have a continuum body in the current configuration $\mathcal{B}(t)$ with the boundary $\partial\mathcal{B}(t)$. This body is now cut by a fictitious surface. Then, let $\boldsymbol{n}$ be a unit vector at position $\boldsymbol{x}$ aligned with the outward normal of an infinitesimal spatial surface element $\mathrm{d}s$ lying in that internal plane of the body. The infinitesimal resultant force vector acting on such an infinitesimal surface element results in

$$\mathrm{d}\mathbf{f} = \boldsymbol{t}(\boldsymbol{x},t,\boldsymbol{n}) \ \mathrm{d}s = \boldsymbol{t}_0 \ \mathrm{d}S \tag{2.27}$$

where $\boldsymbol{t}$ is the Cauchy or true traction vector acting in the current configuration and $\boldsymbol{t}_0$ is the first Piola-Kirchhoff traction vector which is, in contrast to the Cauchy traction vector, normalized with respect to the material surface area $\mathrm{d}S$ that corresponds to $\mathrm{d}s$ in the spatial configuration. Then, Cauchy's stress theorem states the existence of a unique stress tensor $\boldsymbol{\sigma}(\boldsymbol{x}, t)$ that fulfills the following relation:

$$\boldsymbol{t}\left(\boldsymbol{x}, t, \boldsymbol{n}\right) = \boldsymbol{\sigma}(\boldsymbol{x}, t)\boldsymbol{n} \tag{2.28}$$

where $\boldsymbol{\sigma}(\boldsymbol{x}, t)$ is a second order tensor in the spatial configuration called the Cauchy or true stress tensor. Newton's third law of action directly follows from (2.28):

$$\boldsymbol{t}\left(\boldsymbol{x}, t, \boldsymbol{n}\right) = -\boldsymbol{t}\left(\boldsymbol{x}, t, -\boldsymbol{n}\right) \tag{2.29}$$

In linear continuum mechanics (e.g. small displacements) $\boldsymbol{\sigma}$ represents the unique measure of stress, whereas in nonlinear continuum mechanics numerous definitions and names of stress tensors have been proposed. In the following, the most commonly used stress tensors are introduced. Most of them do not have a physical interpretation like the Cauchy stress $\boldsymbol{\sigma}$ but have other advantages like a simpler formulation of certain balance equations or constitutive laws.
A common convenient stress measure to work with is the Kirchhoff stress tensor $\boldsymbol{\tau}$. It is obtained by multiplication of the Cauchy stress tensor with the Jacobian determinant:

$$\boldsymbol{\tau} = J\boldsymbol{\sigma}. \tag{2.30}$$

Another often used stress measure is the first Piola-Kirchhoff stress tensor

$$\boldsymbol{P} = J\boldsymbol{\sigma}\boldsymbol{F}^{-T} \tag{2.31}$$

that can be obtained by inserting (2.28) in (2.27) and applying Nanson's formula (2.5) to transform the unit normal vector $\boldsymbol{n}$ to its counterpart in the reference configuration $\boldsymbol{N}$. The first Piola-Kirchhoff stress tensor is like the deformation gradient a two-point tensor with one basis in the material and the other in the current configuration. The second Piola-Kirchhoff stress tensor $\boldsymbol{S}$ is a stress measure solely defined in the material configuration and results in

$$\boldsymbol{S} = \boldsymbol{F}^{-1}\boldsymbol{P} = J\boldsymbol{F}^{-1}\boldsymbol{\sigma}\boldsymbol{F}^{-T}. \tag{2.32}$$

Solving (2.32) for the Cauchy stress tensor results in

$$\boldsymbol{\sigma} = J^{-1}\boldsymbol{F}\boldsymbol{S}\boldsymbol{F}^{T}. \tag{2.33}$$

2.3 Constitutive Laws

Constitutive laws, which describe the material behavior of a body, form a link between stresses and strains. They can be purely phenomenological, based on experimental findings, or derived from microstructural observations.
The material behavior of an elastic body can typically be described by a so called strain energy function Ψ, which only depends on the current state of deformation. The strain energy function

is a continuous, scalar-valued function and has to be objective, implying that it has to be independent from any rigid body translation or rotation. Therefore, the strain energy can be expressed equivalently as a function of the right stretch tensor $\boldsymbol{U}$, the right Cauchy-Green tensor $\boldsymbol{C}$, or the Green-Lagrange strain $\boldsymbol{E}$:

$$\Psi = \Psi(\boldsymbol{F}) = \Psi(\boldsymbol{U}) = \Psi(\boldsymbol{C}) = \Psi(\boldsymbol{E}). \tag{2.34}$$

The first derivative of the strain energy function in (2.34) with respect to the Green-Lagrange strain results in the second Piola-Kirchhoff stress tensor

$$\boldsymbol{S} = \frac{\partial \Psi(\boldsymbol{E})}{\partial \boldsymbol{E}} = 2\,\frac{\partial \Psi(\boldsymbol{C})}{\partial \boldsymbol{C}}. \tag{2.35}$$

The relation between the derivative of the strain energy function with respect to the Green-Lagrange strain and the right Cauchy-Green tensor is found by applying the chain rule and using (2.12). With (2.33) and (2.35), the Cauchy stress tensor is given by

$$\boldsymbol{\sigma} = 2\,J^{-1}\boldsymbol{F}\cdot\frac{\partial \Psi(\boldsymbol{C})}{\partial \boldsymbol{C}}\cdot\boldsymbol{F}^{T} = J^{-1}\boldsymbol{F}\cdot\frac{\partial \Psi(\boldsymbol{E})}{\partial \boldsymbol{E}}\cdot\boldsymbol{F}^{T}. \tag{2.36}$$

Iterative solution schemes of Newton's type are frequently used to solve a sequence of linearized problems in order to find the solution to a nonlinear (initial boundary-value) problem in finite elasticity. Therefore, the linearization of the second Piola-Kirchhoff stress tensor $\boldsymbol{S}$ presented in (2.35) is required and is given by

$$\mathbb{C} = \frac{\partial \boldsymbol{S}}{\partial \boldsymbol{E}} = \frac{\partial^2 \Psi(\boldsymbol{E})}{\partial \boldsymbol{E}\partial \boldsymbol{E}} = 2\,\frac{\partial \boldsymbol{S}}{\partial \boldsymbol{C}} = 4\,\frac{\partial^2 \Psi(\boldsymbol{C})}{\partial \boldsymbol{C}\partial \boldsymbol{C}}. \tag{2.37}$$

$\mathbb{C}$ is the material representation of the elasticity tensor. It is a fourth-order tensor with major and minor symmetries. Given sufficient smoothness of Ψ, the major symmetry of $\mathbb{C}$ in index notation directly results from (2.37) using Schwarz's theorem

$$\mathbb{C}^{ABCD} = \mathbb{C}^{CDAB}. \tag{2.38}$$

Consequently, the minor symmetries that result from the fact that the second Piola-Kirchhoff stress and the Green-Lagrange strain tensor (or equivalently the right Cauchy-Green tensor) itself are both symmetric are given by

$$\mathbb{C}^{ABCD} = \mathbb{C}^{BACD} = \mathbb{C}^{ABDC}. \tag{2.39}$$

One specific form of a strain energy function is, for example, the compressible isotropic Neo-Hookean material model

$$\Psi = \frac{E}{4\,(1+\nu)}\,\left(\mathrm{tr}(\boldsymbol{C}) - 3 - 2\ln(J)\right) + \frac{E\nu}{2\,(1+\nu)\,(1-2\nu)}\,(J-1)^2 \tag{2.40}$$

with the specific elastic modulus E and the Poisson's ratio ν. To model a wide range of material behaviors, many constitutive laws have been developed, such as the Ogden or Mooney-Rivlin models for rubber-like materials. A more detailed overview of different forms of strain energy functions can be found, for example, in Holzapfel [28] or in Ogden [46].

2.4 Balance Equations

Each mechanical system must follow some basic physical principles. In the following, the global or integral and the local form of the mass balance, the balance of linear, and the balance of angular momentum are given. Only the material description of the balance principles in the special case of statics are presented. All balance principles have to hold for any time t.

Conservation of Mass

The total mass of a continuum body is determined by

$$m = \int_{\mathcal{B}_0} \rho_0 \left(\boldsymbol{X}, t\right) \, \mathrm{d}V = \int_{\mathcal{B}(t)} \rho_t \left(\boldsymbol{x}, t\right) \, \mathrm{d}v \tag{2.41}$$

with the reference mass density $\rho_0 \left(\boldsymbol{X}, t\right)$ in the reference configuration $\mathcal{B}_0$ and the current mass density $\rho_t \left(\boldsymbol{x}, t\right)$ in the current configuration $\mathcal{B}(t)$. Using the Jacobian determinant $J = \det(\boldsymbol{F})$, the reference and current mass density are related as follows

$$\rho_0 = J \rho_t. \tag{2.42}$$

In most of the classical mechanical systems, mass is conserved. Therefore, the mass balance equation in material description, written in global form, reads

$$0 = \frac{\mathrm{d}m}{\mathrm{d}t} = \frac{\mathrm{d}}{\mathrm{d}t} \int_{\mathcal{B}_0} \rho_0 \, \mathrm{d}V. \tag{2.43}$$

The mass balance also has to be fulfilled locally. Neglecting internal mass fluxes, the local form in material description is given by

$$0 = \dot{\rho}_0, \quad \forall \boldsymbol{X} \in \mathcal{B}_0. \tag{2.44}$$

Balance of Mass of an Open System

During growth and remodeling, the mass of a body can either increase through the deposition of new mass (growth) or decrease through the degradation of extant mass (atrophy). Therefore, the balance of mass equations have to be adapted accordingly. For a more detailed explanation, the interested reader is referred to Epstein and Maugin [12].
The total mass of a continuum body is still expressed in the same way as shown in (2.41). The mass balance equation in material description written in global form changes to

$$\frac{\mathrm{d}m}{\mathrm{d}t} = \frac{\mathrm{d}}{\mathrm{d}t} \int_{\mathcal{B}_0} \rho_0 \, \mathrm{d}V = \int_{\mathcal{B}_0} \mathcal{M}_0 \, \mathrm{d}V + \int_{\partial\mathcal{B}_0} \boldsymbol{N}^T \boldsymbol{\mathcal{M}} \, \mathrm{d}A \tag{2.45}$$

where $\mathcal{M}_0$ is a volumetric mass source and $\boldsymbol{\mathcal{M}}$ prescribes the mass flux over the boundary $\partial\mathcal{B}_0$. In this thesis, we do not consider any mass that is transferred over the boundary and therefore the last summand in (2.45) evaluates to zero. Therefore, (2.45) reduces to

$$\frac{\mathrm{d}m}{\mathrm{d}t} = \frac{\mathrm{d}}{\mathrm{d}t} \int_{\mathcal{B}_0} \rho_0 \, \mathrm{d}V = \int_{\mathcal{B}_0} \mathcal{M}_0 \, \mathrm{d}V. \tag{2.46}$$

Neglecting internal mass fluxes, the local form of the adapted mass balance (2.46) is given by

$$\dot{\rho}_0 = \mathcal{M}_0. \tag{2.47}$$

In growth and remodeling models, $\mathcal{M}_0$ is often defined as a function of the local stresses or strains in the body. The fact that we model processes that change the mass of a continuum body does not influence the balance of linear or angular momentum and therefore the standard equations are applicable.

Conservation of Linear Momentum

The global balance of all external forces in the current configuration for a quasi-static problem is given by

$$\int_{\mathcal{B}(t)} \boldsymbol{b} \, \mathrm{d}v + \int_{\partial\mathcal{B}(t)} \boldsymbol{t} \, \mathrm{d}a = \boldsymbol{0} \tag{2.48}$$

with the Cauchy traction vector $\boldsymbol{t}$ and a distributed load (body force) $\boldsymbol{b}$. With Gauss' divergence theorem, the global balance of linear momentum in the current configuration results in

$$\int_{\mathcal{B}(t)} \mathrm{div}(\boldsymbol{\sigma}) + \boldsymbol{b} \, \mathrm{d}v = \boldsymbol{0} \tag{2.49}$$

where $\mathrm{div}(\cdot)$ is the divergence operator w.r.t. the current position vector $\boldsymbol{x}$. Additionally, each infinitesimal mass increment itself has to be in equilibrium and therefore the local form follows to

$$\mathrm{div}(\boldsymbol{\sigma}) + \boldsymbol{b} = \boldsymbol{0}. \tag{2.50}$$

Sometimes, it may be more convenient to formulate the balance of linear momentum on a volume element in the reference configuration. This yields

$$\mathrm{Div}(\boldsymbol{P}) + \boldsymbol{b}_0 = \boldsymbol{0} \tag{2.51}$$

with the divergence operator $\mathrm{Div}(\cdot)$ w.r.t. the material position vector $\boldsymbol{X}$, the first Piola-Kirchhoff stress tensor $\boldsymbol{P}$, and the body force per unit reference volume $\boldsymbol{b}_0$ with $\boldsymbol{b}_0 = J\boldsymbol{b}$.

Conservation of Angular Momentum

In continuum mechanics, a body is in static equilibrium not only if the balance of linear momentum presented in (2.50) and (2.51) holds but also when there is a balance of angular momentum. The global form of the balance of angular momentum with respect to a fixed spatial point $\boldsymbol{r}$ is given by

$$\int_{\mathcal{B}(t)} (\boldsymbol{r} \times \boldsymbol{b}) \; \mathrm{d}v + \int_{\partial\mathcal{B}(t)} (\boldsymbol{r} \times \boldsymbol{t}) \; \mathrm{d}a = \boldsymbol{0}. \tag{2.52}$$

The conservation of angular momentum also has to be fulfilled locally. Therefore, the local form is again obtained by applying Gauss' divergence theorem to the second summand in (2.52) and

performing some basic algebra. It shows that the balance of angular momentum is equivalent to the requirement that the Cauchy stress tensor $\boldsymbol{\sigma}$ is symmetric

$$\boldsymbol{\sigma} = \boldsymbol{\sigma}^T. \tag{2.53}$$

This is often referred to as Cauchy's second equation of motion. Applying the transformation between the different stress measures introduced in (2.30), (2.31), and (2.32) to (2.53) results in

$$\boldsymbol{\tau} = \boldsymbol{\tau}^T \quad , \tag{2.54}$$

$$\boldsymbol{P}\boldsymbol{F}^T = \boldsymbol{F}\boldsymbol{P}^T \quad , \tag{2.55}$$

$$\boldsymbol{S} = \boldsymbol{S}^T \quad . \tag{2.56}$$

The balance of angular momentum does not appear explicitly in any numerical method used in this thesis. The symmetry requirements shown in (2.53), (2.54), (2.55), and (2.56) are directly fulfilled by the specific choice of the constitutive laws (cf. Section 2.3) such that only symmetric second Piola-Kirchhoff stresses occur.

2.5 Initial Boundary Value Problem

The kinematic quantities, several stress measures, and their relation to each other introduced in the previous sections help to better understand and describe mechanical problems. In fact, assuming that a constitutive law is given and that there exist suitable boundary and initial conditions, these quantities allow a complete analysis of a mechanical system that includes the determination of all kinematic quantities and stresses at each point in time.
The boundary value problem in quasi-statics defines a set of nonlinear coupled differential equations consisting of the local balance of linear momentum with appropriate boundary and initial conditions to determine the motion of the body with the displacement field $\boldsymbol{u}(\boldsymbol{X}, t)$ as the only unknown. In order to prescribe boundary conditions, the boundary of the body $\partial\mathcal{B}_0$ is split in two parts

$$\partial\mathcal{B}_0 = \Gamma_{0,d} \cup \Gamma_{0,\sigma} \text{ and } \Gamma_{0,d} \cap \Gamma_{0,\sigma} = \emptyset. \tag{2.57}$$

The Dirichlet (or displacement) boundary conditions, which define the displacement field $\boldsymbol{u}(\boldsymbol{X}, t)$, are prescribed on $\Gamma_{0,d}$ whereas the Neumann (or traction) boundary conditions are prescribed on $\Gamma_{0,\sigma}$ and define the surface tractions $\boldsymbol{t}_0$ in the material configuration. Boundary conditions in space and time are both required. Therefore, initial conditions for the displacement field $\boldsymbol{u}(\boldsymbol{X}, t)$ have to be defined. Consequently, the material formulation of the boundary value problem in quasi-statics is given by the balance of linear momentum

$$\mathrm{Div}(\boldsymbol{P}) + \boldsymbol{b}_0 = \boldsymbol{0} \qquad \text{in } \mathcal{B}_0 \tag{2.58}$$

with Dirichlet and Neumann boundary conditions

$$\boldsymbol{u} = \hat{\boldsymbol{u}} \qquad \text{on } \Gamma_{0,d} \tag{2.59}$$

$$\boldsymbol{t}_0 = \boldsymbol{P} \cdot \boldsymbol{N} = \hat{\boldsymbol{t}}_0 \qquad \text{on } \Gamma_{0,\sigma} \tag{2.60}$$

and the initial condition

$$\boldsymbol{u}\left(\boldsymbol{X}, t=0\right)=\boldsymbol{u}_0(\boldsymbol{X}) \qquad \text{in } \mathcal{B}_0, \tag{2.61}$$

where $\boldsymbol{N}$ is the external material unit normal vector on the boundary, a $\hat{(\cdot)}$ denotes a given boundary condition, and $\boldsymbol{u}_0(\boldsymbol{X})$ represents the initial given condition of the displacement field.

3 Mathematical Models of Growth and Remodeling

Growth and remodeling in soft biological tissues is naturally associated with large deformations. Therefore, the mathematical framework of nonlinear continuum mechanics presented in the previous Chapter 2 is well suited to model these processes. First, the two major approaches to model growth and remodeling processes within the setting of nonlinear continuum mechanics are presented, namely, the kinematic growth (see Section 3.1) and the constrained mixture model (see Section 3.2). Finally, the homogenized constrained mixture model (see Section 3.3) is introduced as it represents the basis of the growth and remodeling model developed in this thesis.

3.1 Kinematic Growth Model

The kinematic growth model was developed by Rodriguez et al. [49] and is similar to mathematical models of plasticity or viscoelasticity. Here, growth is considered as a process that changes the size and the shape of the unloaded stress-free reference configuration $\mathcal{B}_0$. The deformation is

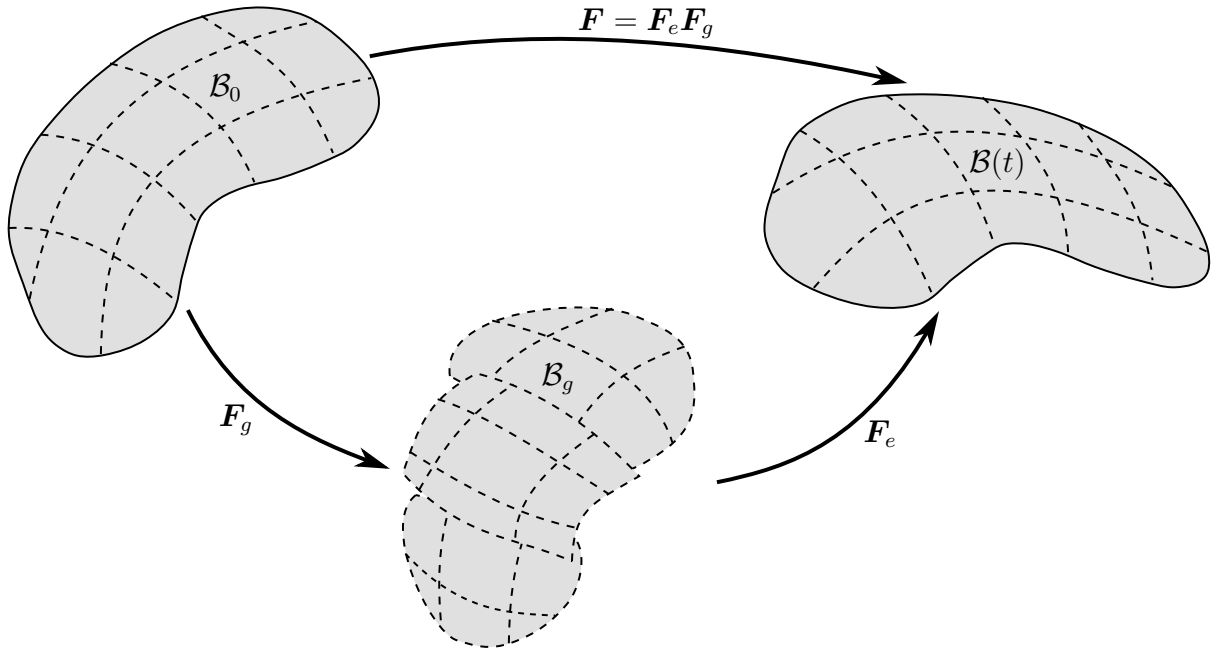

Figure 3.1: Kinematics of the growth model proposed by Rodriguez et al. [49]. The growth theory is based on a multiplicative split of the total deformation gradient $\boldsymbol{F}$ into an elastic part $\boldsymbol{F}_e$ and an inelastic growth part $\boldsymbol{F}_g$ (image adapted from Sebastian L. Fuchs under Creative Commons license) [6].

multiplicatively split into two parts (see Figure 3.1). Changes of mass by deposition or degradation in infinitesimal volume elements are captured by the inelastic growth tensor $\boldsymbol{F}_g$ that deforms the stress-free reference configuration $\mathcal{B}_0$ to an intermediate stress-free configuration $\mathcal{B}_g$. This intermediate "grown" configuration is generally geometrically incompatible, which means that (infinitesimal) volume elements can overlap or have gaps in between. The subsequent elastic deformation caused by the elastic tensor $\boldsymbol{F}_e$ ensures geometrical compatibility and mechanical equilibrium in the current configuration $\mathcal{B}(t)$. Then, the total deformation gradient which maps the reference configuration $\mathcal{B}_0$ to the spatial configuration $\mathcal{B}(t)$ results in

$$\boldsymbol{F} = \boldsymbol{F}_e \boldsymbol{F}_g. \tag{3.1}$$

Assuming that $\boldsymbol{F}_g$ and the stored strain energy which depends on the elastic deformation

$$\Psi = \Psi(\boldsymbol{F}_e(t)) \tag{3.2}$$

are given at each point in time t, the boundary value problem (cf. equations (2.58) - (2.60)) can be solved as usual. So, besides the mechanical constitutive equation (3.2), an additional mechanobiological constitutive equation is required to determine the growth tensor $\boldsymbol{F}_g(t)$ at any time t.
In general, there are two common approaches to define an appropriate constitutive equation for the growth tensor $\boldsymbol{F}_g(t)$. First, one can assume that for some mechanical quantity $\boldsymbol{G}$, which may, for example, be stress or strain, there exists a homeostatic state $\boldsymbol{G}_h$ in soft biological tissues. Then, for simplicity, an appropriate linear evolution equation to model mechano-regulated growth and remodeling can be given by

$$\dot{\boldsymbol{F}}_g = \mathcal{S} : (\boldsymbol{G} - \boldsymbol{G}_h) \tag{3.3}$$

with the fourth order tensor $\mathcal{S}$ determining the amount of growth in the specific directions. Equation (3.3) naturally fulfills the assumption that no growth and remodeling takes place in the homeostatic state

$$\dot{\boldsymbol{F}}_g(\boldsymbol{G} = \boldsymbol{G}_h) = \boldsymbol{0}. \tag{3.4}$$

Second, the growth tensor can simply be defined by some equation of the form

$$\boldsymbol{F}_g = \sum_{j=1}^{n} \beta^j(\boldsymbol{G}, \boldsymbol{G}_h, t) \boldsymbol{B}^j \tag{3.5}$$

with β^j the amount of growth in each growth direction $\boldsymbol{B}^j$. β^j and $\boldsymbol{B}^j$ are defined in a way to match experimental and clinical observations. Again, equation (3.5) needs to fulfill the assumption that no mechano-regulated growth and remodeling takes place in the homeostatic state that leads to the following condition

$$\dot{\beta}^j(\boldsymbol{G} = \boldsymbol{G}_h) = 0. \tag{3.6}$$

The advantage of the kinematic growth model is that it has a simple mathematical foundation and is computationally efficient due to its multiplicative split of the deformation gradient. However, it suffers from a few limitations. First, there are ongoing discussions on how to interpret

the mechanical quantity $\boldsymbol{G}$. For example, Rodriguez et al. [49] identified $\boldsymbol{G}$ with the corotated Cauchy stress, whereas Schmid et al. [50] used the strain, Ambrosi et al. [1] the Eshelby stress, and Himpel et al. [26] the Mandel stress. Second, the kinematic growth model is restricted to one stress-free reference configuration and therefore cannot model different constituents with different natural stress-free configurations and growth kinematics. Third, the model concentrates on mass change and not mass turnover. According to Kroon et al. [33] the continuous turnover of collagen is the driving mechanism in aneurysmal growth. Fourth, as one of the key disadvantages, the definition of $\mathcal{S}$, $\boldsymbol{G}$, β^j, and $\boldsymbol{B}^j$ is most often done on a purely phenomenological basis and not based on any biological or micromechanical processes.

3.2 Multi-Network Constrained Mixture Model

The second major approach to growth and remodeling in soft biological tissues is the multi-network constrained mixture model, herein also referred to classical constrained mixture model, developed by Humphrey et al. [31]. This model is motivated by the idea of multi-network theory [48] and is based on experimental observations, for example, the different half life times of collagen and elastin or the different opening angles of blood vessels after partial lysis of elastin or collagen.

The classical constrained mixture model assumes, in a volume element, n structurally significant constituents such as collagen, elastin, and smooth muscle. All constituents $i \in \{1, 2, \dots, n\}$ deform together so that each constituent exhibits the same total deformation gradient $\boldsymbol{F}$ at any time compared to the reference configuration (see Figure 3.2). In order to model the continuous mass turnover mentioned in the previous section, the constrained mixture model allows for the deposition of individual mass increments of each constituent i at each point in time $\tau \geq 0$ with an elastic prestretch $\boldsymbol{F}_{pre}^{i(\tau)}$ compared to a fictitious stress-free natural configuration $\kappa_{\tau,nat}^{i}$. Then, the total deformation gradient can be split for each mass increment of this constituent i deposited at time τ into an elastic and an inelastic part

$$\boldsymbol{F}(t) = \boldsymbol{F}_e^{i(\tau)}(t)\boldsymbol{F}_{gr}^{i(\tau)}(t), \tag{3.7}$$

where $\boldsymbol{F}_e^{i(\tau)}(t)$ defines the elastic deformation of constituent i deposited at time τ at time t and is given by

$$\boldsymbol{F}_e^{i(\tau)}(t) = \boldsymbol{F}(t)\boldsymbol{F}^{-1}(\tau)\boldsymbol{F}_{pre}^{i(\tau)} \tag{3.8}$$

and the inelastic part $\boldsymbol{F}_{gr}^{i(\tau)}$ has to be defined by a proper evolution equation capturing growth and remodeling. Note that in contrast to the total deformation gradient $\boldsymbol{F}$, its elastic and inelastic parts vary for each constituent i in a differential volume element.

The deposited mass increments have a finite half-life and therefore degrade over time. Thus the total mass density $\rho_0^i(t)$ per unit reference volume of material i at time t results in

$$\rho_0^i(t) = \rho_0^i(0)q^i(t) + \int_0^t \dot{\rho}_{0+}^i(\tau)q^i(t-\tau)\mathrm{d}\tau \tag{3.9}$$

with the rate of mass production $\dot{\rho}_{0+}$, the initial reference mass density $\rho_0^i(0)$ of constituent i, and the survival function $q^i(t-\tau) \in [0, 1]$ which represents the fraction of mass deposited at

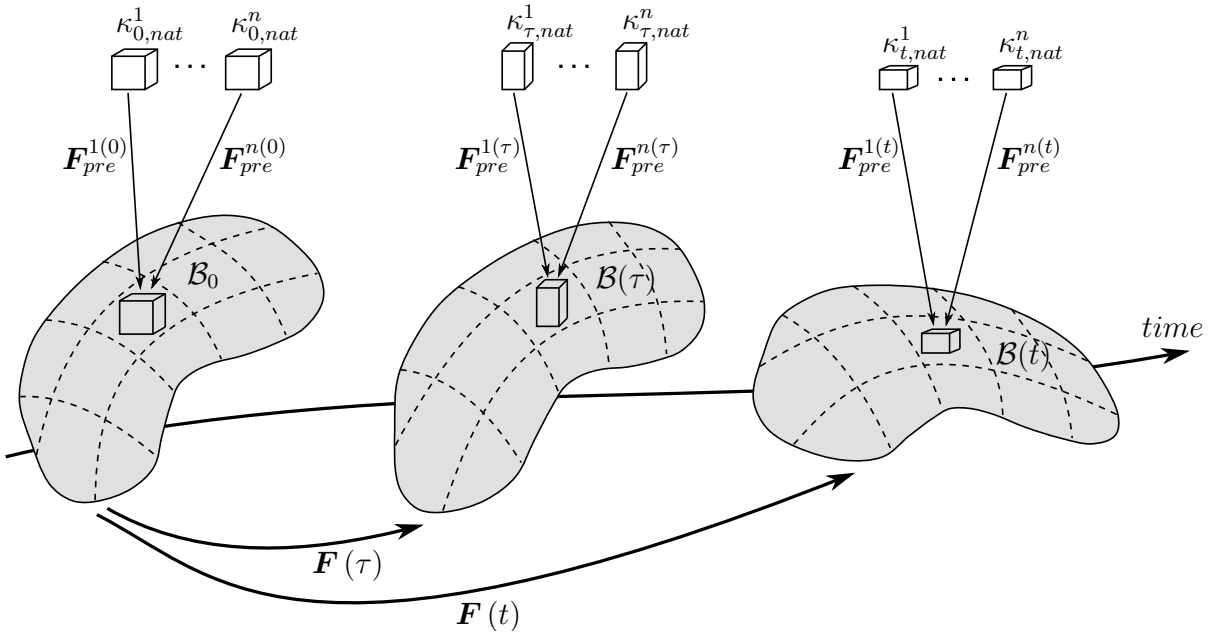

Figure 3.2: External loads as well as growth and remodeling processes deform the reference configuration $\mathcal{B}_0$ into the current configurations $\mathcal{B}(\tau)$ and $\mathcal{B}(t)$. The body is composed of n constituents which are all deformed together by the deformation gradient $\boldsymbol{F}$. Individual mass increments are deposited at any time τ with an elastic deposition prestretch $\boldsymbol{F}^{i(\tau)}_{pre}$ compared to their fictitious stress-free natural configuration $\kappa^i_{\tau,nat}$.

time τ and still surviving at time t. Then, the reference mass density of the whole tissue simply follows as

$$\rho_0(t) = \sum_{i=1}^{n} \rho_0^i(t). \tag{3.10}$$

The strain energy of the whole mixture can be evaluated similar to (3.10) and results in

$$\Psi(t) = \sum_{i=1}^{n} \Psi^i(t). \tag{3.11}$$

with the strain energy of the i-th constituent

$$\Psi^i(t) = \rho_0^i(0) q^i(t) W^i(\boldsymbol{F}_e^{i(0)}(t)) + \int_0^t \dot{\rho}_{0+}^i(\tau) q^i(t-\tau) W^i(\boldsymbol{F}_e^{i(\tau)}(t)) \mathrm{d}\tau. \tag{3.12}$$

Here, W^i represents the strain energy per unit reference mass of each constituent i.
The advantage of the constrained mixture model compared to the kinematic growth model is that it is based on a realistic micromechanical model with parameters that have concrete physiological meanings, e.g. the half-life times of the individual constituents. In detail, the model can account for different constituents with generally different growth kinematics and it allows a continuous turnover of mass. However, to evaluate the integral in (3.12), one has to track a large number of different natural reference configurations for each of the n constituents. Therefore, the classical

constrained mixture model is computationally expensive and the implementation and theory are very complex. Therefore, Cyron et al. [8] developed the homogenized constrained mixture model which tries to combine the advantages of both, the kinematic growth model and the constrained mixture model, respectively.

3.3 Homogenized Constrained Mixture Model

The mathematical model for anisotropic volumetric growth and remodeling developed in this thesis is based on the homogenized constrained mixture model proposed by Cyron et al. [8]. In this section, the concept and the mathematical derivation of the homogenized constrained mixture model are presented in detail. This model combines the computational efficiency and conceptual simplicity of the kinematic growth model (see Section 3.1) with the micromechanical foundation of the classical constrained mixture model (see Section 3.2). An overview of the three different models is given in Figure 3.3.

3.3.1 General Idea

In constrained mixture models, growth and remodeling is understood as a continuous deposition and degradation of differential mass increments of n different constituents, also referred to as mass turnover. Here, it is assumed that new mass is deposited at a rate $\dot{\rho}_{0+}^{i} \geq 0$ with a certain prestress $\boldsymbol{\sigma}_{pre}^{i}$ of the i-th constituent of the mixture into the extant matrix. Simultaneously, extant material is degraded at a rate $\dot{\rho}_{0-}^{i} \leq 0$. Then, the total rate of change of the reference mass density results in

$$\dot{\rho}_{0}^{i} = \dot{\rho}_{0+}^{i} + \dot{\rho}_{0-}^{i}. \tag{3.13}$$

Let us assume that the current stress $\boldsymbol{\sigma}$ of the extant mass which is degraded over time is unequal to the stress of the newly deposited mass $\boldsymbol{\sigma}_{pre}^{i}$. This results in a change of the traction-free configuration of the i-th constituent even if we assume that the total mass stays constant (e.g. $\dot{\rho}_{0}^{i} = 0$). The change of the traction-free state in the absence of any local volume change is referred to as remodeling. However, the traction-free configuration can also change with a change of volume of a differential volume element. Herein, this is referred to as growth.
Classical constrained mixture models can model this change of the traction-free configuration, however, they require keeping track of all the mass increments deposited at different points in time. This leads to a history integral in the strain energy function for each constituent i (see (3.12)). The evaluation of this integral is very involved and computationally expensive. Therefore, Cyron et al. [8] introduced a temporal homogenization over all mass increments deposited at different points in time τ, so that the effect of growth and remodeling can be tracked by an averaged inelastic deformation gradient $\boldsymbol{F}_{gr}^{i}(t)$ that is independent of the time point when an individual mass increment was deposited. Then, equation (3.7) can be rewritten as

$$\boldsymbol{F} = \boldsymbol{F}_{e}^{i}\boldsymbol{F}_{gr}^{i} \tag{3.14}$$

where $\boldsymbol{F}_{e}^{i}$ is the elastic part of the total deformation gradient of constituent i and $\boldsymbol{F}_{gr}^{i}$ is the total inelastic part which can be further split into

$$\boldsymbol{F}_{gr}^{i} = \boldsymbol{F}_{r}^{i}\boldsymbol{F}_{g}^{i}. \tag{3.15}$$

Here, $\boldsymbol{F}_r^i$ captures inelastic changes of the microstructure by mass turnover and $\boldsymbol{F}_g^i$ captures growth related to a change of mass per unit reference volume ρ_0^i. In order to solve for the mechanical equilibrium configuration of the body, one needs to define, in addition to appropriate initial and boundary conditions, mechanical constitutive equations defining the strain energy

$$\Psi = \sum_{i=1}^{n} \rho_0^i W^i \tag{3.16}$$

where Ψ is the total strain energy per unit reference volume of the mixture and W^i is the strain energy per mass of the individual constituents i. The (standard) constitutive equations for soft biological tissues which were developed over the last two decades can be applied here. In addition to that, mechanobiological constitutive equations have to be defined, which prescribe the evolution of $\boldsymbol{F}_r^i$ and $\boldsymbol{F}_g^i$ and the reference mass density ρ_0^i depending on the current mechanical state of the body (e.g. stresses or strains). In the following sections, these mechanobiological evolution equations will be discussed in detail.

3.3.2 Mass Production

One of the most important mechanobiological constitutive equations is the definition of the net mass production. In general, the net mass production can be defined depending on varying quantities describing the current mechanical state of the body. Here, the co-rotated Cauchy stress tensor $\boldsymbol{\sigma}_R^i = \boldsymbol{R}^T \boldsymbol{\sigma}^i \boldsymbol{R}$ in combination with some typically constant homeostatic stress tensor $\boldsymbol{\sigma}_h^i$ is used where $\boldsymbol{R}$ represents the orthonormal rotation tensor from (2.7). Then, the net mass production of each constituent i follows as

$$\dot{\rho}_0^i(t) = \rho_0^i(t) \boldsymbol{K}_\sigma \colon (\boldsymbol{\sigma}_R^i - \boldsymbol{\sigma}_h^i) + \dot{D}^i(t) \tag{3.17}$$

where $\boldsymbol{K}_\sigma$ represents a gain-type fourth-order tensor and $\dot{D}^i(t)$ can be used to prescribe any additional change of mass which is not governed by the Cauchy stress such as a pathological biochemical degradation of a specific constituent of the tissue. It should be noted that for the theory developed by Cyron et al. [8], any other evolution equations can be used to define the net mass production.

3.3.3 Remodeling

Remodeling describes the continuous deposition and degradation of mass. Let us say that new mass (of constituent i) is deposited by a deposition rate $\dot{\rho}_{0+}^i(t)$ per volume reference $\mathrm{d}V$. Hence, the mass increment deposited in a time interval $\mathrm{d}\tau$, at time τ, results in

$$\dot{\rho}_{0+}^i(\tau)\mathrm{d}\tau \geq 0. \tag{3.18}$$

Here, we assume that this mass increment deposited at time τ is continuously degraded by a Poisson process with survival function q^i and

$$\dot{q}^i(t,\tau) = -\frac{1}{T^i} q^i(t,\tau) \tag{3.19}$$

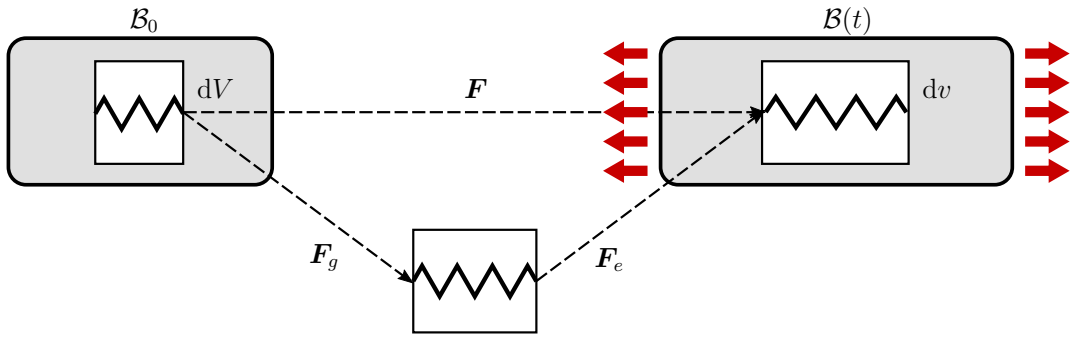

(a) Kinematic growth model proposed by Rodriguez et al. [49]. The total deformation gradient is split into an inelastic growth part $\boldsymbol{F}_g$ and an elastic part $\boldsymbol{F}_e$. See Section 3.1 for more details.

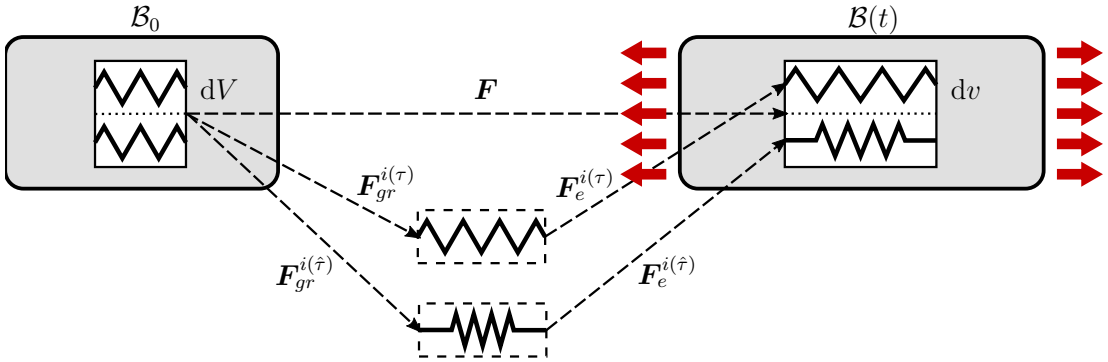

(b) Classical constrained mixture model proposed by Humphrey et al. [31]. In order to keep track of the different stress-free configurations of each mass increment deposited at time τ, an inelastic tensor $\boldsymbol{F}_{gr}^{i(\tau)}$ is introduced individually for each mass increment. See Section 3.2 for more details.

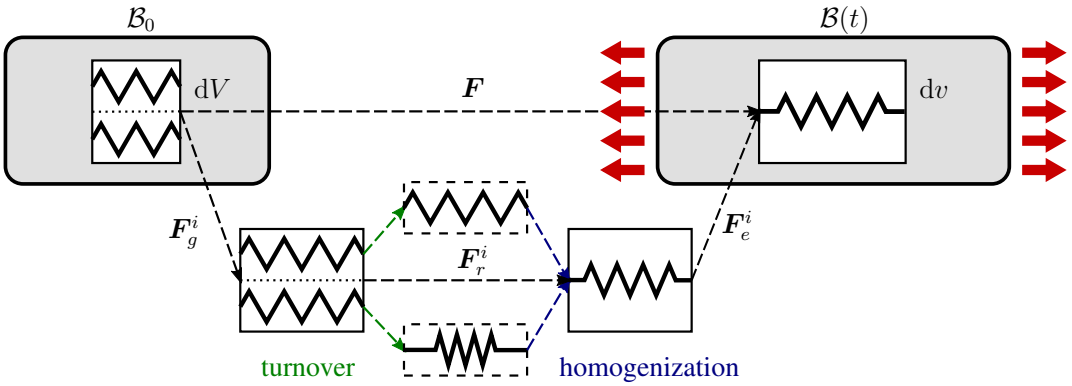

(c) Homogenized constrained mixture model proposed by Cyron et al. [8]. In contrast to the classical constrained mixture model, the stress-free configurations of all mass increments of the i-th constituent are averaged to a single stress-free configuration by a temporally homogenized remodeling tensor $\boldsymbol{F}_r^i$.

Figure 3.3: Overview of three major approaches to model growth and remodeling processes in soft biological tissues. The deposition of new mass is captured by the growth tensor $\boldsymbol{F}_g$ which is visualized by adding coils to the spring. In contrast to that, the inelastic deformation induced by mass turnover is modeled by the remodeling tensor $\boldsymbol{F}_r$ and is visualized by an inelastic stretch or compression of the spring. The elastic stretch and rotation tensor $\boldsymbol{F}_e$ ensures geometrical compatibility and mechanical equilibrium in the current configuration $\mathcal{B}(t)$. It is illustrated by stretched springs and constant coils (image adapted from Sebastian L. Fuchs under Creative Commons license) [6].

with some average turnover time T^i, the period within which a mass increment is on average degraded and replaced by a new mass increment. In the simple case of a constant turnover time T^i, (3.19) leads to an exponential survival function (see also (3.9))

$$q^i\left(t,\tau\right)=\exp\left(\frac{-(t-\tau)}{T^i}\right). \tag{3.20}$$

With (3.19) the rate of mass removal follows as

$$\dot{\rho}^i_{0-}(t)=-\frac{\rho^i_0(t)}{T^i}. \tag{3.21}$$

Similar to (3.18), the mass degraded in a time interval $\mathrm{d}\tau$ at time τ is given by

$$\dot{\rho}^i_{0-}(\tau)\mathrm{d}\tau\leq 0. \tag{3.22}$$

The total rate of change of reference mass density is given by (3.13).
Let us assume that during mass turnover, the total deformation gradient $\boldsymbol{F}$ and the growth tensor $\boldsymbol{F}_g$ are constant. Then, the change of the Cauchy stress in a time interval $\mathrm{d}\tau$ at time τ induced by the deposition of new mass with prestress $\boldsymbol{\sigma}^i_{pre}$ at a rate of $\dot{\rho}^i_{0+}(\tau)$ and the degradation of extant mass at a rate of $\dot{\rho}^i_{0-}(\tau)$ results in

$$\dot{\boldsymbol{\sigma}}^i_r(\tau)\mathrm{d}\tau=\frac{\boldsymbol{\sigma}^i_{pre}\left(\tau\right)\dot{\rho}^i_{0+}\left(\tau\right)\mathrm{d}\tau+\boldsymbol{\sigma}^i\left(\tau\right)\left[\rho^i_0\left(\tau\right)+\dot{\rho}^i_{0-}\left(\tau\right)\mathrm{d}\tau\right]}{\rho^i_0\left(\tau\right)+\dot{\rho}^i_0\left(\tau\right)\mathrm{d}\tau}-\boldsymbol{\sigma}^i(\tau) \tag{3.23}$$

where $\boldsymbol{\sigma}^i(\tau)$ is the mass-averaged Cauchy stress of all mass increments of constituent i forming the mixture. The first term on the right represents the mass-averaged Chauchy stress of constituent i at time $\tau+\mathrm{d}\tau$ and the second summand is the one at time τ. With (3.13), (3.21) and neglecting higher order terms, equation (3.23) can be rewritten as

$$\dot{\boldsymbol{\sigma}}^i_r\left(\tau\right)=-\frac{\dot{\rho}^i_{0+}\left(\tau\right)\left[\boldsymbol{\sigma}^i\left(\tau\right)-\boldsymbol{\sigma}^i_{pre}\left(\tau\right)\right]}{\rho^i_0\left(\tau\right)}=-\left[\frac{\dot{\rho}^i_0\left(\tau\right)}{\rho^i_0\left(\tau\right)}+\frac{1}{T^i}\right]\left[\boldsymbol{\sigma}^i\left(\tau\right)-\boldsymbol{\sigma}^i_{pre}\left(\tau\right)\right]. \tag{3.24}$$

The rate of change of the mass-averaged Cauchy stress $\dot{\boldsymbol{\sigma}}^i_r$ caused only by mass turnover can similarly be expressed by a rate of change of the elastic stretch and rotation tensor $\dot{\boldsymbol{F}}^i_e$ or the elastic right Cauchy-Green tensor $\dot{\boldsymbol{C}}^i_e$, that is,

$$\dot{\boldsymbol{\sigma}}^i_r=\left[\frac{\partial\boldsymbol{\sigma}^i}{\partial\boldsymbol{F}^i_e}:\dot{\boldsymbol{F}}^i_e\right]_{\boldsymbol{F},\boldsymbol{F}^i_g=const}=\left[\frac{\partial\boldsymbol{\sigma}^i}{\partial\boldsymbol{C}^i_e}:\dot{\boldsymbol{C}}^i_e\right]_{\boldsymbol{F},\boldsymbol{F}^i_g=const}. \tag{3.25}$$

with the elastic right Cauchy-Green tensor $\boldsymbol{C}^i_e=(\boldsymbol{F}^i_e)^T\boldsymbol{F}^i_e$ and its rate

$$\dot{\boldsymbol{C}}^i_e=\left(\dot{\boldsymbol{F}}^i_e\right)^T\boldsymbol{F}^i_e+\left(\boldsymbol{F}^i_e\right)^T\dot{\boldsymbol{F}}^i_e. \tag{3.26}$$

Furthermore, the assumption that the total deformation gradient $\boldsymbol{F}$ and the growth tensor $\boldsymbol{F}^i_g$ are constant during mass turnover implies that $\boldsymbol{F}^i_e\boldsymbol{F}^i_r=const$. So, the time derivative of the product $(\boldsymbol{F}^i_e\boldsymbol{F}^i_r)$ follows as

$$\dot{\boldsymbol{F}}^i_e\boldsymbol{F}^i_r+\boldsymbol{F}^i_e\dot{\boldsymbol{F}}^i_r=\boldsymbol{0}. \tag{3.27}$$

The rate of change of the elastic stretch and rotation tensor $\dot{\boldsymbol{F}}_e^i$ results from solving (3.27), that is,

$$\dot{\boldsymbol{F}}_e^i = -\boldsymbol{F}_e^i \dot{\boldsymbol{F}}_r^i \left(\boldsymbol{F}_r^i\right)^{-1} = -\boldsymbol{F}_e^i \boldsymbol{L}_r^i \tag{3.28}$$

with the inelastic remodeling velocity gradient $\boldsymbol{L}_r^i = \dot{\boldsymbol{F}}_r^i \left(\boldsymbol{F}_r^i\right)^{-1}$ (see also (2.23)). Using (3.26) and (3.28) in (3.25) leads to

$$\dot{\boldsymbol{\sigma}}_r^i = -\left[\frac{\partial \boldsymbol{\sigma}^i}{\partial \boldsymbol{C}_e^i} : \left[\boldsymbol{C}_e^i \boldsymbol{L}_r^i + \left(\boldsymbol{L}_r^i\right)^T \boldsymbol{C}_e^i\right]\right]_{\boldsymbol{F}, \boldsymbol{F}_g^i = const}. \tag{3.29}$$

Finally, inserting (3.29) in (3.24) and using the minor symmetry of $\frac{\partial \boldsymbol{\sigma}^i}{\partial \boldsymbol{C}_e^i}$ results in the evolution equation for the remodeling deformation gradient $\boldsymbol{F}_r^i$ of constituent i of the mixture (see equation (28) in [8]), that is,

$$\left[\frac{\dot{\rho}_0^i(t)}{\rho_0^i(t)} + \frac{1}{T^i}\right]\left[\boldsymbol{\sigma}^i - \boldsymbol{\sigma}_{pre}^i\right] = \left[2\frac{\partial \boldsymbol{\sigma}^i}{\partial \boldsymbol{C}_e^i} : \left(\boldsymbol{C}_e^i \boldsymbol{L}_r^i\right)\right]_{\boldsymbol{F}, \boldsymbol{F}_g^i = const}. \tag{3.30}$$

Equation (3.30) can be rewritten in terms of the mass-averaged second Piola-Kirchhoff stress $\boldsymbol{S}^i$ by using the push-forward operation

$$\boldsymbol{\sigma}^i = \frac{1}{J}\boldsymbol{F}\boldsymbol{S}^i\boldsymbol{F}^T \tag{3.31}$$

which results in

$$\left[\frac{\dot{\rho}_0^i(t)}{\rho_0^i(t)} + \frac{1}{T^i}\right]\left[\boldsymbol{S}^i - \boldsymbol{S}_{pre}^i\right] = \left[2\frac{\partial \boldsymbol{S}^i}{\partial \boldsymbol{C}_e^i} : \left(\boldsymbol{C}_e^i \boldsymbol{L}_r^i\right)\right]_{\boldsymbol{F}, \boldsymbol{F}_g^i = const}. \tag{3.32}$$

Note that Cyron et al. [7] showed that $\boldsymbol{\sigma}_{pre}^i$ has to correspond to the homeostatic stress $\boldsymbol{\sigma}_h^i$ introduced in Section 3.3.2 with $\boldsymbol{\sigma}_{pre}^i = \boldsymbol{R}\boldsymbol{\sigma}_h^i\boldsymbol{R}^T$.

3.3.4 Growth

In general, the size of a differential volume element in the body changes by degradation and/or deposition of mass. It is often assumed that soft biological tissues exhibit a nearly incompressible behavior, so that the determinant of the elastic deformation gradient of each constituent i is $\det(\boldsymbol{F}_e^i) = 1$. Furthermore, it is assumed that mass turnover does not change the total tissue mass, which results in an isochoric remodeling tensor, that is, $\det(\boldsymbol{F}_r^i) = 1$. Then the determinant of the total deformation gradient results in

$$\det(\boldsymbol{F}) = \det(\boldsymbol{F}_e^i \boldsymbol{F}_r^i \boldsymbol{F}_g^i) = \det(\boldsymbol{F}_g^i). \tag{3.33}$$

Moreover, we assume that the spatial mass density $\rho(t)$ stays constant during growth so that the packing density of the fibers in the tissue does not change. With this assumption and (3.33), the determinant of the growth deformation gradient $\boldsymbol{F}_g^i$ results in

$$\det(\boldsymbol{F}_g^i) = \frac{\rho_0(t)}{\rho(t)} = \frac{\rho_0(t)}{\rho_0(0)}. \tag{3.34}$$

The full definition of $\boldsymbol{F}_g^i$ (which implies the growth direction) depends on the specific application of the homogenized constrained mixture model. In Section 3.1, two different ways of defining growth tensors were presented which can be used also in homogenized constrained mixture models.

4 Paper A

Homogenized constrained mixture models for anisotropic volumetric growth and remodeling

Summary

Over the last two decades, soft tissue growth and remodeling has attracted increasing attention. The two major approaches to model these processes are the kinematic growth and the multi-network constrained mixture models. However, kinematic growth models are based on rather heuristic mathematical assumptions and classical constrained mixture models suffer from their mathematical complexity and computational inefficiency. To overcome these limitations, recently, the novel concept of homogenized constrained mixture models was introduced. These type of models have the same micromechanical foundation as classical constrained mixture models, yet as efficient and simple as kinematic growth models. Unfortunately, so far, they are limited to two dimensional continua.
To this end, in this paper, the homogenized constrained mixture model is further developed from a purely two-dimensional membrane model to three-dimensional continua. In addition, an anisotropic volumetric growth law for the arterial wall is introduced, which results in the following inelastic (growth) tensor

$$\boldsymbol{F}_g(t) = \frac{\rho_0(t)}{\rho_0(0)} \boldsymbol{a}_0^{\perp} \otimes \boldsymbol{a}_0^{\perp} + (\boldsymbol{I} - \boldsymbol{a}_0^{\perp} \otimes \boldsymbol{a}_0^{\perp}) \tag{4.1}$$

with the reference mass density ρ_0, the unit vector $\boldsymbol{a}_0^{\perp}$ in thickness direction of the arterial wall, and the second order unit tensor $\boldsymbol{I}$. Using this model, the enlargement of an idealized fusiform abdominal aortic aneurysm over 15 years is studied. Depending on the rate of mass production of collagen and smooth muscle, the blood vessel can, on the one hand, attain – after a period of adaptation – a new stable state (high rate of mass production) or, on the other hand, the damage to the elastin layer can result in an unbounded dilatation of the vessel (low rate of mass production). Furthermore, the response of the model aorta due to a sudden and permanent increase in blood pressure is examined. In contrast to previous three dimensional models assuming isotropic growth, the above anisotropic growth law allows for reproduction of the related experimental observations for a specific choice of the rate of mass production of collagen and smooth muscle. Therefore, anisotropic constrained mixture models, as introduced in this paper for the first time, are required to avoid physiologically inaccurate results in simulations of vascular growth and remodeling.

Contribution

I am the principal author of the manuscript. I further developed the homogenized constrained mixture model from a purely two-dimensional membrane model to three dimensions. I implemented the membrane and three dimensional model in our in-house research code BACI (written in C++), designed the study, and carried out all of the computations. I analyzed and critically discussed the results with C.J. Cyron. I drafted the manuscript. C.J. Cyron contributed to the manuscript draft and gave critical reviews. R.C. Aydin supported me with his medical background and contributed valuable comments. A. Seitz contributed with valuable comments on the implementation of the model and the interpretation of the results.

5 Paper B

Anisotropic stiffness and tensional homeostasis induce a natural anisotropy of volumetric growth and remodeling in soft biological tissues

Summary

Volumetric growth in soft biological tissues is often modeled as a local inelastic dilatation of differential tissue volume elements [49] in order to accommodate for the additional mass. This dilation is generally anisotropic, meaning that it is unequal in different directions. Most previous mathematical and theoretical models of growth and remodeling [19, 22, 24, 32, 36, 53, 55] used an inelastic (growth) tensor to capture volumetric growth. In these models and also within the framework of paper A, the definition of this growth tensor is often based on purely heuristic assumptions. To overcome this problem, it is essential to understand and quantify factors governing the anisotropy of the geometric changes induced by growth.
Therefore, in this paper, a new theory is presented to determine the anisotropy of the changes in tissue geometry resulting from volumetric growth in soft biological tissues in a natural way. It is based on two major hypotheses supported by experimental observations reported in the literature:

- Remodeling is driven by tensional homeostasis only.
- The spatial mass density remains constant during volumetric growth.

The proposed theory predicts that differential tissue volume elements dilate mainly in the direction(s) of lowest stiffness. In addition to that, the three dimensional homogenized constrained mixture model is further developed to incorporate the aforementioned theory. To this end, the total strain energy is split into a compressible and a volumetric penalty part. The volumetric penalty-type energy enforces a constant spatial mass density ρ and is given by

$$\Psi^{\#}(t) = \frac{\epsilon}{2}\left(\det(\boldsymbol{F}) - \frac{\rho_0(t)}{\rho}\right)^2 \tag{5.1}$$

with a very large ϵ, the deformation gradient $\boldsymbol{F}$, and the total reference mass density ρ_0. By simply adding this term to the strain energy function, no inelastic (growth) tensor has to be explicitly defined. It is shown that this model is able to reproduce the experimentally observed growth behavior in a host of soft biological tissues without relying on any additional heuristic assumptions or quantities.

Contribution

I am the principal author of the manuscript. I developed the theory that can predict the anisotropy of the changes of the tissue geometry resulting from volumetric growth in soft biological tissues. I implemented this new theory in our in-house research code BACI (written in C++), designed the study, and carried out all of the computations. I analyzed and critically discussed the results with C.J. Cyron. I drafted the manuscript. C.J. Cyron contributed to the manuscript draft, gave critical reviews, and helped to interpret the results. R.C. Aydin supported me with his medical background and contributed valuable comments.

6 Discussion

Parts of this discussion are taken from, derived from, or published in Braeu et al. 2017 [4] and Braeu et al. 2018 [5].
Recently, homogenized constrained mixture models for soft tissue growth and remodeling have been introduced by Cyron et al. [8]. They combine the conceptual simplicity and computational efficiency of kinematic growth models with the micromechanical foundation of classical constrained mixture models. However, so far, they are limited to two dimensions.
To overcome this limitation, in paper A, a three-dimensional homogenized constrained mixture model of anisotropic vascular growth and remodeling was introduced. First, the enlargement of an idealized fusiform abdominal aortic aneurysm over 15 years was studied. In this example, anisotropic growth in thickness direction is assumed and G&R is triggered by a loss of elastin. A good agreement is found between the two-dimensional membrane model developed by Cyron et al. [8] and the three-dimensional anisotropic growth model developed in paper A. Depending on the rate of mass production of collagen and smooth muscle, the blood vessel can, on the one hand, attain – after a period of adaptation – a new stable state (high rate of mass production) or, on the other hand, the damage to the elastin layer can result in an unbounded dilatation of the vessel (low rate of mass production). However, minor differences between both models have been observed which can be explained by the different way elastin is modeled in two and three dimensions.
A weakening of the vessel wall by the loss of elastin should intuitively lead to dilatation of the blood vessel, which can be observed in the model developed in paper A. Yet, previous studies that used constrained mixture models to model growth and remodeling in blood vessels after a loss of elastin, predicted a contraction of the wall, rather than a dilation [13, 22, 53]. The reason for this unphysiological behavior in these models is that they define the growth direction via the incompressibility constraint using a volumetric deviatoric split of the deformation gradient. This leads to an isotropic growth behavior. So, if mass is removed, the tissue will shrink equally in each direction, that means not only the wall thins but the radius of the blood vessel decreases as well. Eriksson et al. [13] tried to overcome this problem by introducing two different kinds of growth mechanisms, namely, constant individual density (CID) and adaptive individual density (AID) growth. With the AID growth approach, Eriksson et al. could mimic a more physiological growth behavior, as in this case, a loss of mass does not lead to any change in tissue volume. However, it is based on an unverified micromechanical foundation. O'Connel et al. in 2008 [45] discussed in detail the structure of elastin in the arterial wall. Thin layers of elastin span along the circumferential and axial directions and are separated by thick layers of smooth muscle and collagen (see Figure 5 in paper A). After a sudden partial loss of elastin, void regions filled with fluid or at least regions with a small resistance against compression would occur between the lamellar sheets of elastin and the collagen/ smooth muscle layer. Because of the blood pressure in thickness direction, these spaces would be expected to close immediately by a motion of the respective layers in thickness direction. This would lead to a thinning of the arterial wall as pre-

dicted by the anisotropic three-dimensional growth model developed in paper A, rather than a change of the mass density of elastin as assumed in the AID concept proposed in Eriksson et al. [13].
Second, the thickening of the arterial wall in hypertension was studied. This example is inspired by an experiment from Matsumoto et al. in 1996 [41], who examined the response of the arterial wall after a sudden and permanent increase in blood pressure. For a specific rate of mass production of collagen and smooth muscle and assuming anisotropic growth in thickness direction, the anisotropic growth model developed in paper A can reproduce these experimental observations, although still with the limitation that the growth anisotropy has to be heuristically predefined in some way. After a transient period, the vessel stabilizes in a new slightly dilated state that corresponds well with the data reported in Matsumoto et al. [41]. In contrast to that, assuming isotropic volumetric growth (similar to [13, 22, 53]) leads to an unbounded dilatation of the blood vessel even for very high rates of mass production of collagen and smooth muscle. Therefore, isotropic growth models, as mostly used previously, cannot reproduce the experimental findings and seem to yield unphysiological results. Slight changes in blood pressure can occur in numerous situations during a lifetime, therefore unbounded dilation, even for a small increase in blood pressure, as observed in isotropic growth models means that aneurysms would be expected in almost the whole population.
The stable behavior in the case of anisotropic growth in the thickness direction and the unstable behavior in the case of isotropic growth can easily be understood from the mechanobiological stability theory [7]. Within this theory, a state where mechanical equilibrium is fulfilled and no mechano-regulated growth and remodeling takes place is called a mechanobiological equilibrium. Healthy soft biological tissues, such as arteries, can typically be assumed to be in mechanobiological equilibrium because they maintain their geometrical shapes over a long period of time. Such a mechanobiological equilibrium is called stable when, after a small perturbation of the equilibrium state by, for example, an increase in blood pressure or a damage to the elastin layer, the system can reattain its original state or at least a state close to the original one. In cylindrical blood vessels, an elevated blood pressure increases the wall stress above the homeostatic value, which leads to growth and remodeling. Anisotropic volumetric growth in the thickness direction helps to reduce the wall stress back to its initial value to restore the mechanobiological equilibrium. On the other hand, remodeling (governed by (3.30) or equivalently (3.32)) leads to a dilatation in the circumferential direction which, according to Laplace' formula (which says that the wall stress increases linearly with the inner radius of the blood vessel), leads to an increase in wall stress. Therefore, by choosing a sufficiently high rate of mass production of collagen and smooth muscle, anisotropic volumetric growth in thickness direction can overrule the effect of remodeling and stabilize the vessel after some adaptation time. In contrast, for the case of isotropic growth, the vessel wall is dilated by the same factor in wall thickness direction (reducing the wall stress) and in circumferential direction (increasing the wall stress). Recalling Laplace' law, these two effects cancel each other out. However, remodeling increases the wall stress, entailing a continued and potentially unbounded dilatation of the vessel. It should be noted here, that in rare cases, stabilization can also occur in the case of isotropic growth. Constituents that do not undergo growth and remodeling (like elastin or a ground matrix) take over a larger and larger wall stress which may enable collagen and smooth muscle to reattain a homeostatic stress state. However, in this case, restabilization would occur only after a large dilatation. Assuming that growth and remodeling should ensure the stability of

the blood vessel in the most efficient way reinforces the assumption of anisotropic growth in the thickness direction. Of course, further studies have to be undertaken to confirm this hypothesis. Nonetheless, it shows that the anisotropy of growth plays a key role in modeling soft biological tissue growth and remodeling. A limitation of paper A is that the anisotropy in wall thickness direction of the blood vessel has to be assumed without relying on more fundamental principles. Therefore, in paper B, a theory was developed to determine the physiological anisotropic changes in tissue geometry resulting from volumetric growth based on two simple hypotheses:

1. The total current mass density remains constant, meaning that a change in tissue mass is directly associated with a proportional change in tissue volume.

2. Remodeling is the only mechanism reorganizing the elastic microstructure of the tissue and is only governed by the principle of tensional homeostasis.

So far, most previous works and also the model developed in paper A try to capture volumetric growth by an inelastic (growth) tensor that is often defined based on purely heuristic assumptions. In contrast to that, the approach presented in paper B has a physiological foundation and allows to model volumetric growth in three dimensions without explicitly defining a growth tensor. As a rule of thumb, volumetric growth and remodeling will result in the approach of paper B in an expansion of differential volume elements mainly in the softest direction(s). Numerous computational studies showed that the theory is able to describe and reproduce the experimentally observed growth behavior in a large number of different load-bearing collagenous soft biological tissues.
Regarding the adaptation of soft biological tissues to external loading, the theory developed in paper B has another interesting consequence. It is well known that fibers rotate in the direction of mechanical loading, which makes loaded directions in soft biological tissues very stiff in general. The theory from paper B predicts that additional mass is deposited in the softest direction(s), thus mainly perpendicular to the loading direction(s). This increases the effective load-bearing cross-section and therefore increases the strength of the soft biological tissue in the most efficient way.
In a large number of situations, it is hard to measure and quantify geometrical changes of soft biological tissues. This theory can not only explain the mechano-regulated adaptation of soft biological tissues but can also help to better understand the complex processes during morphogenesis based on stiffness, which is much easier to model and measure. Future studies should thus try to measure and model stiffness of soft biological tissues in a more accurate way, following previous studies from Gasser et al. [16], Vasta et al. [54], Gizzi et al. [17, 18], Niestrawska et al. [44], and Holzapfel et al. [29]. This might help to better understand complex volumetric growth patterns.
In summary, the three-dimensional homogenized constrained mixture model developed in this thesis is, in combination with the newly developed anisotropic growth theory, an important step towards a novel computational risk assessment method for aneurysms without taking into account any heuristic ad hoc assumptions. This model is an efficient, reliable, and universal tool to model growth and remodeling processes in various kinds of soft biological tissues. In the future, remodeling (i.e. equation (3.30)) could be considered, not only in quasi-one-dimensional fiber materials, but also in fully three dimensional matrix materials. In addition to that, the three-dimensional homogenized constrained mixture model developed in this thesis could be applied

to patient-specific geometries. However, in the proposed growth and remodeling approach, collagen fiber directions have to be accurately defined. Therefore, a procedure needs to be developed to prescribe a reasonable distribution of fiber directions in a patient-specific aorta. Another interesting avenue of future research could be to include biochemical and transport processes which are supposed to influence the volumetric growth behavior of soft biological tissues, along previous studies of Grillo et al. [21], Marino et al. [39], and Mascheroni et al. [40]. Then, a natural next step would be to test the model in a clinical setup. To this end, the data of two subsequent computed tomography (CT) scans of one patient can be used to determine the growth parameter, which controls the rate of mass production of collagen and smooth muscle, with the help of an inverse analysis. Using this calibrated model, the future growth of the aneurysm could be predicted. Since this state is unknown, the proposed procedure has to be intensely validated with follow-up CT scans of the same patient after a fixed number of years. Finally, the further development of the homogenized constrained mixture model to three dimensional continua and the proposed theory that can predict the anisotropy of the changes in tissue geometry resulting from volumetric growth allow application of the model to other soft biological tissues, such as the heart or the eye.

Bibliography

[1] D. Ambrosi and F. Guana, Stress-modulated growth, *Mathematics and Mechanics of Solids* **12**, 319–342, 2007.

[2] C. L. Berry and S. E. Greenwald, Effects of hypertension on the static mechanical properties and chemical composition of the rat aorta1, *Cardiovascular Research* **10**, 437–451, 1976.

[3] J. Bonet and R. D. Wood, *Nonlinear Continuum Mechanics for Finite Element Analysis*, Cambridge University Press, Cambridge, 2nd Edition, 2008.

[4] F. A. Braeu, A. Seitz, R. C. Aydin, and C. J. Cyron, Homogenized constrained mixture models for anisotropic volumetric growth and remodeling, *Biomechanics and Modeling in Mechanobiology* **16**, 889–906, 2017.

[5] F. A. Braeu, R. C. Aydin, and C. J. Cyron, Anisotropic stiffness and tensional homeostasis induce a natural anisotropy of volumetric growth and remodeling in soft biological tissues, *Biomechanics and Modeling in Mechanobiology*, 2018.

[6] Creative Commons License. CC BY-SA 4.0. `https://creativecommons.org/licenses/by-sa/4.0/`, 2019.

[7] C. J. Cyron, J. S. Wilson, and J. D. Humphrey, Mechanobiological stability: a new paradigm to understand the enlargement of aneurysms?, *Journal of the Royal Society Interface* **11**, 20140680, 2014.

[8] C. J. Cyron, R. C. Aydin, and J. D. Humphrey, A homogenized constrained mixture (and mechanical analog) model for growth and remodeling of soft tissue, *Biomechanics and Modeling in Mechanobiology*, 2016.

[9] R. C. Darling, C. Messina, D. C. Brewster, and L. W. Ottinger, Autopsy study of unoperated abdominal aortic aneurysms. the case for early resection., *Circulation* **56 3 Suppl**, II161–4, 1977.

[10] H. Davis, *Conservative Surgery: As Exhibited in Remedying Some of the Mechanical Causes that Operate Injuriously Both in Health and Disease.*, D. Appleton, 1867.

[11] H.-H. Eckstein, D. Böckler, I. Flessenkämper, T. Schmitz-Rixen, S. Debus, and W. Lang, Ultrasonographic screening for the detection of abdominal aortic aneurysms, *Deutsches Ärzteblatt international* **106**, 657–663, 2009.

[12] M. Epstein and G. A. Maugin, Thermomechanics of volumetric growth in uniform bodies, *International Journal of Plasticity* **16**, 951–978, 2000.

[13] T. S. E. Eriksson, P. N. Watton, X. Y. Luo, and Y. Ventikos, Modelling volumetric growth in a thick walled fibre reinforced artery, *Journal of the Mechanics and Physics of Solids* **73**, 134–150, 2014.

[14] C. A. Figueroa, S. Baek, C. A. Taylor, and J. D. Humphrey, A computational framework for fluid-solid-growth modeling in cardiovascular simulations, *Computer Methods in Applied Mechanics and Engineering* **198**, 3583–3602, 2009.

[15] M. F. Fillinger, S. P. Marra, M. L. Raghavan, and F. E. Kennedy, Prediction of rupture risk in abdominal aortic aneurysm during observation: Wall stress versus diameter, *Journal of Vascular Surgery* **37**, 724–732, 2003.

[16] T. C. Gasser, R. W. Ogden, and G. A. Holzapfel, Hyperelastic modelling of arterial layers with distributed collagen fibre orientations, *Journal of The Royal Society Interface* **3**, 15–35, 2006.

[17] A. Gizzi, A. Pandolfi, and M. Vasta, Statistical characterization of the anisotropic strain energy in soft materials with distributed fibers, *Mechanics of Materials* **92**, 119–138, 2016.

[18] A. Gizzi, A. Pandolfi, and M. Vasta, A generalized statistical approach for modeling fiber-reinforced materials, *Journal of Engineering Mathematics*, 2017.

[19] A. Goriely and R. Vandiver, On the mechanical stability of growing arteries, *IMA Journal of Applied Mathematics* **75**, 549–570, 2010.

[20] R. M. Greenhalgh, Comparison of endovascular aneurysm repair with open repair in patients with abdominal aortic aneurysm (evar trial 1), 30-day operative mortality results: randomised controlled trial, *The Lancet* **364**, 843–848, 2004.

[21] A. Grillo, S. Federico, and G. Wittum, Growth, mass transfer, and remodeling in fiber-reinforced, multi-constituent materials, *International Journal of Non-Linear Mechanics* **47**, 388–401, 2012.

[22] A. Grytsan, P. N. Watton, and G. A. Holzapfel, A thick-walled fluid–solid-growth model of abdominal aortic aneurysm evolution: Application to a patient-specific geometry, *Journal of Biomechanical Engineering* **137**, 031008, 2015.

[23] A. Grytsan, T. Eriksson, P. Watton, and T. Gasser, Growth description for vessel wall adaptation: A thick-walled mixture model of abdominal aortic aneurysm evolution, *Materials* **10**, 994, 2017.

[24] R. Grytz, I. A. Sigal, J. W. Ruberti, G. Meschke, and J. C. Downs, Lamina cribrosa thickening in early glaucoma predicted by a microstructure motivated growth and remodeling approach, *Mechanics of Materials : an International Journal* **44**, 99–109, 2012.

[25] D. P. Heider, O. Wolf, C. Reeps, M. H. Hanke, A. Zimmermann, H. Berger, and H. H. Eckstein, Aneurysmen und Dissektionen der thorakalen und abdominellen Aorta, *Der Chirurg* **78**, 600–610, 2007.

[26] M. A. S. P. Himpel G, Kuhl E, Computational modelling of isotropic multiplicative growth, *Computer Modeling in Engineering and Sciences* **8**, 119–134, 2005.

[27] S. Hobbs, M. Claridge, M. Drage, C. Quick, A. Bradbury, and A. Wilmink, Strategies to improve the effectiveness of abdominal aortic aneurysm screening programmes, *Journal of Medical Screening* **11**, 93–96, 2004.

[28] G. A. Holzapfel, *Nonlinear solid mechanics: a continuum approach for engineering*, J. Wiley, Chichester, 2010.

[29] G. A. Holzapfel and R. W. Ogden, Comparison of two model frameworks for fiber dispersion in the elasticity of soft biological tissues, *European Journal of Mechanics - A/Solids* **66**, 193–200, 2017.

[30] J. D. Humphrey and G. A. Holzapfel, Mechanics, mechanobiology, and modeling of human abdominal aorta and aneurysms, *Journal of biomechanics* **45**, 805–814, 2012.

[31] J. D. Humphrey and K. R. Rajagopal, A constrained mixture model for growth and remodeling of soft tissues, *Mathematical Models and Methods in Applied Sciences* **12**, 407–430, 2002.

[32] I. Karšaj, J. Sorić, and J. D. Humphrey, A 3-D framework for arterial growth and remodeling in response to altered hemodynamics, *International Journal of Engineering Science* **48**, 1357–1372, 2010.

[33] M. Kroon and G. A. Holzapfel, A model for saccular cerebral aneurysm growth by collagen fibre remodelling, *Journal of Theoretical Biology* **247**, 775–87, 2007.

[34] M. Kroon and G. A. Holzapfel, A theoretical model for fibroblast-controlled growth of saccular cerebral aneurysms, *Journal of Theoretical Biology* **257**, 73–83, 2009.

[35] W. J. Lin, M. D. Iafrati, R. A. Peattie, and L. Dorfmann, Growth and remodeling with application to abdominal aortic aneurysms, *Journal of Engineering Mathematics* **109**, 113–137, 2018.

[36] M. Lindquist Liljeqvist, R. Hultgren, T. C. Gasser, and J. Roy, Volume growth of abdominal aortic aneurysms correlates with baseline volume and increasing finite element analysis-derived rupture risk, *Journal of Vascular Surgery* **63**, 1434–1442.e3, 2016.

[37] S. Loerakker, T. Ristori, and F. P. T. Baaijens, A computational analysis of cell-mediated compaction and collagen remodeling in tissue-engineered heart valves, *Journal of the Mechanical Behavior of Biomedical Materials* **58**, 173–187, 2016.

[38] A. Maier, M. W. Gee, C. Reeps, J. Pongratz, H.-H. Eckstein, and W. A. Wall, A comparison of diameter, wall stress, and rupture potential index for abdominal aortic aneurysm rupture risk prediction, *Annals of Biomedical Engineering* **38**, 3124–3134, 2010.

[39] M. Marino, G. Pontrelli, G. Vairo, and P. Wriggers, A chemo-mechano-biological formulation for the effects of biochemical alterations on arterial mechanics: the role of molecular transport and multiscale tissue remodelling, *Journal of The Royal Society Interface* **14**, 2017.

[40] P. Mascheroni, M. Carfagna, A. Grillo, D. P. Boso, and B. A. Schrefler, An avascular tumor growth model based on porous media mechanics and evolving natural states, *Mathematics and Mechanics of Solids* **23**, 686–712, 2017.

[41] T. Matsumoto and K. Hayashi, Response of arterial wall to hypertension and residual stress, In *Biomechanics: Functional Adaptation and Remodeling*, pages 93–119, Springer Japan, Tokyo, 1996.

[42] M. Müller, Gefäßchirurgie - arterielle Aneurysmen, In *Chirurgie für Studium und Praxis*, pages 58–61, Breisach: Medizinische Verlags- und Informationsdienste, 2004/05.

[43] Y. Nakagawa, M. Totsuka, T. Sato, Y. Fukuda, and K. Hirota, Effect of disuse on the ultrastructure of the achilles tendon in rats, *European Journal of Applied Physiology and Occupational Physiology* **59**, 239–242, 1989.

[44] J. A. Niestrawska, C. Viertler, P. Regitnig, T. U. Cohnert, G. Sommer, and G. A. Holzapfel, Microstructure and mechanics of healthy and aneurysmatic abdominal aortas: experimental analysis and modelling, *Journal of The Royal Society Interface* **13**, 2016.

[45] M. K. O'Connell, S. Murthy, S. Phan, C. Xu, J. Buchanan, R. Spilker, R. L. Dalman, C. K. Zarins, W. Denk, and C. A. Taylor, The three-dimensional micro- and nanostructure of the aortic medial lamellar unit measured using 3d confocal and electron microscopy imaging, *Matrix biology: journal of the International Society for Matrix Biology* **27**, 171–181, 2008.

[46] R. Ogden, *Non-linear Elastic Deformations*, Dover Publications, 1997.

[47] R. A. P Scott, P. Tisi, H. A. Ashton, and D. R. Allen, *Abdominal aortic aneurysm rupture rates: A 7-year follow-up of the entire abdominal aortic aneurysm population detected by screening*, Volume 28, 1998.

[48] K. R. Rajagopal and A. S. Wineman, A constitutive equation for nonlinear solids which undergo deformation induced microstructural changes, *International Journal of Plasticity* **8**, 385–395, 1992.

[49] E. K. Rodriguez, A. Hoger, and A. D. McCulloch, Stress-dependent finite growth in soft elastic tissues, *Journal of Biomechanics* **27**, 455–467, 1994.

[50] H. Schmid, L. Pauli, A. Paulus, E. Kuhl, and M. Itskov, Consistent formulation of the growth process at the kinematic and constitutive level for soft tissues composed of multiple constituents, *Computer Methods in Biomechanics and Biomedical Engineering* **15**, 547–561, 2012.

[51] P. Sáez, E. Peña, M. A. Martínez, and E. Kuhl, Computational modeling of hypertensive growth in the human carotid artery, *Computational Mechanics* **53**, 1183–1196, 2014.

[52] C. Truesdell and W. Noll, *The Non-Linear Field Theories of Mechanics*, Springer Berlin Heidelberg, Berlin, Heidelberg, 1965.

[53] A. Valentín, J. D. Humphrey, and G. A. Holzapfel, A finite element-based constrained mixture implementation for arterial growth, remodeling, and adaptation: Theory and numerical verification, *International Journal for Numerical Methods in Biomedical Engineering* **29**, 822–849, 2013.

[54] M. Vasta, A. Gizzi, and A. Pandolfi, On three- and two-dimensional fiber distributed models of biological tissues, *Probabilistic Engineering Mechanics* **37**, 170–179, 2014.

[55] L. Virag, J. S. Wilson, J. D. Humphrey, and I. Karšaj, Potential biomechanical roles of risk factors in the evolution of thrombus-laden abdominal aortic aneurysms, *International Journal for Numerical Methods in Biomedical Engineering* **33**, e2893, 2017.

[56] D. A. Vorp, Biomechanics of abdominal aortic aneurysm, *Journal of Biomechanics* **40**, 1887–1902, 2007.

[57] P. N. Watton, A. Selimovic, N. B. Raberger, P. Huang, G. A. Holzapfel, and Y. Ventikos, Modelling evolution and the evolving mechanical environment of saccular cerebral aneurysms, *Biomechanics and Modeling in Mechanobiology* **10**, 109–132, 2011.

[58] J. Wolff, *Das Gesetz der Transformation der Knochen*, A. Hirschwald, 1892.

[59] World Health Organization. Cardiovascular diseases (cvds). `https://www.who.int/news-room/fact-sheets/detail/cardiovascular-diseases-(cvds)`. Accessed: 2019-01-24.

[60] A. M. Zöllner, M. A. Holland, K. S. Honda, A. K. Gosain, and E. Kuhl, Growth on demand: Reviewing the mechanobiology of stretched skin, *Journal of the Mechanical Behavior of Biomedical Materials* **28**, 495–509, 2013.

A Full Text: Paper A

SPRINGER NATURE LICENSE
TERMS AND CONDITIONS

Mar 06, 2019

This Agreement between Mr. Fabian Braeu ("You") and Springer Nature ("Springer Nature") consists of your license details and the terms and conditions provided by Springer Nature and Copyright Clearance Center.

License Number	4527401298676
License date	Feb 13, 2019
Licensed Content Publisher	Springer Nature
Licensed Content Publication	Biomechanics and Modeling in Mechanobiology
Licensed Content Title	Homogenized constrained mixture models for anisotropic volumetric growth and remodeling
Licensed Content Author	F. A. Braeu, A. Seitz, R. C. Aydin et al
Licensed Content Date	Jan 1, 2016
Licensed Content Volume	16
Licensed Content Issue	3
Type of Use	Thesis/Dissertation
Requestor type	academic/university or research institute
Format	print and electronic
Portion	full article/chapter
Will you be translating?	no
Circulation/distribution	<501
Author of this Springer Nature content	yes
Title	Homogenized constrained mixture models for anisotropic volumetric growth and remodeling
Institution name	Institute for Computational Mechanics, Technical University of Munich, Garching, Germany
Expected presentation date	Apr 2019
Requestor Location	Mr. Fabian Braeu Paracelsusstr. 12a München, 80939 Germany Attn: Mr. Fabian Braeu
Customer VAT ID	DE811193231
Billing Type	Invoice
Billing Address	Mr. Fabian Braeu Paracelsusstr. 12a München, Germany 80939 Attn: Mr. Fabian Braeu
Total	0.00 EUR
Terms and Conditions	

Springer Nature Terms and Conditions for RightsLink Permissions

Springer Nature Customer Service Centre GmbH (the Licensor) hereby grants you a non-exclusive, world-wide licence to reproduce the material and for the purpose and requirements specified in the attached copy of your order form, and for no other use, subject to the conditions below:

1. The Licensor warrants that it has, to the best of its knowledge, the rights to license reuse of this material. However, you should ensure that the material you are requesting is original to the Licensor and does not carry the copyright of another entity (as credited in the published version).

   If the credit line on any part of the material you have requested indicates that it was reprinted or adapted with permission from another source, then you should also seek permission from that source to reuse the material.

2. Where **print only** permission has been granted for a fee, separate permission must be obtained for any additional electronic re-use.

3. Permission granted **free of charge** for material in print is also usually granted for any electronic version of that work, provided that the material is incidental to your work as a whole and that the electronic version is essentially equivalent to, or substitutes for, the print version.

4. A licence for 'post on a website' is valid for 12 months from the licence date. This licence does not cover use of full text articles on websites.

5. Where **'reuse in a dissertation/thesis'** has been selected the following terms apply: Print rights of the final author's accepted manuscript (for clarity, NOT the published version) for up to 100 copies, electronic rights for use only on a personal website or institutional repository as defined by the Sherpa guideline (www.sherpa.ac.uk/romeo/).

6. Permission granted for books and journals is granted for the lifetime of the first edition and does not apply to second and subsequent editions (except where the first edition permission was granted free of charge or for signatories to the STM Permissions Guidelines http://www.stm-assoc.org/copyright-legal-affairs/permissions/permissions-guidelines/), and does not apply for editions in other languages unless additional translation rights have been granted separately in the licence.

7. Rights for additional components such as custom editions and derivatives require additional permission and may be subject to an additional fee. Please apply to Journalpermissions@springernature.com/bookpermissions@springernature.com for these rights.

8. The Licensor's permission must be acknowledged next to the licensed material in print. In electronic form, this acknowledgement must be visible at the same time as the figures/tables/illustrations or abstract, and must be hyperlinked to the journal/book's homepage. Our required acknowledgement format is in the Appendix below.

9. Use of the material for incidental promotional use, minor editing privileges (this does not include cropping, adapting, omitting material or any other changes that affect the meaning, intention or moral rights of the author) and copies for the disabled are permitted under this licence.

10. Minor adaptations of single figures (changes of format, colour and style) do not require the Licensor's approval. However, the adaptation should be credited as shown in Appendix below.

Biomech Model Mechanobiol
DOI 10.1007/s10237-016-0859-1

ORIGINAL PAPER

Homogenized constrained mixture models for anisotropic volumetric growth and remodeling

F. A. Braeu[1] · A. Seitz[1] · R. C. Aydin[1] · C. J. Cyron[1]

Received: 20 September 2016 / Accepted: 18 November 2016
© Springer-Verlag Berlin Heidelberg 2016

Abstract Constrained mixture models for soft tissue growth and remodeling have attracted increasing attention over the last decade. They can capture the effects of the simultaneous presence of multiple constituents that are continuously deposited and degraded at in general different rates, which is important to understand essential features of living soft tissues that cannot be captured by simple kinematic growth models. Recently the novel concept of homogenized constrained mixture models was introduced. It was shown that these models produce results which are very similar (and in certain limit cases even identical) to the ones of constrained mixture models based on multi-network theory. At the same time, the computational cost and complexity of homogenized constrained mixture models are much lower. This paper discusses the theory and implementation of homogenized constrained mixture models for anisotropic volumetric growth and remodeling in three dimensions. Previous constrained mixture models of volumetric growth in three dimensions were limited to the special case of isotropic growth. By numerical examples, comparison with experimental data and a theoretical discussion, we demonstrate that there is some evidence raising doubts whether isotropic growth models are appropriate to represent growth and remodeling of soft tissue in the vasculature. Anisotropic constrained mixture models, as introduced in this paper for the first time, may be required to avoid unphysiological results in simulations of vascular growth and remodeling.

Keywords Growth and remodeling · Volumetric · Mechanobiology · Aneurysm · Computational modeling

1 Introduction

Growth and remodeling of biological soft tissues have attracted increasing interest over the last two decades. For a comprehensive recent review, the reader is referred to (Cyron and Humphrey 2016). Naturally associated with large deformations, they are best addressed within the mathematical framework of nonlinear continuum mechanics. To this end, Rodriguez et al. developed a kinematic growth theory based on a simple multiplicative split of the deformation gradient into an elastic part and an inelastic (growth) part, similar to mathematical models of plasticity or viscoelastic fluids (Rodriguez et al. 1994). Thanks to its conceptual simplicity and computational efficiency, this kinematic growth theory is still widely used (Ambrosi et al. 2011; Menzel and Kuhl 2012) and has been applied to various types of soft tissues and biomaterials (e.g., Göktepe 2010; Zöllner 2012, 2013; Ambrosi and Guana 2007; Grytz 2012; Albero et al. 2014; Ben Amar and Goriely 2005; Goriely and Vandiver 2010; Böl and Bolea Albero 2014; Taber and Eggers 1996; Ambrosi and Mollica 2004; Vandiver and Goriely 2009). It suffers, however, from a couple of severe limitations. In particular, it neglects the simultaneous production and degradation processes of multiple constituents (such as elastin and collagen) that is characteristic of living tissues. These processes are key to understand and capture phenomena such as the change of the opening angle of arteries after application of proteases (Cyron et al. 2016a) or in hypertension (Matsumoto and Hayashi 1996). To incorporate these processes, so-called constrained mixture models

✉ C. J. Cyron
cyron@lnm.mw.tum.de

[1] Institute for Computational Mechanics, Technical University of Munich, Boltzmannstrasse 15, 85748 Garching, Germany

Published online: 05 December 2016

were developed (Humphrey and Rajagopal 2002), motivated by the idea of multi-network theory (Rajagopal and Wineman 1992). These models have now been established as a second major approach to growth and remodeling in soft tissues (Figueroa 2009; Baek et al. 2006; Valentin 2009; Wilson et al. 2013; Zeinali-Davarani et al. 2011; Kroon and Holzapfel 2008, 2007). They describe growth and remodeling as a superposition of continuous degradation and deposition processes of differential mass increments of multiple constituents in each differential volume element. To avoid the high complexity and computational cost of these models, Watton et al. developed, motivated by Humphrey (1999), an alternative constrained mixture model that is not based on multi-network theory but only tracks for each constituent a so-called recruitment stretch that accounts for deposition and degradation of mass increments in a lumped manner (e.g., Eriksson 2014; Watton et al. 2004, 2011).

With simple kinematic growth models, both isotropic and anisotropic volumetric growth can be modeled straightforwardly. For constrained mixture models, the implementation of volumetric growth is more challenging. Such models have therefore most often been combined with mechanical membrane models, where growth was simply described as a change of the thickness parameter of the membrane (Figueroa 2009; Baek et al. 2006; Wilson et al. 2013; Watton et al. 2004, 2011; Wilson et al. 2012; Zeinali-Davarani and Baek 2012; Watton and Hill 2009). After some extensions to thick-walled axisymmetric blood vessels (Virag 2015; Karšaj et al. 2010), only recently constrained mixture models for volumetric growth in general geometries were proposed (Eriksson 2014; Grytsan et al. 2015; Valentín et al. 2013). They were, however, limited to isotropic volumetric growth.

Recently the so-called homogenized constrained mixture models were introduced (Cyron et al. 2016b). They are essentially based on the same micromechanical model of growth and remodeling as classical constrained mixture models based on multi-network theory. However, using a form of temporal homogenization across differential mass increments deposited at different times, they can capture the effects of growth and remodeling by a split into an elastic and inelastic deformation gradient of each constituent comparable to the one used in kinematic growth models. This way, homogenized constrained mixture models combine the realistic micromechanical foundation of classical constrained mixture models based on multi-network theory with the conceptual simplicity and low computational cost of kinematic growth models. Moreover, they enable a straightforward incorporation of both isotropic and anisotropic volumetric growth. By Cyron et al. (2016b) mainly the mathematical and mechanical foundations of homogenized constrained mixture models were introduced, illustrated only by the simple example of growth in a two-dimensional curved membrane continuum.

In this paper, we discuss in detail how homogenized constrained mixture models can be applied to study anisotropic volumetric growth in three dimensions. We demonstrate general good agreement but also some quantitative differences between the results of three-dimensional solid models compared to equivalent two-dimensional membrane models. This supports on the one hand the appropriateness of previous membrane models for general academic studies but also indicates that three-dimensional models may be an indispensable tool to ensure the model accuracy that may be required in future clinical applications. Moreover, we present some evidence raising doubts whether isotropic volumetric growth models are appropriate to study vascular growth and remodeling in three dimensions. Isotropic models apparently exhibit some difficulties in reproducing the growth response of arteries to hypertension, and they also appear to suffer from an inherent susceptibility to mechanobiological instability.

In this paper, first- and second-order tensors are printed in boldface and double contraction products of two tensors are denoted by a colon and time derivatives by an overdot. For constrained mixtures composed of n constituents (i.e., material types like collagen or elastin), a superscript $i = 1, \ldots, n$ denotes a mechanical quantity of the ith constituent. Determinants of second-order tensors are denoted by $|.|$, traces by $\mathrm{tr}\,(.)$. For tensor products, the symbol $\otimes$ is used.

2 Kinematics and balance equations

Let $B_0 \subset \mathbb{R}^3$ be a reference configuration of a continuous body mapped at time $t \geq 0$ to a current configuration $B(t)$. Each material point $\boldsymbol{X} \in B_0$ is mapped to its current position $\boldsymbol{x}(t, \boldsymbol{X}) \in B(t)$ by

$$\boldsymbol{x} : \mathbb{R}_0^+ \times B_0 \to \mathbb{R}^3, \qquad (t, \boldsymbol{X}) \mapsto \boldsymbol{x}(t, \boldsymbol{X}), \tag{1}$$

with deformation gradient

$$\boldsymbol{F} = \frac{\partial \boldsymbol{x}}{\partial \boldsymbol{X}}. \tag{2}$$

Without loss of generality, we assume herein the initial condition $B(0) = B_0$. Note that B_0 can be an arbitrary configuration and need not satisfy any specific mechanical conditions. In practice, B_0 will be most often the in vivo configuration of a biological tissue before some specific event starts a certain growth and remodeling process of interest. For example, it can be the healthy configuration of a blood vessel right before the vessel suffers some mechanical or biochemical damage that initiates the growth of an aneurysm. Reference volume elements dV in B_0 are mapped to volume

elements $dv = JdV$ in the current configuration $B(t)$ with the Jacobian determinant $J = |\boldsymbol{F}| > 0$. Each volume element consists of a constrained mixture of n different constituents (e.g., collagen, elastin, or smooth muscle) that are supposed to undergo the same deformation over time. That is, the total deformation gradient $\boldsymbol{F}$ in (2) is the same for all constituents. The local stress-free state may, however, differ between the constituents and in fact in general even between the differential mass increments of these constituents deposited at different times τ. That is, for each differential mass increment of the ith constituent deposited at time τ we split the deformation gradient into an individual elastic part $\boldsymbol{F}_{\mathrm{e}}^{i(\tau)}$ and inelastic part $\boldsymbol{F}_{\mathrm{gr}}^{i(\tau)}$ so that

$$\boldsymbol{F} = \boldsymbol{F}_{\mathrm{e}}^{i(\tau)} \boldsymbol{F}_{\mathrm{gr}}^{i(\tau)}. \tag{3}$$

Here $\boldsymbol{F}_{\mathrm{gr}}^{i(\tau)}$ captures the differences between the local stress-free configurations of different mass increments due to deposition at a different time and in a different configuration as well as continuous growth and remodeling. Growth and remodeling happen on slow time scales (at least hours, typically days to months) and can thus be modeled as a quasi-static process so that dynamic effects like inertia or viscoelasticity can usually be neglected and the balance of linear momentum becomes in the interior of the body

$$\operatorname{div}(\boldsymbol{P}) + \varrho_0 \boldsymbol{b}_0 = \boldsymbol{0}, \tag{4}$$

with body force vector $\boldsymbol{b}_0$ (per unit mass) and the first Piola–Kirchhoff stress $\boldsymbol{P}$. The total mass density (per unit reference volume)

$$\varrho_0 = \sum_{i=1}^{n} \varrho_0^i \tag{5}$$

is the sum of the mass densities ϱ_0^i of the individual constituents. Following Eqs. (2.51) and (4.6) from Holzapfel (2000), the mass density ϱ in the current spatial configuration is computed from the mass density in the reference configuration by

$$\varrho = \varrho_0 / |\boldsymbol{F}|. \tag{6}$$

Note that Equation (4.6) in Holzapfel (2000) was derived under the assumption of conservation of mass but that it holds true also generally if the amount of mass in reference volume elements changes over time so that it can be used herein.

The first Piola–Kirchhoff stress $\boldsymbol{P} = \partial \Psi / \partial \boldsymbol{F}$ can be computed from the total strain energy function (per unit reference volume)

$$\Psi = \sum_{i=1}^{n} \Psi^i = \sum_{i=1}^{n} \varrho_0^i W^i \tag{7}$$

where Ψ^i and W^i are the strain energies per unit reference volume and mass of each constituent, respectively. W^i depends in general only on the elastic deformation of each mass increment, that is, on the elastic right Cauchy–Green tensor

$$\boldsymbol{C}_{\mathrm{e}}^{i(\tau)} = \left(\boldsymbol{F}_{\mathrm{e}}^{i(\tau)}\right)^{\mathrm{T}} \boldsymbol{F}_{\mathrm{e}}^{i(\tau)} \tag{8}$$

or, equivalently, on its invariants. For isotropic materials, there exist only three invariants, and for anisotropic materials, additional pseudo-invariants have to be considered (cf. section 6 in Holzapfel 2000). Below, we will use not only the first Piola–Kirchhoff stress $\boldsymbol{P}$ but also the second Piola–Kirchhoff stress

$$\boldsymbol{S} = \frac{\partial \Psi}{\partial \boldsymbol{E}} = \sum_{i=1}^{n} \varrho_0^i \frac{\partial W^i}{\partial \boldsymbol{E}} = \sum_{i=1}^{n} \varphi^i \boldsymbol{S}^i \tag{9}$$

where $\boldsymbol{E} = \left(\boldsymbol{F}^{\mathrm{T}}\boldsymbol{F} - \boldsymbol{I}\right)/2$ is the Green–Lagrange strain tensor, $\boldsymbol{I}$ is the identity tensor, and

$$\boldsymbol{S}^i = \frac{\varrho_0^i}{\varphi^i} \frac{\partial W^i}{\partial \boldsymbol{E}} \tag{10}$$

is the second Piola–Kirchhoff stress of the ith constituent and φ^i its volume fraction in the current configuration. The push-forward of $\boldsymbol{S}^i$ renders

$$\boldsymbol{\sigma}^i = \frac{1}{|\boldsymbol{F}|} \boldsymbol{F} \boldsymbol{S}^i \boldsymbol{F}^{\mathrm{T}}. \tag{11}$$

which can be interpreted as the Cauchy stress in the fictitious case that the volume fraction φ^i of the ith constituent equals one.

In a given configuration $B(t)$, the balance of linear momentum (4) can be evaluated at any point in time using (5)–(8) if the W^i, ϱ_0^i, and $\boldsymbol{F}_{\mathrm{gr}}^{i(\tau)}$ are known or if at least some additional equations are given to compute them at any time. The above equations represent a common basis of all constrained mixture models for growth and remodeling proposed so far. The difference between these models is mainly the way how the ϱ_0^i and $\boldsymbol{F}_{\mathrm{gr}}^{i(\tau)}$ are computed, respectively. In the following section, we will point out in detail how these quantities can be computed in homogenized constrained mixture models for anisotropic volumetric growth and remodeling.

3 Homogenized constrained mixture models

3.1 General

In constrained mixture models, growth and remodeling are conceptualized as a simultaneous continuous degradation

and deposition of n different constituents, which is also referred to as mass turnover. New mass is assumed to be deposited into the extant matrix with a certain prestress $\boldsymbol{\sigma}^i_{\text{pre}}$ at a rate $\dot{\varrho}^i_{0+} \geq 0$. At the same time, extant mass is continuously degraded at a rate $\dot{\varrho}^i_{0-} \geq 0$ so that the net rate of mass production is

$$\dot{\varrho}^i_0 = \dot{\varrho}^i_{0+} - \dot{\varrho}^i_{0-}. \tag{12}$$

Given that in general the prestress $\boldsymbol{\sigma}^i_{\text{pre}}$ with which new mass is deposited is unequal to the current stress $\boldsymbol{\sigma}^i$ of the extant mass that is being degraded, mass turnover changes in general the current average stress and thus also traction-free state of a constituent even when mass deposition and degradation balance (i.e., $\dot{\varrho}^i_0 = 0$). This change of the traction-free state in the absence of any change of local mass density or volume is necessarily associated with some change of the microstructure of the tissue that is referred to herein as remodeling. The local traction-free configuration of a constituent will in general not only change by this kind of turnover-based remodeling but also by growth, that is, a change of mass. If $\dot{\varrho}^i_{0+}$ and $\dot{\varrho}^i_{0-}$ do not balance in (12) so that $\dot{\varrho}^i_0 \neq 0$ the resulting change of mass is in general associated with a local change of the volume required to accommodate the mass in a certain region of the body. This growth-related local change of volume can be, similarly as the above-described remodeling, expressed as inelastic change of the local traction-free configuration of a certain constituent.

To account for changes of the traction-free state resulting from growth and remodeling, classical constrained mixture models keep track of all mass increments deposited at different times τ. For each constituent, the strain energy Ψ^i is computed on the basis of a history integral incorporating each of these mass increments and its individual stress-free configuration. Computing this history integral is involved and time consuming. Therefore, Cyron et al. (2016b) introduced a homogenization across the different mass increments deposited at different times. This homogenization is based on the idea that the gross effect of growth and remodeling can be captured by some average inelastic deformation gradient $\boldsymbol{F}^i_{\text{gr}}$ for all mass increments of the ith constituent. That is, $\boldsymbol{F}^{i(\tau)}_{\text{gr}} = \boldsymbol{F}^i_{\text{gr}}$ for all τ in (3) and we can rewrite (3) as

$$\boldsymbol{F} = \boldsymbol{F}^i_{\text{e}} \boldsymbol{F}^i_{\text{gr}} \tag{13}$$

where $\boldsymbol{F}^i_{\text{gr}}$ can be decomposed multiplicatively as

$$\boldsymbol{F}^i_{\text{gr}} = \boldsymbol{F}^i_{\text{r}} \boldsymbol{F}^i_{\text{g}}. \tag{14}$$

Here the remodeling part $\boldsymbol{F}^i_{\text{r}}$ captures changes in the microstructure by mass turnover. The growth part $\boldsymbol{F}^i_{\text{g}}$ is directly related to a change of the mass per unit reference volume ϱ^i_0. Then, to close the system of equations (1)–(8) and enable a computation of the mechanical equilibrium configuration of the body at each time, one needs, in addition to proper initial and boundary conditions, two kinds of constitutive equations. First, one needs mechanical constitutive equations defining the strain energies W^i of the constituents. Numerous such constitutive equations have been developed over the last two decades for soft tissues. All these equations could be used in the framework developed herein. For simplicity, we will rely in this paper largely on the ideas introduced by Holzapfel et al. (2000) and discuss their application briefly in Sect. 3.3 below. Second, one needs mechanobiological constitutive equations defining the evolution of the inelastic deformation gradients $\boldsymbol{F}^i_{\text{r}}$ and $\boldsymbol{F}^i_{\text{g}}$ as well as of the mass densities ϱ^i_0 depending on mechanical stimuli such as stress or strain. These mechanobiological evolution equations will be discussed in the following Sect. 3.2.

3.2 Mechanobiological constitutive equations

3.2.1 Mass production

The most important mechanobiological constitutive equations are the ones defining the net mass production rates of each constituent in the current mechanical state. Following Cyron et al. (2016b) (and thereby the assumptions previously made, for example, also by Figueroa 2009; Wilson et al. 2013, 2012; Cyron et al. 2014), we assume that the net mass production (i.e., the difference between mass production and mass degradation) is governed by the difference between the co-rotated Cauchy stress tensor $\boldsymbol{\sigma}^i_R = \boldsymbol{R}^{\text{T}} \boldsymbol{\sigma}^i \boldsymbol{R}$ and some (typically constant) homeostatic stress $\boldsymbol{\sigma}_{\text{h}}$. Here $\boldsymbol{R}$ is the orthonormal rotation tensor in the polar decomposition of the deformation gradient $\boldsymbol{F} = \boldsymbol{R}\boldsymbol{U}$ with $\boldsymbol{U}$ the material stretch tensor. Then the net mass production can be written as

$$\dot{\varrho}^i_0(t) = \varrho^i_0(t)\, \boldsymbol{K}^i_\sigma : \left(\boldsymbol{\sigma}^i_R - \boldsymbol{\sigma}^i_{\text{h}}\right) + \dot{D}^i(t) \tag{15}$$

with some (typically constant) gain-type second-order tensor $\boldsymbol{K}^i_\sigma$. Here the first summand on the right-hand side is the mechano-regulated net mass production rate (depending on the current stress). The second summand $\dot{D}^i(t)$ is a generic rate function that can be used to describe additional deposition or also damage processes that affect the net mass production but are not driven by Cauchy stress but other factors (such as mechanical fatigue and chemical degradation processes). For the theory developed herein also any other constitutive equation defining $\dot{\varrho}^i_0$ could be chosen.

Collagen and smooth muscle, the major constituents subject to growth and remodeling in load-bearing soft tissues such as arteries, are often modeled using quasi-

one-dimensional fiber families. Then, in both the co-rotated Cauchy stress tensor $\boldsymbol{\sigma}^i_R$ and the homeostatic stress tensor $\boldsymbol{\sigma}^i_{\mathrm{h}}$ only the components in reference fiber direction $\boldsymbol{a}^i_0$ are unequal to zero and denoted by $\sigma^i = \left(\boldsymbol{a}^i_0 \otimes \boldsymbol{a}^i_0\right) : \boldsymbol{\sigma}^i_R$ and $\sigma^i_{\mathrm{h}} = \left(\boldsymbol{a}^i_0 \otimes \boldsymbol{a}^i_0\right) : \boldsymbol{\sigma}^i_{\mathrm{h}}$, respectively, and one can rewrite (15) as

$$\dot{\varrho}^i_0(t) = \varrho^i_0(t)\, k^i_\sigma \frac{\sigma^i - \sigma^i_{\mathrm{h}}}{\sigma^i_{\mathrm{h}}} + \dot{D}^i(t) \tag{16}$$

with $k^i_\sigma = \sigma^i_{\mathrm{h}} \boldsymbol{K}^i_\sigma : \left(\boldsymbol{a}^i_0 \otimes \boldsymbol{a}^i_0\right)$.

3.2.2 Remodeling

For a known net mass production rate $\dot{\varrho}^i_0$ and a deposition prestress $\boldsymbol{\sigma}^i_{\mathrm{pre}}$, it was demonstrated in Cyron et al. (2016b) that the evolution of the inelastic remodeling deformation gradient $\boldsymbol{F}^i_{\mathrm{r}}$ is given by (cf. Eq. (17) and Eq. (31) in Cyron et al. (2016b) and note the symmetry of $\partial \boldsymbol{S}^i / \partial \boldsymbol{C}^i_{\mathrm{e}}$)

$$\left[\frac{\dot{\varrho}^i_0(t)}{\varrho^i_0(t)} + \frac{1}{T^i}\right]\left[\boldsymbol{S}^i - \boldsymbol{S}^i_{\mathrm{pre}}\right] = \left[2\frac{\partial \boldsymbol{S}^i}{\partial \boldsymbol{C}^i_{\mathrm{e}}} : \left(\boldsymbol{C}^i_{\mathrm{e}} \boldsymbol{L}^i_{\mathrm{r}}\right)\right]_{\boldsymbol{F}, \boldsymbol{F}^i_{\mathrm{g}} = const}. \tag{17}$$

Here $\boldsymbol{L}^i_{\mathrm{r}} = \dot{\boldsymbol{F}}^i_{\mathrm{r}} (\boldsymbol{F}^i_{\mathrm{r}})^{-1}$ is the remodeling velocity gradient, $\boldsymbol{S}^i = |\boldsymbol{F}|\, \boldsymbol{F}^{-1} \boldsymbol{\sigma}^i \boldsymbol{F}^{-\mathrm{T}}$ and $\boldsymbol{S}^i_{\mathrm{pre}} = |\boldsymbol{F}|\, \boldsymbol{F}^{-1} \boldsymbol{\sigma}^i_{\mathrm{pre}} \boldsymbol{F}^{-\mathrm{T}}$ are the second Piola–Kirchhoff stress and deposition prestress, and T^i is the average turnover time, that is, the period within which a mass increment is degraded and replaced by a new mass increment. This time is related to the half-life time measured experimentally, for example, by radioactive labeling by Nissen et al. (1978) and Etminan (2014), by the factor $ln\,(2)$. Modeling mass turnover as a continuous replacement of fibers by new fibers in the same material direction, the rotational part of $\boldsymbol{F}^i_{\mathrm{r}}$ is zero and $\boldsymbol{F}^i_{\mathrm{r}}$ thus symmetric so that (17) provides in d dimensions a system of $d\,(d+1)\,/2$ independent equations for computing the same number of unknown components of $\dot{\boldsymbol{F}}^i_{\mathrm{r}}$ in any given mechanical state. $\boldsymbol{S}^i_{\mathrm{pre}}(t)$ is the elastic stress of new mass that is produced at time t at a rate $\dot{\varrho}^i_{0+}$. At the same time, extant mass with stress $\boldsymbol{S}^i$ is degraded at a rate $\dot{\varrho}^i_{0-}$. Note that in our model we do not consider single mass increments produced and degraded but only keep track of the net change of the elastic stress in each constituent that results from such a combined production and degradation process. This net change of elastic stress can be expressed in terms of an inelastic remodeling rate $\dot{\boldsymbol{F}}^i_{\mathrm{r}}$ that is computed by (17). As shown in Proposition 1 of Cyron and Humphrey (2014), the prestress $\boldsymbol{\sigma}^i_{\mathrm{pre}}$ has to correspond to the homeostatic stress introduced in Sect. 3.2.1, that is, $\boldsymbol{\sigma}^i_{\mathrm{pre}} = \boldsymbol{R} \boldsymbol{\sigma}^i_{\mathrm{h}} \boldsymbol{R}^{\mathrm{T}}$.

3.2.3 Growth

An increase or decrease in mass of a differential material element in the body is in general associated with an increase or decrease of its volume, noting that the space a material element occupies depends (for a given density) on its mass. This change of volume can be captured by an inelastic growth deformation gradient $\boldsymbol{F}^i_{\mathrm{g}}$ describing the change of size and shape of the differential volume element by deposition or degradation of mass. The local inelastic deformation gradient resulting from a certain change of mass depends in general on the micromechanical and geometric characteristics of the underlying growth process. The development of appropriate constitutive equations defining the evolution of $\boldsymbol{F}^i_{\mathrm{g}}$ in time is thus non-trivial and a comprehensive discussion of the relation between the growth process on the micro-scale and the resulting $\boldsymbol{F}^i_{\mathrm{g}}$ on the continuum-scale would go beyond the scope of this paper. Instead, we focus on a particularly simple model. We assume that deposition or degradation of mass of any constituent can be imagined as a process that changes (per unit time) the shape of volume elements in which it happens by an inelastic deformation gradient rate $\dot{\boldsymbol{G}}^i$. This change of shape is assumed herein to occur by way of an inelastic reorganization of the whole volume element that affects all constituents equally. Therefore, all constituents are experiencing the same inelastic growth deformation gradient $\boldsymbol{F}_{\mathrm{g}} = \boldsymbol{F}^i_{\mathrm{g}}$. Its rate equals the sum of the growth-related deformation gradient rates $\dot{\boldsymbol{G}}^i$ contributed by the individual constituents:

$$\dot{\boldsymbol{F}}_{\mathrm{g}} = \dot{\boldsymbol{F}}^i_{\mathrm{g}} = \sum_{i=1}^{n} \dot{\boldsymbol{G}}^i. \tag{18}$$

For living soft tissue, it is often assumed that growth occurs as a change of volume while the spatial density ϱ remains constant in time. Moreover, due to its high volume fraction of water, living soft tissue is typically modeled as an incompressible material, that is, its elastic deformation is supposed to be isochoric. This paper mainly focuses on the discussion of a theoretical framework rather than physiological details. Therefore, although more complex models could be thought of and might describe more realistically the relation between fluid and solid constituents in soft tissue, we assume herein for simplicity that also the elastic deformation of each individual constituent is isochoric, that is, $\left|\boldsymbol{F}^i_{\mathrm{e}}\right| = 1$. Isochoric elastic deformation implies via (17) automatically also an isochoric remodeling deformation gradient, that is, $\left|\boldsymbol{F}^i_{\mathrm{r}}\right| = 1$. Then, with (13) and (14)

$$|\boldsymbol{F}| = \left|\boldsymbol{F}^i_{\mathrm{e}}\right| \left|\boldsymbol{F}^i_{\mathrm{r}}\right| \left|\boldsymbol{F}^i_{\mathrm{g}}\right| = \left|\boldsymbol{F}^i_{\mathrm{g}}\right|. \tag{19}$$

From (6), (19), and $|\boldsymbol{F}(0)| = 1$, we conclude

$$\left|\boldsymbol{F}_{\mathrm{g}}(t)\right| = \frac{\varrho_0(t)}{\varrho_0(0)} \tag{20}$$

and thus

$$\frac{\dot{\varrho}_0(t)}{\varrho_0(0)} = \frac{d\left|\boldsymbol{F}_{\mathrm{g}}(t)\right|}{dt} = \frac{\partial\left|\boldsymbol{F}_{\mathrm{g}}\right|}{\partial \boldsymbol{F}_{\mathrm{g}}} : \dot{\boldsymbol{F}}_{\mathrm{g}} = \frac{\partial\left|\boldsymbol{F}_{\mathrm{g}}\right|}{\partial \boldsymbol{F}_{\mathrm{g}}} : \left(\sum_{i=1}^{n} \dot{\boldsymbol{G}}^i\right). \tag{21}$$

This equation has to hold for any net mass production rate of any constituent and thus also for the special case that only the net mass production of a single constituent whose index is without loss of generality i is not equal to zero. Then with (5), $\dot{\varrho}_0(t) = \dot{\varrho}_0^i(t)$ and all summands on the right-hand side of (21) except for the ith one are equal to zero so that (with Eq. (1.241) in Holzapfel 2000)

$$\frac{\dot{\varrho}_0^i(t)}{\varrho_0(0)} = \left|\boldsymbol{F}_{\mathrm{g}}^i\right| \left(\boldsymbol{F}_{\mathrm{g}}^i\right)^{-\mathrm{T}} : \dot{\boldsymbol{G}}^i. \tag{22}$$

The rate $\dot{\boldsymbol{G}}^i$ can in general be written as

$$\dot{\boldsymbol{G}}^i = \beta^i \boldsymbol{B}^i \tag{23}$$

where the second-order tensor $\boldsymbol{B}^i$ defines the growth direction and is normalized without loss of generality such that $\mathrm{tr}\left(\boldsymbol{B}^i\right) = 1$. From (22) and (23), we conclude

$$\beta^i = \frac{\dot{\varrho}_0^i(t)}{\varrho_0(0)\left|\boldsymbol{F}_{\mathrm{g}}^i\right|\left[\left(\boldsymbol{F}_{\mathrm{g}}^i\right)^{-\mathrm{T}} : \boldsymbol{B}^i\right]} \tag{24}$$

and thus, with (23) and (20)

$$\begin{aligned}\dot{\boldsymbol{G}}^i &= \frac{\dot{\varrho}_0^i(t)}{\varrho_0(0)\left|\boldsymbol{F}_{\mathrm{g}}^i\right|\left[\left(\boldsymbol{F}_{\mathrm{g}}^i\right)^{-\mathrm{T}} : \boldsymbol{B}^i\right]}\boldsymbol{B}^i \\ &= \frac{\dot{\varrho}_0^i(t)}{\varrho_0(t)\left[\left(\boldsymbol{F}_{\mathrm{g}}^i\right)^{-\mathrm{T}} : \boldsymbol{B}^i\right]}\boldsymbol{B}^i.\end{aligned} \tag{25}$$

Note that (18) and (25) uniquely determine the evolution of the growth deformation gradient $\boldsymbol{F}_{\mathrm{g}}^i$ for given mass density $\varrho_0(t)$, mass production rates $\dot{\varrho}_0^i(t)$, and growth directions $\boldsymbol{B}^i$. The mass production rates (and thus also current mass) are determined by (15). Thus, only the growth direction $\boldsymbol{B}^i$ has to be defined in addition to (15) or (16). Like (17) with regard to remodeling, (18) and (25) account for the effect of growth in a homogenized sense. That is, they do not consider separately the individual effects of all the mass increments deposited at different times in the tissue but only their gross effect by way of the total increase of mass.

3.3 Mechanical constitutive equations

Numerous mechanical constitutive equations for soft biological tissue have been published over the last decades. The homogenized constrained mixture model developed herein can be combined with arbitrary strain energy functions for the different constituents of the constrained mixture. Nevertheless, we will specify in this section a set of such functions that has been turned out particularly suitable for vascular biomechanics in the past (Wilson et al. 2013; Zeinali-Davarani et al. 2011; Wilson et al. 2012; Cyron et al. 2014) and which is therefore also used in the examples in Sect. 4. The arterial wall is modeled as a constrained mixture of elastin, (circumferential) smooth muscle and four families of collagen fibers oriented in circumferential, axial, and diagonal ($+/-45°$) direction (cf. Fig. 1). If in the following a certain parameter

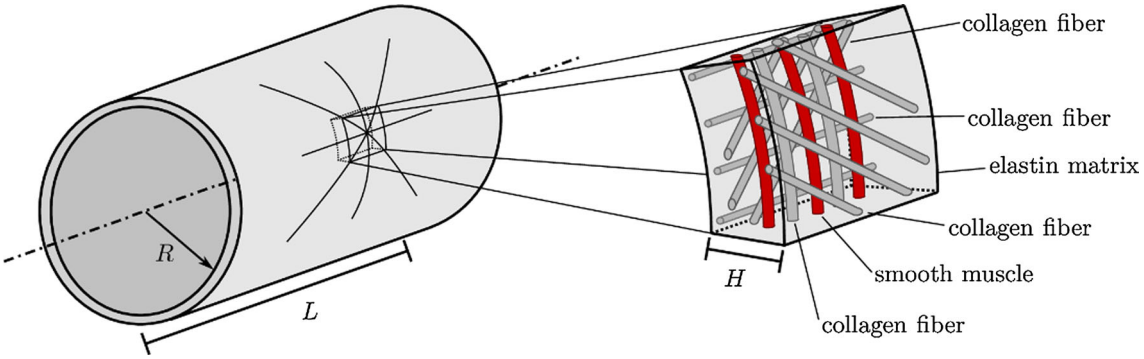

Fig. 1 Cylindrical model aorta of radius R, length L, and wall thickness H whose wall is composed by four families of collagen fibers (axially, circumferentially, and diagonally aligned), circumferential smooth muscle and an elastin matrix (image provided by Sebastian Fuchs under Creative Commons license) (Creative Commons License 2016)

or quantity relates specifically to elastin, collagen, or smooth muscle, we will use the superscript el, co, or sm, respectively. In this section, we omit superscripts in $\boldsymbol{F}_{\mathrm{gr}}$ and $\boldsymbol{F}_{\mathrm{e}}$, given that in each equation it is evident to which constituent in the constrained mixture they refer.

Collagen and the passive elasticity of smooth muscle are represented by quasi-one-dimensional fiber families, respectively. Assume these are aligned with the unit direction vector $\boldsymbol{a}_0$ in reference configuration and the unit direction vector $\boldsymbol{a}_{\mathrm{gr}} = \boldsymbol{F}_{\mathrm{gr}}\boldsymbol{a}_0/\|\boldsymbol{F}_{\mathrm{gr}}\boldsymbol{a}_0\|$ in the inelastically deformed intermediate configuration, where $\boldsymbol{F}_{\mathrm{gr}}$ is the inelastic deformation gradient of the respective fiber family. Then we introduce the pseudo-invariant

$$I_a = \boldsymbol{C}_{\mathrm{e}} : (\boldsymbol{a}_{\mathrm{gr}} \otimes \boldsymbol{a}_{\mathrm{gr}}) = \lambda_{\mathrm{e}}^2 \tag{26}$$

where $\boldsymbol{C}_{\mathrm{e}}$ is the elastic Cauchy–Green deformation tensor and λ_{e} the elastic stretch in fiber direction of the respective constituent. The strain energy of a collagen fiber family is then a Fung-type exponential function

$$W^{\mathrm{co}} = \frac{k_1^{\mathrm{co}}}{2k_2^{\mathrm{co}}}\left(e^{k_2^{\mathrm{co}}(I_a-1)^2} - 1\right) \tag{27}$$

with material parameters k_1^{co} and k_2^{co}. For smooth muscle, we use the strain energy function

$$W^{\mathrm{sm}} = W^{\mathrm{sm}}_{\mathrm{pas}} + W^{\mathrm{sm}}_{\mathrm{act}} \tag{28}$$

with a passive Fung-type part

$$W^{\mathrm{sm}}_{\mathrm{pas}} = \frac{k_1^{\mathrm{sm}}}{2k_2^{\mathrm{sm}}}\left(e^{k_2^{\mathrm{sm}}(I_a-1)^2} - 1\right) \tag{29}$$

with material parameters k_1^{sm} and k_2^{sm}. Given the general importance of active smooth muscle tone (Murtada et al. 2012; Murtada and Holzapfel 2014; Murtada et al. 2010a, b, 2015) in the vasculature, we also incorporate a simple model of active smooth muscle tension based on the strain energy function

$$W^{\mathrm{sm}}_{\mathrm{act}} = \frac{\sigma_{\mathrm{actmax}}}{\varrho_0\,(0)}\left(\lambda_{\mathrm{act}} + \frac{1}{3}\frac{(\lambda_m - \lambda_{\mathrm{act}})^3}{(\lambda_m - \lambda_0)^2}\right) \tag{30}$$

with λ_{act} the active stretch in fiber direction, σ_{actmax} the maximal active Cauchy stress, and λ_m and λ_0 the active stretches at maximum and zero active stress. Consistent with other studies (Wilson et al. 2013), one assumes that $\lambda_{\mathrm{act}} = \lambda/\hat{\lambda}_{\mathrm{act}}$ where $\hat{\lambda}_{\mathrm{act}}$ equals, due to fast muscle remodeling, at every point in time the total stretch in muscle direction in mechanical equilibrium so that in any equilibrium configuration with total stretch λ in fiber direction (compared to the reference configuration) we have $\lambda_{\mathrm{act}} = 1$ but yet $\partial\lambda_{\mathrm{act}}/\partial\lambda = 1/\hat{\lambda}_{\mathrm{act}} = 1/\lambda$, which is important to compute the stress resulting from (30).

As pointed out already in Sect. 3.2.3, we assume herein that each individual constituent is incompressible under elastic deformation, that is, $|\boldsymbol{F}_{\mathrm{e}}| = 1$. For constituents represented by uniaxial fiber families, (26)–(30) define via the equilibrium of linear momentum only the elastic stretch λ_{e} in fiber direction. Incompressibility is then enforced by the simple kinematic assumption that the elastic stretch of the fiber material perpendicular to the fiber axis equals $1/\sqrt{\lambda_{\mathrm{e}}}$ so that the elastic deformation gradient of a fiber material becomes

$$\boldsymbol{F}_{\mathrm{e}} = \lambda_{\mathrm{e}}\boldsymbol{a}_{\mathrm{gr}} \otimes \boldsymbol{a}_{\mathrm{gr}} + \frac{1}{\sqrt{\lambda_{\mathrm{e}}}}\left(\boldsymbol{I} - \boldsymbol{a}_{\mathrm{gr}} \otimes \boldsymbol{a}_{\mathrm{gr}}\right) \tag{31}$$

with identity tensor $\boldsymbol{I}$.

In two-dimensional membrane models of arteries (e.g., Wilson et al. 2013; Zeinali-Davarani et al. 2011; Wilson et al. 2012; Cyron et al. 2014), elastin is often represented by an isotropic two-dimensional neo-Hookean strain energy function

$$W^{\mathrm{el}}_{\mathrm{2D}} = \frac{\mu^{\mathrm{el}}_{\mathrm{2D}}}{2}\left[\boldsymbol{C}_{\mathrm{e}} : \boldsymbol{A}^{\parallel}_{\mathrm{gr}} + \frac{1}{\left|\boldsymbol{A}^{\parallel}_{\mathrm{gr}}\boldsymbol{C}_{\mathrm{e}}\boldsymbol{A}^{\parallel}_{\mathrm{gr}} + \boldsymbol{A}^{\perp}_{\mathrm{gr}}\right|} - 3\right] \tag{32}$$

where $\boldsymbol{C}_{\mathrm{e}}$ is the elastic Cauchy–Green deformation tensor of elastin, $\boldsymbol{a}^{\perp}_{\mathrm{gr}}$ defines a unit vector in wall thickness direction in the inelastically deformed intermediate configuration of elastin, $\boldsymbol{A}^{\perp}_{\mathrm{gr}} = \boldsymbol{a}^{\perp}_{\mathrm{gr}} \otimes \boldsymbol{a}^{\perp}_{\mathrm{gr}}$ is the structural tensor in wall thickness direction, and $\boldsymbol{A}^{\parallel}_{\mathrm{gr}} = \boldsymbol{I} - \boldsymbol{a}^{\perp}_{\mathrm{gr}} \otimes \boldsymbol{a}^{\perp}_{\mathrm{gr}}$ a structural tensor for the tangential plane to the vessel wall. Note that $\boldsymbol{a}^{\perp}_{\mathrm{gr}} = \boldsymbol{F}_{\mathrm{gr}}\boldsymbol{a}^{\perp}_0/\|\boldsymbol{F}_{\mathrm{gr}}\boldsymbol{a}^{\perp}_0\|$ with the unit vector $\boldsymbol{a}^{\perp}_0$ in wall thickness direction in the reference configuration and the inelastic deformation gradient $\boldsymbol{F}_{\mathrm{gr}}$ (capturing growth and remodeling) of elastin. Note that (32) is identical to, for example, Equation (2.6) in Wilson et al. (2013), that is, it exactly represents the strain energy that is typically used in two-dimensional membrane models for elastin, using only a notation that is generall enough to deal with arbitrary three-dimensional geometries. In this paper, we do not primarily focus on constitutive modeling of the arterial wall. Rather we aim at establishing a new mathematical framework for growth and remodeling in three dimensions. To test this framework, it is instructive to compare the results of our three-dimensional simulations with previously reported results from two-dimensional membrane models. Therefore, we herein do not fully exploit the freedom our three-dimensional model is granting to develop a detailed constitutive model that accounts for the inhomogeneity of the arterial wall in thickness direction. Instead we rather use a constitutive model as similar as possible to the ones used in previous two-dimensional models.

The above constitutive equations (26)–(32) are identical to the constitutive framework used previously in two dimensions (e.g., Wilson et al. 2013, 2012; Cyron et al. 2016b, 2014). The only modification we add to this framework in this paper is an additional strain energy contribution for elastin that ensures that the degrees of freedom that appear additionally in three dimensions compared to two dimensions are endowed with a proper stiffness (in order to avoid numerical problems). To this end, a three-dimensional isotropic neo-Hookean strain energy W_{3D}^{el} is added to the elastin strain energy from (32) to constrain shear deformation. Thereby, one uses the isochoric elastic deformation gradient

$$\bar{\boldsymbol{F}}_e = \frac{1}{|\boldsymbol{F}_e|^{1/3}} \boldsymbol{F}_e \tag{33}$$

with $\boldsymbol{F}_e$ the elastic deformation gradient of elastin and $|\bar{\boldsymbol{F}}_e| = 1$. The related isochoric elastic right Cauchy–Green tensor of elastin is $\bar{\boldsymbol{C}}_e = \bar{\boldsymbol{F}}_e^T \bar{\boldsymbol{F}}_e$, and its first invariant is $\mathrm{tr}\left(\bar{\boldsymbol{C}}_e\right)$. Using these quantities, we define a three-dimensional isotropic neo-Hookean strain energy contribution of elastin in the form

$$W_{3D}^{el} = \frac{\mu_{3D}^{el}}{2} \left[\left(\mathrm{tr}\left(\bar{\boldsymbol{C}}_e\right) - 3 \right) \right] \tag{34}$$

with the material parameter μ_{3D}^{el} governing the shear stiffness. For elastin, incompressibility cannot be enforced by a simple kinematic assumption like (31). Therefore, we use the volumetric penalty function

$$W_{vol}^{el} = \varepsilon \left(|\boldsymbol{F}_e| - 1 \right)^2 \tag{35}$$

where a sufficiently high penalty parameter ε is used to enforce a nearly incompressible behavior of elastin. The total strain energy of elastin is then composed by the contributions from (32), (34), and (35) and becomes

$$W^{el} = W_{2D}^{el} + W_{3D}^{el} + W_{vol}^{el}. \tag{36}$$

For a numerical implementation, the first and second derivatives of the above strain energy functions with respect to the Green–Lagrange strain $\boldsymbol{E}$ are required. These are provided in Appendix 2.

4 Numerical examples

4.1 General

We implemented the homogenized constrained mixture model developed in Sect. 3 in our in-house research code BACI (written in C++) and studied volumetric growth and remodeling in a simple model aorta that is represented by a thick-walled cylinder of length L, inner radius R, and wall thickness H with an internal (blood) pressure p. This thick-walled cylinder was discretized with 8-noded hexahedral finite elements. An Fbar method was applied to avoid problems with locking (de Souza Neto et al. 1996). Based on a convergence study that was performed to ensure a negligible numerical error, we discretized the geometry with 552,960 elements (480 elements in axial direction, 6 elements in radial direction, and 192 elements in circumferential direction). The evolution of growth and remodeling (i.e., (16)–(18), and (25)) was solved using a backward Euler time integration scheme (cf. Appendix 3) with a time step size ten times smaller than the smallest turnover time T^i (cf. (17)) of any constituent. The direction vectors of fiber families representing collagen and smooth muscle were averaged within each finite element. So far, volumetric constrained mixture models of arterial growth assumed isotropic growth (Eriksson 2014; Grytsan et al. 2015; Valentín et al. 2013). However, experiments suggest in particular for arteries rather anisotropic growth, that is, material deposition or degradation (at least mainly) in thickness direction (Matsumoto and Hayashi 1996). Therefore, we study below both the case of isotropic growth represented by $\boldsymbol{B}^i = \boldsymbol{I}/3$ in (25) and the case of anisotropic growth in thickness direction represented by $\boldsymbol{B}^i = \boldsymbol{a}_0^\perp \otimes \boldsymbol{a}_0^\perp$ with the unit vector $\boldsymbol{a}_0^\perp$ in wall thickness direction (in reference configuration). In case of isotropic growth, we conclude from (18) and (25) that the time derivative of the growth deformation gradient and thus, because of the initial condition $\boldsymbol{F}_g^i(t=0) = \boldsymbol{I}$, also the growth deformation gradient itself can be written as some scalar prefactor times the identity tensor. With (20) this prefactor can be computed as $\varrho_0(t)/\varrho_0(0)$ such that

$$\boldsymbol{F}_g^i = \left(\frac{\varrho_0(t)}{\varrho_0(0)} \right)^{1/3} \boldsymbol{I}. \tag{37}$$

Similarly, one concludes in case of anisotropic growth in wall thickness direction

$$\boldsymbol{F}_g^i = \frac{\varrho_0(t)}{\varrho_0(0)} \boldsymbol{a}_0^\perp \otimes \boldsymbol{a}_0^\perp + \left(\boldsymbol{I} - \boldsymbol{a}_0^\perp \otimes \boldsymbol{a}_0^\perp \right). \tag{38}$$

There is some evidence that in adult arterial tissue mechanically functional elastin is not produced any longer but only slowly degraded with a half-life time of several decades (Cyron and Humphrey 2016). Thus, elastin growth can be characterized by the mass production rate $\dot{\varrho}_0^{el}(t) = -\varrho_0^{el}(t)/T^{el}$ rendering in (17) the remodeling velocity gradient $\boldsymbol{L}_r^{el} = \boldsymbol{0}$ and thus $\boldsymbol{F}_r^{el}(t) = \boldsymbol{F}_r^{el}(0)$ at any time. Collagen and smooth muscle are modeled by quasi-one-dimensional fiber families. Note that in this case (17) defines the remodeling deformation gradient uniquely only via the

additional kinematic assumption of incompressibility, that is, (31), which confines the space of possible elastic and remodeling deformations (cf. also Appendix 1 in Cyron et al. (2016b)).

Herein we simulate growth and remodeling starting from a homeostatic initial configuration (i.e., a mechanical equilibrium configuration where no mechano-regulated growth and remodeling occur). This means that for constituents subject to growth and remodeling (i.e., collagen and smooth muscle), the initial elastic stress or equivalently stretch has to equal the respective homeostatic one (which itself typically equals the deposition stretch, cf. Proposition 1 in Cyron and Humphrey (2014)). It is then an important question how the elastic stretch of elastin has to be chosen so that under this constraint mechanical equilibrium in a given initial configuration is fulfilled. In a membrane, the answer to this question is straightforward. However, in a general three-dimensional solid it is in general non-trivial (cf. also page 10 in Eriksson (2014)). To overcome this problem, we use herein the procedure described in Appendix 1. Essentially, in this procedure we slightly vary the two-dimensional stiffness parameter $\mu_{2\mathrm{D}}^{\mathrm{el}}$ and initial radial elastic stretch of elastin $\lambda_{\mathrm{e}}^{\mathrm{el}\perp}$ $(t=0)$ over the wall thickness such that both mechanical equilibrium and a homeostatic state of collagen and smooth muscle are ensured in the given initial configuration. Note that only these two parameters are varied in wall thickness direction, whereas all other parameters are kept constant to keep the model particularly similar to previously published membrane models and allow thereby instructive comparisons. All simulation parameters are summarized in Table 1 and chosen identical to the parameter values used in previous computational studies of aortic aneurysms with two-dimensional membrane models and reported in Table 1 of Wilson et al. (2013). Originally, these parameter values were determined by Wilson et al. (2012) from biaxial mechanical testing data reported by Geest et al. (2004) by nonlinear regression. The only additional parameters we used in this paper are $\mu_{2\mathrm{D}}^{\mathrm{el}}$ and $\lambda_{\mathrm{e}}^{\mathrm{el}\perp}$ $(t=0)$, which are computed as pointed out in Appendix 1, and the damage parameters. The latter have been chosen heuristically for our specific computational example in Sect. 4.2 in order to resemble a typical damage in the vascular wall as it may occur during the initiation of an aneurysm.

4.2 Enlargement of axisymmetric model aneurysm

In the first example, we study the enlargement of an idealized fusiform abdominal aortic aneurysm over 15 years, starting from the above-described axisymmetric cylindrical geometry. Generally, anisotropic growth in thickness direction is assumed in this section [cf. (38) in Sect. 4.1]. Elastin is assumed to be subject to a damage rate function

$$\dot{D}^{\mathrm{el}}(\boldsymbol{X},t)=-\frac{1}{T^{\mathrm{el}}}\varrho_0^{\mathrm{el}}(\boldsymbol{X},t)-\left[\frac{D_{\max}}{t_{\mathrm{dam}}}\exp\left[-0.5\left(\frac{X_3}{L_{\mathrm{dam}}}\right)^2\right]\exp\left[-\frac{t}{t_{\mathrm{dam}}}\right]\right]\varrho_0^{\mathrm{el}}(\boldsymbol{X},0) \tag{39}$$

where we use a coordinate system with origin in the center of the cylinder and X_3-axis aligned with the symmetry axis of the cylinder so that $X_3\epsilon\,[-L/2;\,L/2]$. The first summand on the right-hand side of (39) corresponds to a normal age-related degradation (driven by a Poisson process with time constant T^{el}), the second summand to an additional damage (e.g., by proteolytic activity in the vessel wall) that starts at $t=0$ and spreads out along the vessel axis (beginning in the center) following a Gaussian-type function. It finally degrades up to a fraction $D_{\max}$ of the initial elastin in the vessel wall. We compared the response of our three-dimensional model aorta to the damage from (39) with the response of a two-dimensional membrane model where also a homogenized constrained mixture model for growth and remodeling was used (cf. section 3.2 of Cyron et al. (2016b)). We performed the comparison for a range of gain parameters $k_\sigma^{\mathrm{co}}=k_\sigma^{\mathrm{sm}}\in[0.05,0.07,0.09,0.11,0.13,0.15]\,/\,T^{\mathrm{co}}$. The results are shown in Fig. 2. Generally, the agreement between the solution of the two-dimensional membrane model and the three-dimensional model developed herein is good. To examine the origin of the minor differences between both, we performed further computational studies. These suggested that the differences mainly result from the different ways how elastin is modeled in two and three dimensions, respectively. In the two-dimensional membrane model, the strain energy of elastin is given by the two-dimensional neo-Hookean function in (32) only where the elasticity parameter is chosen $\mu_{2\mathrm{D}}^{\mathrm{el}}=72\,\mathrm{J/kg}$. In the three-dimensional model, the strain energy of elastin includes additionally a three-dimensional neo-Hookean contribution and a volumetric penalty term as can be seen in (36). Moreover, in three dimensions, we use $\mu_{3\mathrm{D}}^{\mathrm{el}}=72\,\mathrm{J/kg}$ and compute $\mu_{2\mathrm{D}}^{\mathrm{el}}$ from the condition of mechanical equilibrium in the initial configuration, which provides values in the range $9\,\mathrm{J/kg}\leq\mu_{2\mathrm{D}}^{\mathrm{el}}\leq 40\,\mathrm{J/kg}$. These minor differences between the model in two and three dimensions could not be avoided due to the additional degrees of freedom in three dimensions and the requirement to ensure initial mechanical equilibrium with respect to all of them. Yet, altogether the behavior of the two- and three-dimensional model is very similar. In both models, the vessel responds to the elastin damage specified in (39) for small gain parameters by an unbounded enlargement (mechanobiological instability). By contrast, for large gain parameters, the blood vessel can apparently, after a transient period of enlargement, reattain a new stable and only slightly dilated configuration, which is in good agreement with the theory of mechanobiological stability proposed by Cyron et al.

Table 1 Simulation parameters of the idealized cylindrical blood vessel studied in Sect. 4

Geometry/load		
Inner radius	R	10 mm
Wall thickness	H	1.41 mm
Length	L	180 mm
Mean blood pressure	p	100 mmHg
Material parameters		
Elastin: 2D neo-Hookean parameter	$\mu_{2\mathrm{D}}^{\mathrm{el}}$	$\in$[9; 40]J/kg
Elastin: 3D neo-Hookean shear parameter	$\mu_{3\mathrm{D}}^{\mathrm{el}}$	72 J/kg
Elastin: volumetric penalty function	ε	720 J/kg
Collagen: Fung exponential parameters	k_1^{co}	568 J/kg
	k_2^{co}	11.2
Smooth muscle: passive contribution	k_1^{sm}	7.6 J/kg
	k_2^{sm}	11.4
Smooth muscle: active contribution	σ_{actmax}	54 kPa
	λ_0	0.8
	λ_m	1.4
Initial reference mass densities		
Elastin	$\varrho_0^{\mathrm{el}}(t=0)$	241.5 kg/m^3
Collagen: circumferential	$\varrho_0^{\mathrm{co}(0^\circ)}(t=0)$	65.1 kg/m^3
Collagen: axial	$\varrho_0^{\mathrm{co}(90^\circ)}(t=0)$	65.1 kg/m^3
Collagen: diagonal	$\varrho_0^{\mathrm{co}(45^\circ)}(t=0)$, $\varrho_0^{\mathrm{co}(-45^\circ)}(t=0)$	260.4 kg/m^3
Smooth muscle	$\varrho_0^{\mathrm{sm}}(t=0)$	157.5 kg/m^3
Total initial reference mass density	$\varrho_0(t=0)$	1050 kg/m^3
Growth and remodeling parameters		
Collagen/smooth muscle: turnover time	$T^{\mathrm{co}} = T^{\mathrm{sm}}$	101 days
Collagen/smooth muscle: gain parameter	$k_\sigma^{\mathrm{co}} = k_\sigma^{\mathrm{sm}}$	[0.05, 0.07, 0.09, 0.11, 0.13, 0.15]/T^{co}
Elastin: mean life time	T^{el}	101 years
Elastin: gain parameter	k_σ^{el}	0
Initial elastic stretch (equal to homeostatic stretch/deposition stretch for collagen and smooth muscle)		
Elastin: axial direction	$\lambda_{\mathrm{e}}^{\mathrm{el}(90^\circ)}(t=0)$	1.25
Elastin: circumferential direction	$\lambda_{\mathrm{e}}^{\mathrm{el}(0^\circ)}(t=0)$	1.34
Elastin: radial direction	$\lambda_{\mathrm{e}}^{\mathrm{el}\perp}(t=0)$	$\in$[0.60; 0.64]
Collagen (in fiber direction)	$\lambda_{\mathrm{e}}^{\mathrm{co}}(t=0)$	1.062
Smooth muscle (in fiber direction)	$\lambda_{\mathrm{e}}^{\mathrm{sm}}(t=0)$	1.1
Damage parameters in model aneurysm		
Damage spread in space	L_{dam}	10 mm
Damage spread in time	t_{dam}	40 days
Maximal damage	D_{max}	0.5

To distinguish between different collagen fiber families, we use, when appropriate, superscripts co(0°), co(90°), co(45°), and co(−45°) for circumferential, axial and diagonal fibers. For collagen and smooth muscle, the elastic stretch in the initial configuration equals the homeostatic stretch in fiber direction (that is equivalent to a certain homeostatic Cauchy stress). For μ_{2D}^{el} and $\lambda_{\mathrm{e}}^{\mathrm{el}\perp}(t=0)$ not a single value is given but rather a parameter interval within which these parameters are varied in wall thickness direction according to the procedure described in Appendix 1 in order to ensure both mechanical and mechanobiological equilibrium in the given initial geometry

(2014), Cyron and Humphrey (2014). To illustrate the simulations discussed in this section, the von Mises stress and the normalized collagen mass density at different points in time and for two different growth parameters $k_\sigma^{\mathrm{co}} = k_\sigma^{\mathrm{sm}} = 0.15/T^{\mathrm{co}}$ and $k_\sigma^{\mathrm{co}} = k_\sigma^{\mathrm{sm}} = 0.05/T^{\mathrm{co}}$ are shown in Figs. 3 and 4.

In previous three-dimensional constrained mixture models of arterial growth and remodeling (Eriksson 2014; Valen-

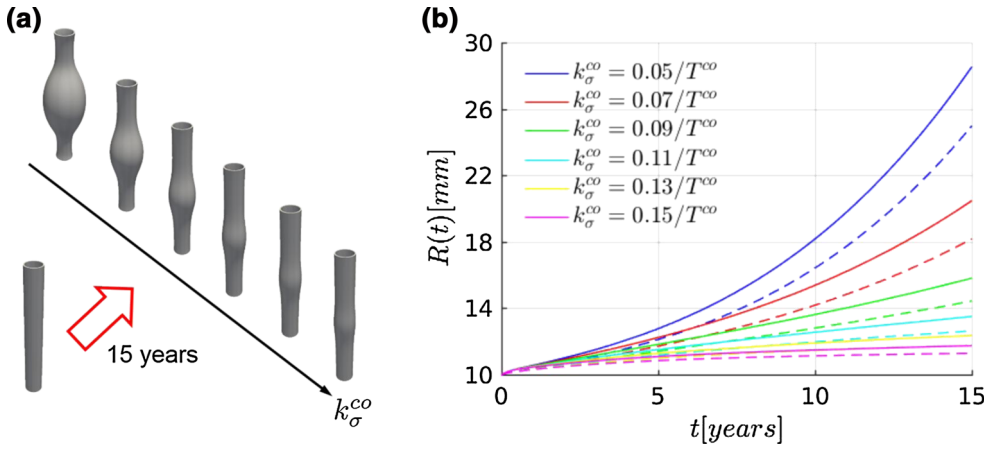

Fig. 2 Expansion of an idealized fusiform abdominal aortic aneurysm over 15 years following a focal loss of elastin for different gain factors k_σ^{co}. **a** Shape of initial geometry and geometries after 15 years for increasing values of k_σ^{co}. **b** Maximal inner radius of aneurysm over 15 years. The results of the three-dimensional volumetric model developed herein (*solid lines*) are compared with a membrane-based homogenized constrained mixture model used also by Cyron et al. (2016b) (*dashed lines*)

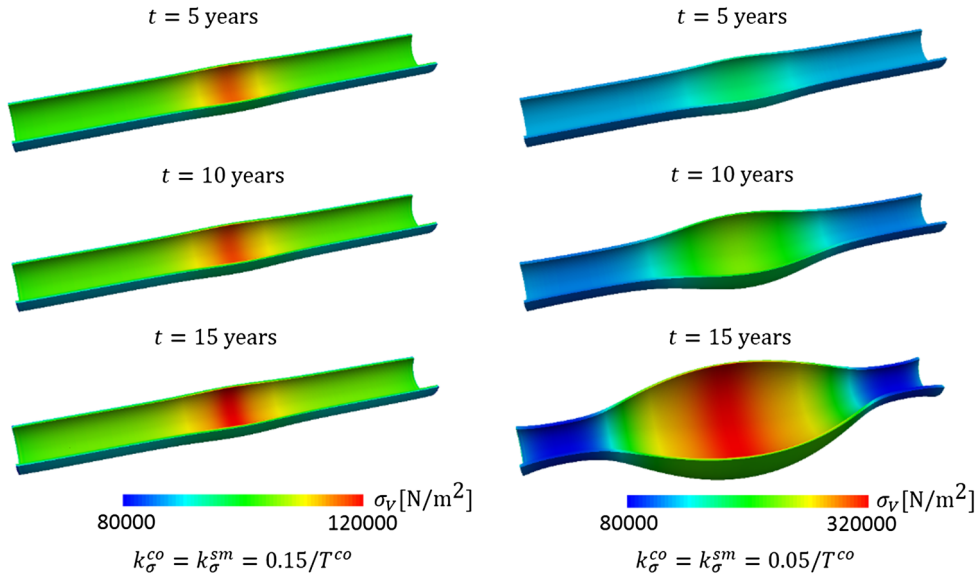

Fig. 3 Von Mises stresses σ_V in a cylindrical model aorta in response to the damage defined in (39) at three different points in time t. For a high gain parameter $k_\sigma^{co} = k_\sigma^{sm} = 0.15/T^{co}$ the vessel quickly stabilizes in an only slightly dilated configuration with moderately elevated stress (*left*). For a low gain parameter $k_\sigma^{co} = k_\sigma^{sm} = 0.05/T^{co}$ (*right*) an unbounded increase in the vessel diameter and wall stress are observed as expected for aneurysms evolving toward rupture

tín et al. 2013; Grytsan et al. 2015), a loss of elastin was in general associated with a contraction of the vessel radius rather than a dilatation as one would intuitively expect after a weakening of the wall. The reason for this unphysical behavior was the way how volumetric growth was conceptualized in these models. The growth direction was implicitly determined by the incompressibility constraint using a volumetric deviatoric split of the deformation gradient. This way only isotropic growth could be modeled. So, if elastin was degraded and the total tissue volume decreased, the tissue contracted equally in all spatial directions and thus also in circumferential direction so that the radius significantly decreased. To overcome this apparently unphysical behavior, Eriksson (2014) introduced the distinction between constant individual density (CID) and adaptive individual density (AID) growth. In AID growth, a loss of mass does not change the tissue volume itself and so a loss of elastin does not entail a contraction of the artery. While this idea can, from a practical perspective, help avoid an unphysical contraction of the artery after a loss of elastin, its micromechanical foundation appears controversial in several respects. The medial layer of arteries is organized in a sandwich-like structure as discussed in detail by O'Connell (2008). Thin lamellar sheets of elastin spanning in circumferential and

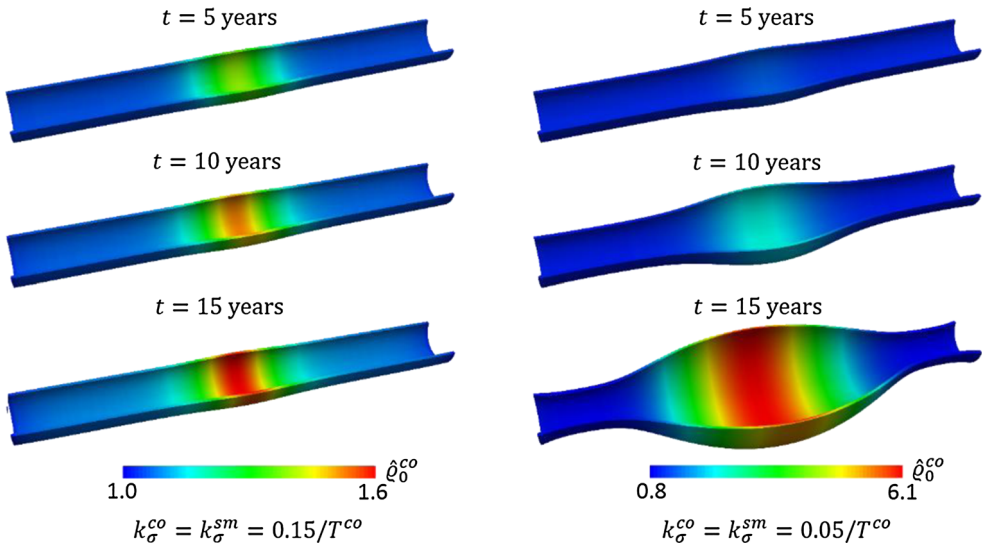

Fig. 4 Normalized reference mass density of collagen $\hat{\varrho}_0^{co}$ (that is, current divided by initial reference mass density of all collagen fiber families together) in a cylindrical model aorta in response to the damage defined in (39) at three different points in time t for a mechanobiologically stable (*left*, $k_\sigma^{co} = k_\sigma^{sm} = 0.15/T^{co}$) and unstable (*right*, $k_\sigma^{co} = k_\sigma^{sm} = 0.05/T^{co}$) case

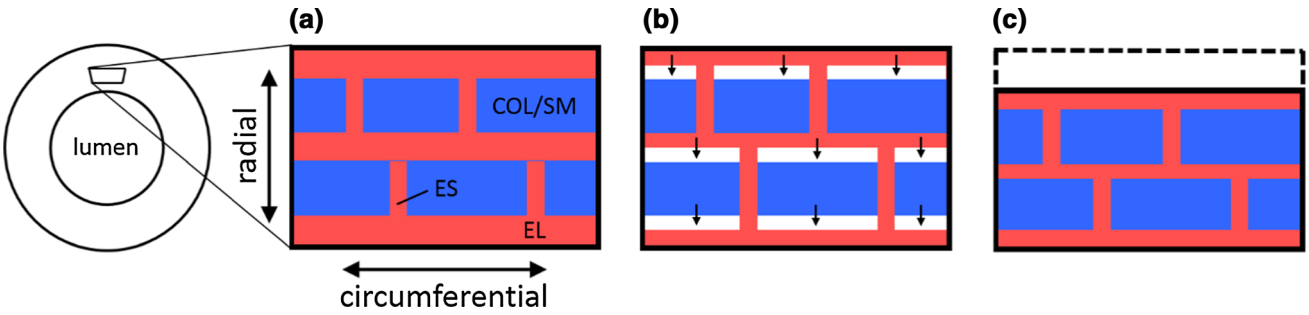

Fig. 5 Cross section of circular cylindrical model aorta (*left*) and illustration of shrinking of the media after degradation of elastin in a magnified region: **a** healthy media consisting of thin elastic lamellar layers (EL: *red*) which are connected to each other by elastin struts (ES: *red*) and collagen/smooth muscle layers (COL/SM: *blue*) which fill the space between the elastin layers. **b** Media directly after degradation of elastin. Void (that is, fluid-filled) spaces (*white*) are expected to rapidly fill by a relative motion of the adjacent material layers due to the pressure in radial direction throughout the wall, which leads to a reduced wall thickness as illustrated in **c**

axial direction separate thick layers of smooth muscle and collagen fibers (cf. Fig. 5). A sudden loss of elastin mass would mean that the lamellar sheets are partially replaced by void (that is, only fluid-filled) spaces or at least spaces of massively reduced resistance against compression. Noting the pressure in the thickness direction of the vessel wall, these spaces would be expected to close rapidly by a relative motion of the adjacent material layers in wall thickness direction. Thus, it appears at least questionable whether a loss of elastin would really change the mass density of the tissue as implicitly assumed by the AID concept proposed in Eriksson (2014) or whether it would not rather locally shrink the tissue in thickness direction of the vessel wall. Such shrinking in thickness direction is exactly what the anisotropic volumetric growth model developed herein describes. It is important to note that previous isotropic volumetric constrained mixture growth models were in principle not able to capture a thinning of the vessel wall by a partial loss of tissue mass without altering significantly the traction-free configuration of the remaining mass in circumferential direction, which leads to the above-mentioned unphysical contraction. By contrast, the anisotropic growth model developed herein overcomes this problem in a fairly natural way (cf. Fig. 5).

4.3 Thickening of arterial wall in hypertension

Matsumoto and Hayashi (1996) examined the response of the aorta to a sudden and permanent increase in blood pressure. In this section, we study a similar situation with the parameters from Table 1. Unlike in Sect. 4.2, no damage of elastin is considered noting the short period studied compared to the long half-life time of elastin and the absence of particular

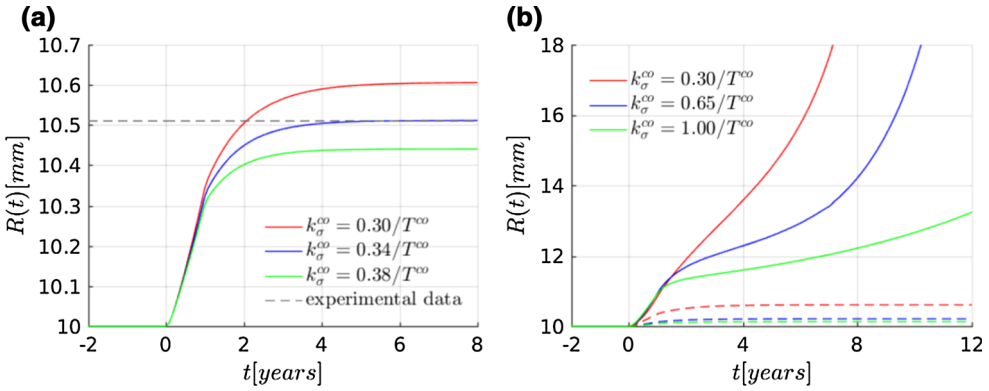

Fig. 6 Adaptation of a healthy aorta to a minor increase in blood pressure $\delta p = 20\,\text{mmHg}$ for different gain parameters k_σ^{co} governing collagen production. The maximal inner radius is plotted over time. Note that the system is initially in a homeostatic state so that the maximal radius does not change until the system is perturbed at time $t = 0$. **a** Anisotropic growth: simulated vessels (*solid lines*) stabilize for $k_\sigma^{co} = 0.34/T^{co}$ around radius expected from experiments (*dashed line*). **b** While for anisotropic growth (*dashed lines*) vessel geometry stabilizes quickly after perturbation, isotropic growth (*solid lines*) leads for the same gain parameters $k_\sigma^{co} = 0.30/T^{co}, 0.65/T^{co}, 1.00/T^{co}$ to unstable growth and remodeling (continued dilatation of the vessel over time instead of stabilization around a new equilibrium state); this observation suggests a generally higher susceptibility of isotropic growth to mechanobiological instability

proteolytic insults that could be expected to accelerate elastin degradation. At time $t = 0$, the blood vessel is subjected to a sudden increase in blood pressure p from 100mmHg to 120 mmHg. With a gain parameter $k_\sigma^{\text{co}} = k_\sigma^{\text{sm}} = 0.34/T^{\text{co}}$ and assuming anisotropic growth in thickness direction of the vessel wall, the vessel is observed to stabilize, after a transient growth period, in a new slightly dilated state that corresponds well to the one expected from the experimental observations of Matsumoto and Hayashi (1996) (cf. Fig. 6a). For a discussion how the data from experiments with rats in Matsumoto and Hayashi (1996) are compared with the dilatation of a human aorta as described by the parameters in Table 1, the reader is referred to section 3.3 of Cyron et al. (2014). Again the results obtained with the three-dimensional model developed in this paper are nearly identical to the ones obtained with the membrane model used by Cyron et al. (2014).

Interestingly, the results change completely if in the three-dimensional model isotropic volumetric growth is assumed (similar to Eriksson 2014; Valentín et al. 2013; Grytsan et al. 2015). In this case, the vessel undergoes an unstable dilatation even for gain parameters as large as $k_\sigma^{\text{co}} = k_\sigma^{\text{sm}} = 1.00/T^{\text{co}}$ (cf. Fig. 6b). Not only is this behavior completely different from the stabilizing behavior observed experimentally by Matsumoto and Hayashi (1996), it also appears highly unphysiological. Blood vessels are expected to be subject to minor changes of blood pressure in numerous situations and if these always resulted in an unbounded unstable dilatation, aneurysms would be expected in nearly the whole and also younger population (rather than only 5–10% of the elderly population). The reason for the unstable dilatation in case of isotropic growth can be understood easily from the theory of mechanobiological stability (Cyron et al. 2014; Cyron and Humphrey 2014). In this theory, one considers in general some state of mechanobiological equilibrium like the initial configuration in this example (where mechanical equilibrium is satisfied and no mechano-regulated growth and remodeling occur). Such an equilibrium state is called mechanobiologically stable if the system considered can reattain after small perturbations a mechanobiological equilibrium state identical to or close to the original one. In cylindrical blood vessels, after an increase in blood pressure, thickening of the wall helps restore a homeostatic stress state because it decreases the wall stress back to the initial level. On the other hand, circumferential dilatation of the wall further increases the wall stress due to Laplace' formula (which says that the wall stress increases linearly with the inner radius of the vessel). In case of anisotropic growth in thickness direction, dilatation in circumferential direction results only from remodeling (i.e., the dynamics of $\boldsymbol{F}_{\text{r}}^{i}$ governed by (17)) and can thus easily be overruled by sufficient growth (i.e., wall thickening) driven by $\boldsymbol{F}_{\text{g}}^{i}$ if the gain parameters k_σ^{co} and k_σ^{sm} are chosen high enough. Therefore, anisotropic growth in thickness direction can easily restabilize a blood vessel after a small perturbation. The situation is completely different in case of isotropic growth. There, by definition, the growth deformation gradient $\boldsymbol{F}_{\text{g}}^{i}$ entails an equal dilatation in wall thickness direction and in circumferential direction. While the wall thickening decreases the average wall stress, the dilatation of the circumference increases wall stress by the same factor, recalling Laplace' formula. Noting that the dilatation in circumferential direction is, however, additionally promoted by the remodeling deformation gradient $\boldsymbol{F}_{\text{r}}^{i}$, it can easily overrule the effect of wall thickening, entailing a continued (and potentially unstable) dilatation of the vessel. It is worth noting that also in case of isotropic growth one may eventually observe a restabilization because constituents not subject to

growth and remodeling (like elastin) will take over a larger and larger fraction of the wall stress as the vessel keeps dilating, which may enable collagen and smooth muscle to reattain at some point a homeostatic stress state. However, our computational studies suggest that for isotropic growth such a restabilization may occur only for large gain parameters (that is a very high collagen production) and after a considerable dilatation of the blood vessel. That is, isotropic growth appears to make blood vessels at least much more susceptible to unstable dilatation than anisotropic growth in thickness direction. If one assumes that growth and remodeling should ensure stability and functional adaptation of blood vessels as efficiently as possible, this raises the question whether or why blood vessels should rely on isotropic instead of anisotropic growth. In fact, Matsumoto et al. report experimental observations (in particular in Table 2 of Matsumoto and Hayashi (1996)) which suggest that growth and remodeling of blood vessels in response to hypertension are not isotropic. Rather the ratio of wall thickness and vessel radius increases significantly, which supports the idea that anisotropic growth in wall thickness direction rather than isotropic growth may be an appropriate model for vascular growth and remodeling. Further studies are, of course, required to definitely confirm or reject this hypothesis.

5 Conclusions

Mathematical modeling of soft tissue growth and remodeling has been based so far mainly on two major approaches. The kinematic growth theory of Rodriguez et al. (1994) relies on a simple multiplicative split of the deformation gradient into an inelastic growth part accounting for local changes of mass and volume and an elastic part ensuring mechanical equilibrium and geometric compatibility. While conceptually simple and computationally efficient, this approach suffers, from an inherent inability to account for the separate growth and remodeling of several distinct structurally significant constituents. To overcome this limitation, Humphrey and Rajagopal introduced the so-called constrained mixture models (Humphrey and Rajagopal 2002) where growth and remodeling are conceptualized as a continuous degradation and deposition of differential mass increments. These constrained mixture models realistically mimic the situation in vivo where cells such as fibroblasts and smooth muscle cells are continuously secreting new extracellular matrix and degrading extant matrix at the same time, for example, by matrix metalloproteinases (MMPs). However, the implementation of classical constrained mixture models based on multi-network theory is involved and their computational cost is significantly higher than the one of the simple kinematic growth models. To combine the advantages of simple kinematic growth models and constrained mixture models, recently a new class of models was introduced, the so-called homogenized constrained mixture models (Cyron et al. 2016b). They share the realistic micromechanical foundation of the classical constrained mixture models and produce results that are in many cases nearly identical or at least very similar to the ones of classical constrained mixture models. Yet, their implementation is nearly as simple as the one of the kinematic growth models and their computational cost is similarly low. By Cyron et al. (2016b) introduced homogenized constrained mixture models with a main focus on theoretical aspects.

In this paper, we pointed out in detail how homogenized constrained mixture models can be used for anisotropic volumetric growth and remodeling in three dimensions. Using the example of a circular–cylindrical model aorta, we demonstrated that homogenized constrained mixture models can reproduce realistically both pathological growth (as observed in aneurysms) and adaptive growth in healthy vessels (e.g., in response to hypertension). A major advantage of the homogenized constrained mixture models developed in this paper is the natural incorporation of anisotropic volumetric growth. Constrained mixture models for volumetric soft tissue growth and remodeling published previously were limited to isotropic volumetric growth. However, experimental observations, for example, by Matsumoto and Hayashi (1996), rather suggest that arterial growth is anisotropic and is likely to occur (at least mainly) in thickness direction of the vessel wall. As discussed in Sect. 4.3, the reason may be that anisotropic growth can ensure the stability of blood vessels under perturbations more efficiently than isotropic growth. Therefore, the ability of the homogenized constrained mixture model developed herein to incorporate straightforwardly anisotropic growth may make it an ideal tool to study growth and remodeling in the vasculature. In this paper, we used only a particularly simple constitutive model for the arterial wall with the intention to keep constitutive modeling as similar as possible to previously published two-dimensional studies and enable thereby instructive comparisons. Combining the framework for growth and remodeling developed herein with more sophisticated and realistic three-dimensional constitutive models such as the ones used by Eriksson (2014), Holzapfel et al. (2015) will be a natural next step.

Acknowledgements This work was supported by the International Graduate School for Science and Engineering (IGSSE) of the Technical University of Munich and the Emmy Noether program of the German Research Foundation DFG (CY 75/2-1). The authors thank Sebastian Fuchs for providing Fig. 1 under a Creative Commons License.

Compliance with ethical standards

Conflict of interest The authors declare that they have no conflict of interest.

Appendix 1

In mechanobiological equilibrium, mechanical equilibrium is satisfied and at the same time no growth and remodeling occur because the stress of each constituent subject to growth and remodeling equals the homeostatic value (Cyron and Humphrey 2014). In two-dimensional membrane models of blood vessels, it is easy to define for a given vascular geometry an initial state in mechanobiological equilibrium. The reason is that in the balance of momentum only the membrane stress rather than the Cauchy stress appears (cf. Equation (2.2) in Cyron et al. (2014)). So, one can first solve this equation to ensure mechanical equilibrium. Subsequently, one can separately vary the remaining parameters (in particular wall thickness and mass fractions) to ensure that the Cauchy stress of each constituent equals the homeostatic value.
By contrast, in three dimensions the definition of an initial state in mechanobiological equilibrium is not straightforward. In Sect. 4, we applied, inspired by Gee et al. (2010), the following procedure to initialize the simulations in mechanobiological equilibrium:

1. First, the homeostatic stress (or equivalently stretch) of collagen and smooth muscle in fiber direction has to be defined. Herein, we adopt the values used already by Wilson et al. (2013) and presented in Table 1. The elastic stretches $\lambda_e^{co}(t=0)$ and $\lambda_e^{sm}(t=0)$ of collagen and smooth muscle in the initial configuration are then computed so that they correspond to these homeostatic stresses (or are equal to the chosen homeostatic stretches).
2. Second, the elastic in vivo stretches of elastin in axial and circumferential direction have to be defined. Herein, we adopt the values used already by Wilson et al. (2013) and presented in Table 1. These stretches are equal to the initial stretch of elastin in axial direction $\lambda_e^{el(90°)}(t=0)$ and circumferential direction $\lambda_e^{el(0°)}(t=0)$.
3. Third, the elastic stretch $\lambda_e^{el\perp}(t=0,r)$ of elastin in wall thickness direction in the initial configuration at time $t=0$ is computed. The stretch depends on the distance r from the cylinder axis and is computed such that the Cauchy stress $\sigma^{\perp}(r)$ of the whole constrained mixture in wall thickness direction linearly increases from the value $\sigma^{\perp}(r=R) = -p$ at the inner radius of the cylinder to the $\sigma^{\perp}(r=R+H) = 0$ at the outer radius of the cylinder. That is, we use the condition

$$p\left(1-\frac{r-R}{H}\right)+\sigma^{\perp}\left(\lambda_e^{el\perp}(t=0,r)\right)=0 \tag{40}$$

With given strain energies from Sect. 3.3, given initial mass fractions (cf. Table 1), given initial (homeostatic) stretches of collagen and smooth muscle (cf. 1)) as well as given initial axial and circumferential stretch of elastin (cf. 2)), $\sigma^{\perp}$ in (40) becomes a function of only the parameter $\lambda_e^{el\perp}(t=0,r)$, which can thus be computed from (40). Note that the only other so far unknown parameter μ_{2D}^{el} does not appear in (40) because it affects only the axial and circumferential wall stress but not the radial one due to the two-dimensional elasticity of (32). Equation (40) is solved for $\lambda_e^{el\perp}(t=0,r)$ by applying a Newton–Raphson method.
4. Fourth, the material parameter $\mu_{2D}^{el}(r)$ is defined such that it ensures a constant circumferential Cauchy stress of elastin despite the variation of $\lambda_e^{el\perp}(t=0,r)$ in radial direction. This ensures mechanical equilibrium for the $\lambda_e^{el\perp}(t=0,r)$ computed according to 3) and requires

$$\sum_{i=1}^{n}\sigma^{i(0°)}(t=0)=\frac{pR}{H} \tag{41}$$

with $\sigma^{i(0°)}(t=0)$ the Cauchy stress of the ith constituent in circumferential direction in the initial configuration at time $t=0$. Equation (41) has to hold for any $r \in [R;R+H]$, and it is solved analytically for the material parameter $\mu_{2D}^{el}(r)$. Note that all parameters that are required to compute the Cauchy stresses $\sigma^{i(0°)}$ from the strain energies defined in Sect. 3.3 are known at this point except for μ_{2D}^{el}. Also note that, as the elastic radial prestretch of elastin $\lambda_e^{el\perp}(t=0,r)$ varies in wall thickness direction, also the material parameter $\mu_{2D}^{el}(r)$ has to.

An initially stress-free thick-walled homogeneous cylinder on which an internal pressure is imposed exhibits in general a parabolic stress profile both of the circumferential stress $\sigma^{(0°)}$ and radial stress $\sigma^{\perp}$ as illustrated in Fig. 7a. By contrast, the prestressing procedure described in this appendix leads to a configuration with constant circumferential stress $\sigma^{(0°)}$ and linearly increasing radial stress $\sigma^{\perp}$ (cf. Fig. 7b) in case of uniform mass fractions and fiber orientations throughout the wall. The real stress profile over the wall thickness in arteries is currently not exactly known so that the prestressing procedure used herein should be understood as a simple way to initialize our simulations in a state of mechanobiological equilibrium rather than as a physiologically accurate procedure.

Appendix 2

In this appendix, we provide the first and second derivatives of the strain energy functions W^{co}, W^{sm}, and W^{el} in (27), (28), and (36) with respect to the total Green–Lagrange strain $\boldsymbol{E}$. For each constituent, we assume a multiplicative split of the deformation gradient into an elastic part $\boldsymbol{F}_e$ and an inelas-

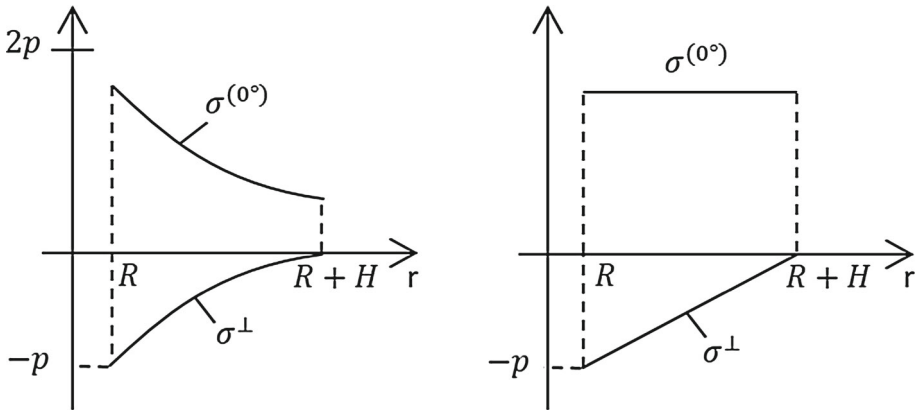

Fig. 7 Circumferential ($\sigma^{(0°)}$) and radial ($\sigma^{\perp}$) stress in a thick-walled cylinder from the inner radius R to the outer radius $R + H$ in an initially stress-free cylinder under internal pressure p (*left*) compared to the prestressed configuration produced by the procedure described in this appendix (*right*)

tic part $\boldsymbol{F}_{\mathrm{gr}}$ (cf. (13)) and the partial derivative with respect to the total strain is computed assuming that $\boldsymbol{F}_{\mathrm{gr}}$ is constant so that a variation of $\boldsymbol{E}$ translates into a variation of $\boldsymbol{F}_{\mathrm{e}}$ only. Note that in this appendix we omit superscripts in $\boldsymbol{F}_{\mathrm{gr}}$ and $\boldsymbol{F}_{\mathrm{e}}$, given that in each equation it is evident to which constituent in the constrained mixture they refer.

For collagen in (27), we have

$$\frac{\partial W^{\mathrm{co}}}{\partial \boldsymbol{E}} = \frac{2\left[k_1^{\mathrm{co}}\left(I_a-1\right)e^{k_2^{\mathrm{co}}(I_a-1)^2}\right]}{\|\boldsymbol{F}_{\mathrm{gr}}\boldsymbol{a}_0\|^2}\boldsymbol{a}_0\otimes\boldsymbol{a}_0 \tag{42}$$

where $\boldsymbol{a}_0$ is the unit direction vector in reference configuration of the collagen fiber family. The second derivative of the strain energy function is

$$\frac{\partial^2 W^{\mathrm{co}}}{\partial \boldsymbol{E}\partial \boldsymbol{E}} = \frac{4k_1^{\mathrm{co}}\left[1+2k_2^{\mathrm{co}}\left(I_a-1\right)^2\right]e^{k_2^{\mathrm{co}}(I_a-1)^2}}{\|\boldsymbol{F}_{\mathrm{gr}}\boldsymbol{a}_0\|^4}\boldsymbol{a}_0 \otimes\boldsymbol{a}_0\otimes\boldsymbol{a}_0\otimes\boldsymbol{a}_0. \tag{43}$$

The stress and elasticity of smooth muscle fiber families aligned with the unit vector $\boldsymbol{a}_0$ in reference configuration are governed by

$$\frac{\partial W^{\mathrm{sm}}_{\mathrm{pas}}}{\partial \boldsymbol{E}} = \frac{2\left[k_1^{\mathrm{sm}}\left(I_a-1\right)e^{k_2^{\mathrm{sm}}(I_a-1)^2}\right]}{\|\boldsymbol{F}_{\mathrm{gr}}\boldsymbol{a}_0\|^2}\boldsymbol{a}_0\otimes\boldsymbol{a}_0, \tag{44}$$

$$\frac{\partial^2 W^{\mathrm{sm}}_{\mathrm{pas}}}{\partial \boldsymbol{E}\partial \boldsymbol{E}} = \frac{4k_1^{\mathrm{sm}}\left[1+2k_2^{\mathrm{sm}}\left(I_a-1\right)^2\right]e^{k_2^{\mathrm{sm}}(I_a-1)^2}}{\|\boldsymbol{F}_{\mathrm{gr}}\boldsymbol{a}_0\|^4}\boldsymbol{a}_0\otimes\boldsymbol{a}_0 \otimes\boldsymbol{a}_0\otimes\boldsymbol{a}_0\otimes\boldsymbol{a}_0, \tag{45}$$

$$\frac{\partial W^{\mathrm{sm}}_{\mathrm{act}}}{\partial \boldsymbol{E}} = \frac{\sigma_{\mathrm{actmax}}}{\varrho_0\left(0\right)\left[\boldsymbol{C}:\left(\boldsymbol{a}_0\otimes\boldsymbol{a}_0\right)\right]}\left(1-\frac{\left(\lambda_m-\lambda_{\mathrm{act}}\right)^2}{\left(\lambda_m-\lambda_0\right)^2}\right) \boldsymbol{a}_0\otimes\boldsymbol{a}_0, \tag{46}$$

$$\frac{\partial^2 W^{\mathrm{sm}}_{\mathrm{act}}}{\partial \boldsymbol{E}\partial \boldsymbol{E}} = -2\frac{\sigma_{\mathrm{actmax}}}{\varrho_0\left(0\right)\left[\boldsymbol{C}:\left(\boldsymbol{a}_0\otimes\boldsymbol{a}_0\right)\right]^2} \left(1-\frac{\left(\lambda_m-\lambda_{\mathrm{act}}\right)^2}{\left(\lambda_m-\lambda_0\right)^2}\right)\boldsymbol{a}_0\otimes\boldsymbol{a}_0\otimes\boldsymbol{a}_0\otimes\boldsymbol{a}_0. \tag{47}$$

For elastin we have, according to (36), $W^{\mathrm{el}} = W^{\mathrm{el}}_{\mathrm{2D}} + W^{\mathrm{el}}_{\mathrm{3D}} + W^{\mathrm{el}}_{\mathrm{vol}}$ with

$$\frac{\partial W^{\mathrm{el}}_{\mathrm{2D}}}{\partial \boldsymbol{E}} = \mu^{\mathrm{el}}_{\mathrm{2D}}\left(\boldsymbol{F}_{\mathrm{gr}}^{-1}\boldsymbol{A}^{\parallel}_{\mathrm{gr}}\boldsymbol{F}_{\mathrm{gr}}^{-\mathrm{T}} - \frac{1}{\left|\boldsymbol{A}^{\parallel}_{\mathrm{gr}}\boldsymbol{C}_{\mathrm{e}}\boldsymbol{A}^{\parallel}_{\mathrm{gr}}+\boldsymbol{A}^{\perp}_{\mathrm{gr}}\right|}\boldsymbol{A}^{\parallel}_0\right), \tag{48}$$

$$\frac{\partial^2 W^{\mathrm{el}}_{\mathrm{2D}}}{\partial \boldsymbol{E}\partial \boldsymbol{E}} = \frac{2\mu^{\mathrm{el}}_{\mathrm{2D}}}{\left|\boldsymbol{A}^{\parallel}_{\mathrm{gr}}\boldsymbol{C}_{\mathrm{e}}\boldsymbol{A}^{\parallel}_{\mathrm{gr}}+\boldsymbol{A}^{\perp}_{\mathrm{gr}}\right|}\left(\boldsymbol{A}^{\parallel}_0\otimes\boldsymbol{A}^{\parallel}_0+\boldsymbol{A}^{\parallel}_0\odot\boldsymbol{A}^{\parallel}_0\right), \tag{49}$$

where $\boldsymbol{C}_{\mathrm{e}}$ is the elastic Cauchy–Green deformation tensor of elastin, $\boldsymbol{F}_{\mathrm{gr}}$ its inelastic deformation gradient, $\boldsymbol{A}^{\parallel}_0 = \boldsymbol{F}^{-1}\boldsymbol{A}^{\parallel}_{\mathrm{gr}}\boldsymbol{F}^{-\mathrm{T}}$ and the special tensor product $\odot$ is defined such that in index notation $\left(\boldsymbol{A}\odot\boldsymbol{B}\right)_{ijkl} = \left(\boldsymbol{A}_{ik}\boldsymbol{B}_{jl}+\boldsymbol{A}_{jk}\boldsymbol{B}_{il}\right)/2$. The three-dimensional neo-Hookean contribution of elastin leads to

$$\frac{\partial W^{\mathrm{el}}_{\mathrm{3D}}}{\partial \boldsymbol{E}} = \mu^{\mathrm{el}}_{\mathrm{3D}}\left|\boldsymbol{C}_{\mathrm{e}}\right|^{-1/3}\left(\boldsymbol{C}_{\mathrm{gr}}^{-1}-\frac{1}{3}\mathrm{tr}\left(\boldsymbol{C}_{\mathrm{e}}\right)\boldsymbol{C}^{-1}\right) \tag{50}$$

and

$$\frac{\partial^2 W^{\mathrm{el}}_{\mathrm{3D}}}{\partial \boldsymbol{E}\partial \boldsymbol{E}} = \frac{2}{3}\mu^{\mathrm{el}}_{\mathrm{3D}}\left|\boldsymbol{C}_{\mathrm{e}}\right|^{-\frac{1}{3}}\left[-\left(\boldsymbol{C}_{\mathrm{gr}}^{-1}\otimes\boldsymbol{C}^{-1}+\boldsymbol{C}^{-1}\otimes\boldsymbol{C}_{\mathrm{gr}}^{-1}\right) +\frac{1}{3}\mathrm{tr}\left(\boldsymbol{C}_{\mathrm{e}}\right)\boldsymbol{C}^{-1}\otimes\boldsymbol{C}^{-1}+\mathrm{tr}\left(\boldsymbol{C}_{\mathrm{e}}\right)\boldsymbol{C}^{-1}\odot\boldsymbol{C}^{-1}\right] \tag{51}$$

with $\boldsymbol{C}_{\mathrm{gr}} = \boldsymbol{F}^{\mathrm{T}}_{\mathrm{gr}}\boldsymbol{F}_{\mathrm{gr}}$ and the standard Cauchy–Green deformation tensor $\boldsymbol{C} = \boldsymbol{F}^{\mathrm{T}}\boldsymbol{F}$. The volumetric penalty term ensuring an isochoric elastic deformation of elastin leads to

$$\frac{\partial W^{\mathrm{el}}_{\mathrm{vol}}}{\partial \boldsymbol{E}} = 2\varepsilon\left|\boldsymbol{C}_{\mathrm{e}}\right|^{1/2}\left(\left|\boldsymbol{C}_{\mathrm{e}}\right|^{1/2}-1\right)\boldsymbol{C}^{-1} \tag{52}$$

and

$$\frac{\partial^2 W_{\text{vol}}^{\text{el}}}{\partial \boldsymbol{E} \partial \boldsymbol{E}} = 4\varepsilon \left|\boldsymbol{C}_{\text{e}}\right|^{1/2} \left[\left(\left|\boldsymbol{C}_{\text{e}}\right|^{1/2} - \frac{1}{2} \right) \boldsymbol{C}^{-1} \otimes \boldsymbol{C}^{-1} - \left(\left|\boldsymbol{C}_{\text{e}}\right|^{1/2} - 1 \right) \boldsymbol{C}^{-1} \odot \boldsymbol{C}^{-1} \right]. \tag{53}$$

The above equations (42), (44), (46), (48), (50), and (52) can directly be used in (9) to compute for given reference mass densities of the different constituents the second Piola–Kirchhoff stress at each point. The elasticity tensor of the constrained mixture that is required to compute the tangent stiffness matrix is, as usual, given by

$$\mathbb{C} = \frac{\partial \boldsymbol{S}}{\partial \boldsymbol{E}} = \frac{\partial^2 \Psi}{\partial \boldsymbol{E} \partial \boldsymbol{E}} = \sum_{i=1}^{n} \varrho_0^i \frac{\partial^2 W^i}{\partial \boldsymbol{E} \partial \boldsymbol{E}}. \tag{54}$$

where the second derivatives of the strain energies W^i can be computed using (43), (45), (47), (49), (51), and (53).

Appendix 3

Time integration of growth and remodeling in a finite element scheme requires updating in each time step both the inelastic deformation gradients $\boldsymbol{F}_{\text{gr}}^i$ at each Gauss point and the total displacements at each node. For our homogenized constrained mixture model, we tested two time integration schemes. In both we discretized time by a series of n discrete points in time $t = t^1, \ldots, t^n$ with $t^1 = 0$. The distance between two subsequent points in time was $\Delta t = t^{k+1} - t^k$. The total deformation gradient and inelastic deformation gradients at time t^k are $\boldsymbol{F}\left(t^k\right)$ and $\boldsymbol{F}_{\text{gr}}^i\left(t^k\right)$, respectively.

In the first, explicit time integration scheme we compute at time point t^k from a given total deformation gradient $\boldsymbol{F}\left(t^k\right)$ and inelastic deformation gradient $\boldsymbol{F}_{\text{gr}}^i\left(t^k\right)$ via the evolution equations (16)–(18) and (25) the rate $\dot{\boldsymbol{F}}_{\text{gr}}^i$ and approximate $\boldsymbol{F}_{\text{gr}}^i\left(t^{k+1}\right) = \boldsymbol{F}_{\text{gr}}^i\left(t^k\right) + \dot{\boldsymbol{F}}_{\text{gr}}^i\left(\boldsymbol{F}_{\text{gr}}^i\left(t^k\right), \boldsymbol{F}\left(t^k\right)\right) \Delta t$. Then we compute from this $\boldsymbol{F}_{\text{gr}}^i\left(t^{k+1}\right)$, using the balance of linear momentum (4) and the equations provided in Appendix 2, iteratively the mechanical equilibrium configuration at t^{k+1}, that is, $\boldsymbol{F}\left(t^{k+1}\right)$.

In the second, implicit time integration scheme we first compute an estimate of $\boldsymbol{F}_{\text{gr}}^i\left(t^{k+1}\right)$ by solving (iteratively) the implicit equation $\boldsymbol{F}_{\text{gr}}^i\left(t^{k+1}\right) = \boldsymbol{F}_{\text{gr}}^i\left(t^k\right) + \dot{\boldsymbol{F}}_{\text{gr}}^i\left(\boldsymbol{F}_{\text{gr}}^i\left(t^{k+1}\right), \boldsymbol{F}\left(t^k\right)\right) \Delta t$, where $\dot{\boldsymbol{F}}_{\text{gr}}^i$ is again computed using the evolution equations (16)–(18) and (25). Subsequently, we compute an estimate of the mechanical equilibrium configuration at time t^{k+1}, that is, $\boldsymbol{F}\left(t^{k+1}\right)$, by solving (iteratively) the balance of linear momentum (4), using the equations provided in Appendix 2. Then we compute an updated estimate of $\boldsymbol{F}_{\text{gr}}^i\left(t^{k+1}\right)$ based on our estimate of $\boldsymbol{F}\left(t^{k+1}\right)$ instead of $\boldsymbol{F}\left(t^k\right)$. This updated estimate of $\boldsymbol{F}_{\text{gr}}^i\left(t^{k+1}\right)$ is used to update also the estimate of $\boldsymbol{F}\left(t^{k+1}\right)$, and these updates of $\boldsymbol{F}_{\text{gr}}^i\left(t^{k+1}\right)$ and $\boldsymbol{F}\left(t^{k+1}\right)$ are iterated until $\boldsymbol{F}$ has converged.

Both in the explicit and implicit time integration scheme, the balance of linear momentum (4) has to be solved iteratively to compute $\boldsymbol{F}\left(t^{k+1}\right)$. To this end, Newton–Raphson iterations can be used. Note that the tangent stiffness matrix used in these iterations can be directly based on (54) in Appendix 2 in an explicit time integration scheme. In an implicit time integration scheme, however, to obtain quadratic convergence of the Newton–Raphson iterations, one has to add to the second derivatives of the strain energies in (54) an additional fourth-order tensor accounting for expected changes of the inelastic deformation gradient through the iterations of the displacement field. This additional fourth-order tensor can be computed for the ith constituent as

$$\mathbb{C}_{\text{implicit}}^i = \left[\frac{\partial}{\partial \boldsymbol{F}_{\text{gr}}^i} \left(\frac{\partial W^i}{\partial \boldsymbol{E}} \right) \right] : \frac{\partial \boldsymbol{F}_{\text{gr}}^i}{\partial \boldsymbol{E}}. \tag{55}$$

The computational results shown in Sect. 4 were all computed using the above-described implicit time integration scheme. Note that explicit and implicit refer in the above discussion to the update of the inelastic deformation gradient only. The balance of linear momentum is always obtained via the solution of an implicit system of equations.

References

Albero AB, Ehret AE, Böl M (2014) A new approach to the simulation of microbial biofilms by a theory of fluid-like pressure-restricted finite growth. Comput Methods Appl Mech Eng 272:271–289

Ambrosi D, Guana F (2007) Stress-modulated growth. Math Mech Solids 12(3):319–342

Ambrosi D, Mollica F (2004) The role of stress in the growth of a multicell spheroid. J Math Biol 48(5):477–99

Ambrosi D et al (2011) Perspectives on biological growth and remodeling. J Mech Phys Solids 59(4):863–883

Baek S, Rajagopal KR, Humphrey JD (2006) A theoretical model of enlarging intracranial fusiform aneurysms. J Biomech Eng 128(1):142–9

Ben Amar M, Goriely A (2005) Growth and instability in elastic tissues. J Mech Phys Solids 53(10):2284–2319

Böl M, Bolea Albero A (2014) On a new model for inhomogeneous volume growth of elastic bodies. J Mech Behav Biomed Mater 29:582–593

Creative Commons License (2016) CC BY-SA 4.0. http://creativecommons.org/licenses/by-sa/4.0/

Cyron CJ, Humphrey JD (2014) Vascular homeostasis and the concept of mechanobiological stability. Int J Eng Sci 85:203–223

Cyron CJ, Humphrey JD (2016) Growth and remodeling of load-bearing biological soft tissues. Meccanica 1–20. doi:10.1007/s11012-016-0472-5

Cyron CJ, Wilson JS, Humphrey JD (2014) Mechanobiological stability: a new paradigm to understand the enlargement of aneurysms? J R Soc Interface 11(100):20140680

Cyron CJ, Wilson JS, Humphrey JD (2016a) Constitutive formulations for soft tissue growth and remodeling. In: Payan Y, Ohayon J (eds) Biomechanics of living organs: hyperelastic constitutive laws for finite element modeling. Elsevier, Amsterdam (forthcoming)

Cyron CJ, Aydin RC, Humphrey JD (2016b) A homogenized constrained mixture (and mechanical analog) model for growth and remodeling of soft tissue. Biomech Model Mechanobiol 15(6):1389–1403

de Souza Neto EA et al (1996) Design of simple low order finite elements for large strain analysis of nearly incompressible solids. Int J Solids Struct 33(20):3277–3296

Eriksson TSE et al (2014) Modelling volumetric growth in a thick walled fibre reinforced artery. J Mech Phys Solids 73:134–150

Etminan N et al (2014) Age of collagen in intracranial saccular aneurysms. Stroke 45(6):1757–63

Figueroa CA et al (2009) A computational framework for fluid-solid-growth modeling in cardiovascular simulations. Comput Methods Appl Mech Eng 198(45–46):3583–3602

Gee MW, Förster C, Wall WA (2010) A computational strategy for prestressing patient-specific biomechanical problems under finite deformation. Int J Numer Methods Biomed Eng 26(1):52–72

Geest JPV, Sacks MS, Vorp DA (2004) Age dependency of the biaxial biomechanical behavior of human abdominal aorta. J Biomech E 126(6):815–822

Göktepe S et al (2010) A multiscale model for eccentric and concentric cardiac growth through sarcomerogenesis. J Theor Biol 265(3):433–442

Goriely A, Vandiver R (2010) On the mechanical stability of growing arteries. IMA J Appl Math 75:549–570

Grytsan A, Watton PN, Holzapfel GA (2015) A thick-walled fluid-solid-growth model of abdominal aortic aneurysm evolution: application to a patient-specific geometry. J Biomech Eng 137(3):031008

Grytz R et al (2012) Lamina cribrosa thickening in early glaucoma predicted by a microstructure motivated growth and remodeling approach. Mech Mater 44:99–109

Holzapfel G (2000) Nonlinear solid mechanics: a continuum approach for engineering. Wiley, New York

Holzapfel G, Gasser T, Ogden R (2000) A new constitutive framework for arterial wall mechanics and a comparative study of material models. J Elast Phys Sci Solids 61(1–3):1–48

Holzapfel GA et al (2015) Modelling non-symmetric collagen fibre dispersion in arterial walls. J R Soc Interface 12(106):20150188

Humphrey JD (1999) Remodeling of a collagenous tissue at fixed lengths. J Biomech Eng 121(6):591–7

Humphrey JD, Rajagopal KR (2002) A constrained mixture model for growth and remodeling of soft tissues. Math Models Methods Appl Sci 12(03):407–430

Karšaj I, Sorić J, Humphrey JD (2010) A 3-D framework for arterial growth and remodeling in response to altered hemodynamics. Int J Eng Sci 48(11):1357–1372

Kroon M, Holzapfel GA (2007) A model for saccular cerebral aneurysm growth by collagen fibre remodelling. J Theor Biol 247(4):775–787

Kroon M, Holzapfel GA (2008) Modeling of saccular aneurysm growth in a human middle cerebral artery. J Biomech Eng 130(5):051012

Matsumoto T, Hayashi K (1996) Response of arterial wall to hypertension and residual stress. In: Hayashi K, Kamiya A, Ono K (eds) Biomechanics. Springer, Berlin, pp 93–119

Menzel A, Kuhl E (2012) Frontiers in growth and remodeling. Mech Res Commun 42:1–14

Murtada S-I, Holzapfel GA (2014) Investigating the role of smooth muscle cells in large elastic arteries: a finite element analysis. J Theor Biol 358:1–10

Murtada S-I, Kroon M, Holzapfel GA (2010a) Modeling the dispersion effects of contractile fibers in smooth muscles. J Mech Phys Solids 58(12):2065–2082

Murtada S-I, Kroon M, Holzapfel GA (2010b) A calcium-driven mechanochemical model for prediction of force generation in smooth muscle. Biomech Model Mechanobiol 9(6):749–762

Murtada SC, Arner A, Holzapfel GA (2012) Experiments and mechanochemical modeling of smooth muscle contraction: significance of filament overlap. J Theor Biol 297:176–86

Murtada S-I et al (2015) Adaptation of active tone in the mouse descending thoracic aorta under acute changes in loading. Biomech Model Mechanobiol 15(3):589–592

Nissen R, Cardinale GJ, Udenfriend S (1978) Increased turnover of arterial collagen in hypertensive rats. Proc Natl Acad Sci USA 75(1):451–453

O'Connell MK et al (2008) The three-dimensional micro-and nanostructure of the aortic medial lamellar unit measured using 3D confocal and electron microscopy imaging. Matrix Biology 27(3):171–181

Rajagopal K, Wineman A (1992) A constitutive equation for nonlinear solids which undergo deformation induced microstructural changes. Int J Plast 8(4):385–395

Rodriguez EK, Hoger A, McCulloch AD (1994) Stress-dependent finite growth in soft elastic tissues. J Biomech 27(4):455–67

Taber LA, Eggers DW (1996) Theoretical study of stress-modulated growth in the aorta. J Theor Biol 180(4):343–357

Valentin A et al (2009) Complementary vasoactivity and matrix remodelling in arterial adaptations to altered flow and pressure. J R Soc Interface 6(32):293–306

Valentín A, Humphrey J, Holzapfel GA (2013) A finite element-based constrained mixture implementation for arterial growth, remodeling, and adaptation: theory and numerical verification. Int J Numer Methods Biomed Eng 29(8):822–849

Vandiver R, Goriely A (2009) Morpho-elastodynamics: the long-time dynamics of elastic growth. J Biol Dyn 3(2–3):180–195

Virag L et al (2015) A computational model of biochemomechanical effects of intraluminal thrombus on the enlargement of abdominal aortic aneurysms. Ann Biomed Eng 43(12):2852–2867

Watton PN, Hill NA (2009) Evolving mechanical properties of a model of abdominal aortic aneurysm. Biomech Model Mechanobiol 8(1):25–42

Watton P, Hill N, Heil M (2004) A mathematical model for the growth of the abdominal aortic aneurysm. Biomech Model Mechanobiol 3(2):98–113

Watton PN et al (2011) Modelling evolution and the evolving mechanical environment of saccular cerebral aneurysms. Biomech Model Mechanobiol 10(1):109–32

Wilson JS, Baek S, Humphrey JD (2012) Importance of initial aortic properties on the evolving regional anisotropy, stiffness and wall thickness of human abdominal aortic aneurysms. J R Soc Interface 9(74):2047–58

Wilson JS, Baek S, Humphrey JD (2013) Parametric study of effects of collagen turnover on the natural history of abdominal aortic aneurysms. Proc R Soc A 469(2150):20120556

Zeinali-Davarani S, Baek S (2012) Medical image-based simulation of abdominal aortic aneurysm growth. Mech Res Commun 42:107–117

Zeinali-Davarani S, Sheidaei A, Baek S (2011) A finite element model of stress-mediated vascular adaptation: application to abdominal aortic aneurysms. Comput Methods Biomech Biomed Eng 14(9):803–817

Zöllner AM et al (2012) Stretching skeletal muscle: chronic muscle lengthening through sarcomerogenesis. PLoS ONE 7(10):e45661

Zöllner AM et al (2013) Growth on demand: reviewing the mechanobiology of stretched skin. J Mech Behav Biomed Mater 28:495–509

B Full Text: Paper B

SPRINGER NATURE LICENSE
TERMS AND CONDITIONS

Mar 12, 2019

This Agreement between Mr. Fabian Braeu ("You") and Springer Nature ("Springer Nature") consists of your license details and the terms and conditions provided by Springer Nature and Copyright Clearance Center.

License Number	4527450186641
License date	Feb 14, 2019
Licensed Content Publisher	Springer Nature
Licensed Content Publication	Biomechanics and Modeling in Mechanobiology
Licensed Content Title	Anisotropic stiffness and tensional homeostasis induce a natural anisotropy of volumetric growth and remodeling in soft biological tissues
Licensed Content Author	F. A. Braeu, R. C. Aydin, Christian J. Cyron
Licensed Content Date	Jan 1, 2018
Type of Use	Thesis/Dissertation
Requestor type	academic/university or research institute
Format	print and electronic
Portion	full article/chapter
Will you be translating?	no
Circulation/distribution	<501
Author of this Springer Nature content	yes
Title	Multiscale Modeling of Vascular Growth and Remodeling in Aneurysm
Institution name	Institute for Computational Mechanics, Technical University of Munich, Garching, Germany
Expected presentation date	Apr 2019
Requestor Location	Mr. Fabian Braeu Paracelsusstr. 12a München, 80939 Germany Attn: Mr. Fabian Braeu
Customer VAT ID	DE811193231
Billing Type	Invoice
Billing Address	Mr. Fabian Braeu Paracelsusstr. 12a München, Germany 80939 Attn: Mr. Fabian Braeu
Total	0.00 EUR
Terms and Conditions	

Springer Nature Terms and Conditions for RightsLink Permissions

Springer Nature Customer Service Centre GmbH (the Licensor) hereby grants you a non-exclusive, world-wide licence to reproduce the material and for the purpose and requirements specified in the attached copy of your order form, and for no other use, subject to the conditions below:

1. The Licensor warrants that it has, to the best of its knowledge, the rights to license reuse of this material. However, you should ensure that the material you are requesting is original to the Licensor and does not carry the copyright of another entity (as credited in the published version).

   If the credit line on any part of the material you have requested indicates that it was reprinted or adapted with permission from another source, then you should also seek permission from that source to reuse the material.

2. Where **print only** permission has been granted for a fee, separate permission must be obtained for any additional electronic re-use.

3. Permission granted **free of charge** for material in print is also usually granted for any electronic version of that work, provided that the material is incidental to your work as a whole and that the electronic version is essentially equivalent to, or substitutes for, the print version.

4. A licence for 'post on a website' is valid for 12 months from the licence date. This licence does not cover use of full text articles on websites.

5. Where **'reuse in a dissertation/thesis'** has been selected the following terms apply: Print rights of the final author's accepted manuscript (for clarity, NOT the published version) for up to 100 copies, electronic rights for use only on a personal website or institutional repository as defined by the Sherpa guideline (www.sherpa.ac.uk/romeo/).

6. Permission granted for books and journals is granted for the lifetime of the first edition and does not apply to second and subsequent editions (except where the first edition permission was granted free of charge or for signatories to the STM Permissions Guidelines http://www.stm-assoc.org/copyright-legal-affairs/permissions/permissions-guidelines/), and does not apply for editions in other languages unless additional translation rights have been granted separately in the licence.

7. Rights for additional components such as custom editions and derivatives require additional permission and may be subject to an additional fee. Please apply to Journalpermissions@springernature.com/bookpermissions@springernature.com for these rights.

8. The Licensor's permission must be acknowledged next to the licensed material in print. In electronic form, this acknowledgement must be visible at the same time as the figures/tables/illustrations or abstract, and must be hyperlinked to the journal/book's homepage. Our required acknowledgement format is in the Appendix below.

9. Use of the material for incidental promotional use, minor editing privileges (this does not include cropping, adapting, omitting material or any other changes that affect the meaning, intention or moral rights of the author) and copies for the disabled are permitted under this licence.

10. Minor adaptations of single figures (changes of format, colour and style) do not require the Licensor's approval. However, the adaptation should be credited as shown in Appendix below.

Biomechanics and Modeling in Mechanobiology
https://doi.org/10.1007/s10237-018-1084-x

ORIGINAL PAPER

Anisotropic stiffness and tensional homeostasis induce a natural anisotropy of volumetric growth and remodeling in soft biological tissues

F. A. Braeu[1] · R. C. Aydin[1] · Christian J. Cyron[2,3]

Received: 15 March 2018 / Accepted: 16 October 2018
© Springer-Verlag GmbH Germany, part of Springer Nature 2018

Abstract
Growth in soft biological tissues in general results in anisotropic changes of the tissue geometry. It remains a key challenge in biomechanics to understand, quantify, and predict this anisotropy. In this paper, we demonstrate that anisotropic tissue stiffness and the well-known mechanism of tensional homeostasis induce a natural anisotropy of the geometric changes resulting from volumetric growth in soft biological tissues. As a rule of thumb, this natural anisotropy makes differential tissue volume elements dilate mainly in the direction(s) of lowest stiffness. This simple principle is shown to explain the experimentally observed growth behavior in a host of different soft biological tissues without relying on any additional heuristic assumptions or quantities (such as ad hoc defined growth tensors).

Keywords Growth and remodeling · Volumetric · Mechanobiology · Aneurysm · Computational modeling · Anisotropic growth

1 Introduction

In biological tissues, one frequently observes growth, that is, production or degradation of tissue mass along with directly associated changes of the tissue geometry. Growth can be divided into two categories. Surface growth results from deposition of mass on external or also internal surfaces of tissues or organs. Examples are the growth of biofilms, horns, nails, hair, or seashells (Skalak et al. 1997; Soleimani et al. 2016). By contrast, in volumetric growth material is deposited throughout the whole volume of tissues. For example, growth of collagenous soft tissues results from collagen production by smooth muscle cells or fibroblasts distributed all over the volume of, for example, blood vessels or tendons (Humphrey et al. 2014). If mass is produced in a differential tissue volume element, the volume element in general has to expand in order to accommodate the additional mass. Therefore, volumetric growth is usually modeled as a local inelastic dilatation (Rodriguez et al. 1994) of differential tissue volume elements. This dilatation is in general anisotropic (i.e., unequal in different spatial directions) as illustrated also in Fig. 1. Its anisotropy plays a key role in soft tissue biomechanics. For example, it enables arteries to increase wall thickness under increased blood pressure. Without such ability, arteries might be prone to rupture in particular in early life where the shape of and load on tissues and organs change continuously and considerably. For developing theoretical and computational models of volumetric growth in soft biological tissues, it is thus essential to understand and quantify the factors governing the anisotropy of the geometric changes induced by growth.

Theoretical and computational models of the growth and remodeling of living soft tissues have attracted rapidly increasing attention over the last decade (Goriely and Vandiver 2010; Karšaj et al. 2010; Grytz et al. 2011; 2012; Valentín et al. 2013; Grytsan et al. 2015; Lindquist Liljeqvist et al. 2016; Braeu et al. 2017; Virag et al. 2017). Recently, there have been attempts to inform such models by experiments measuring the in general anisotropic changes of tissue geometry during growth (Tsamis et al. 2012).

✉ Christian J. Cyron
christian.cyron@tuhh.de

1 Institute for Computational Mechanics, Technical University of Munich, Munich, Germany

2 Institute of Continuum Mechanics and Materials Mechanics, Hamburg University of Technology, Eissendorfer Strasse 42, 21073 Hamburg, Germany

3 Institute of Materials Research, Materials Mechanics, Helmholtz-Zentrum Geesthacht, Geesthacht, Germany

Published online: 09 November 2018

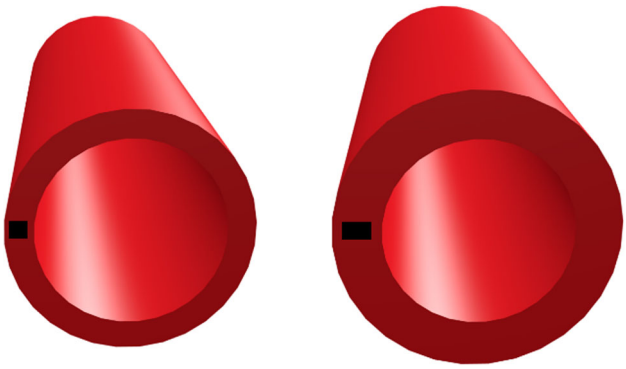

Fig. 1 If blood pressure in an artery (left) is increased, the wall thickens (right). Thereby, differential volume elements (black) dilate not isotropically (i.e., equally in circumferential direction and wall thickness direction) but anisotropically (i.e., mainly in wall thickness direction). This way, differential volume elements with initial square cross section become rectangular with an elongated side in wall thickness direction. So far, the origin of this anisotropy and similar other observations related to volumetric growth in soft biological tissues remain poorly understood

However, the natural difficulties to obtain such information in vivo limit the application of such approaches so far significantly. Therefore, theories have been developed on how anisotropic shape changes of differential volume elements might be defined in the absence of specific experimental information. DiCarlo and Quiligotti (2002) and Ambrosi and Guana (2007) proposed the hypothesis that they might be governed by an Eshelby-like stress tensor. Despite its theoretical elegance, this approach is currently not widely used, possibly because of its difficulties to explain without further assumptions the experimentally observed growth behavior in important situations, for example, in blood vessels in hypertension. As a consequence, currently most theoretical and computational models of volumetric growth of soft living tissues still rely on mainly heuristic assumptions about the anisotropy of the geometric changes resulting from the growth process. These assumptions are usually simply made such that reasonable results are obtained in the end. Obviously, this prevents truly predictive simulations. Moreover, simplistic assumptions such as the one of isotropic growth are widely used but render for many relevant applications results that are in strong disagreement with experimental observations as pointed out in (Braeu et al. 2017).

It is thus widely acknowledged that there remains a pressing need for a theory that can predict the anisotropy of the changes of the tissue geometry resulting from volumetric growth in soft biological tissues in good agreement with experimental observations and on the basis of some fundamental mathematical or mechanical ideas (Ambrosi et al. 2011). Such a theory could significantly help to understand the geometric evolution of living organisms during morphogenesis early in life as well as the mechanobiological adaptation processes in adult tissues, for example, in aneurysmatic or hypertensive blood vessels (Eriksson et al. 2014; Sáez et al. 2014; Grytsan et al. 2015, 2017, Lin et al. 2017). Moreover, it could provide a powerful tool for the development of new and efficient methods in tissue engineering, a field where volumetric growth processes are of particular importance. Finally, it could be key to understand the interplay between mechanical and chemical factors (e.g., genetic factors) governing soft tissue growth.

In this paper, we examine the problem of volumetric growth specifically in soft biological tissues subject to tensional homeostasis. Tensional homeostasis is a mechanism that relies on a coupling between mechanics and biology and seeks to establish or maintain in tissues some preferred mechanical state (Cyron and Humphrey 2017). It can be expected to govern growth and remodeling in load-bearing soft collagenous tissues such as blood vessels, tendons, the bladder, or stomach as well as general connective tissue. Osseous tissues are not considered herein. Also nervous tissues are not considered here because the role of tensional homeostasis in such tissues is unclear to date.

In Sect. 2, we first briefly delineate a general mathematical model of volumetric growth and remodeling in load-bearing soft biological tissues, largely in line with previous work. In Sect. 3, we discuss the micromechanical and physiological foundations of growth and remodeling in soft biological tissues, in particular the production and degradation of tissue mass and the reorganization of the tissue microstructure following the principle of tensional homeostasis. In Sect. 4, we demonstrate that anisotropic tissue stiffness and the mechanism of tensional homeostasis, which has been observed to be a fundamental property of various biological tissues, induce a natural anisotropy of volumetric growth in load-bearing soft biological tissues. As a rule of thumb, this natural growth anisotropy will make differential tissue volume elements dilate mainly in the direction(s) of lowest stiffness during volumetric growth. In Sect. 5, we demonstrate how these ideas give rise to a new type of computational model that can capture volumetric growth and remodeling in a host of soft biological tissues without any ad hoc definition of a growth tensor.

2 Continuum mechanics

Relying on the general theory of nonlinear continuum mechanics, we model soft biological tissues as mechanical bodies whose material points $\boldsymbol{X} \in B_0$ are mapped at times $t \geq 0$ by a deformation to their current position $\boldsymbol{x}(t, \boldsymbol{X}) \in B(t)$, see also Fig. 2. The Jacobi matrix of this deformation is the so-called deformation gradient

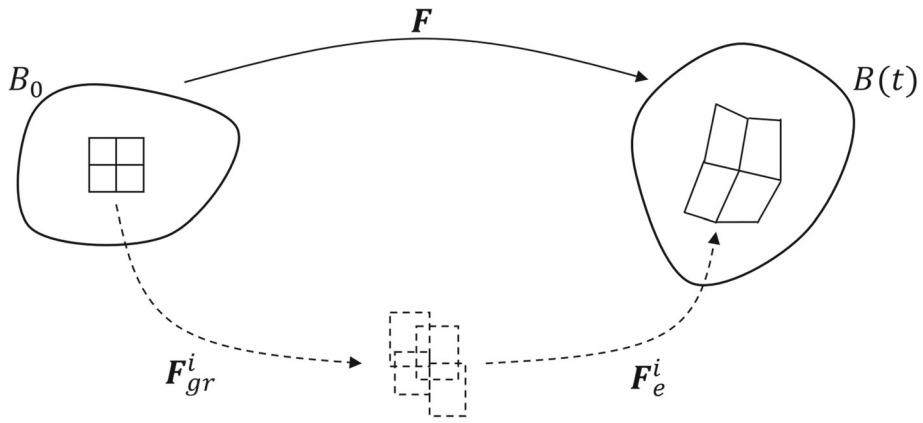

Fig. 2 Illustration of the kinematics of volumetric growth and remodeling. The deformation gradient $\boldsymbol{F}$ can be split at each point into an inelastic part $\boldsymbol{F}^i_{gr}$ and an elastic part $\boldsymbol{F}^i_e$. The inelastic $\boldsymbol{F}^i_{gr}$ accounts for inelastic changes of the stress-free configuration of individual constituents in differential volume elements that may be associated with growth and remodeling. Volume elements in the reference configuration B_0 are deformed by $\boldsymbol{F}^i_{gr}$ into an intermediate configuration which is in general not geometrically compatible so that neighboring volume elements may overlap or form gaps. The elastic deformation gradient $\boldsymbol{F}^i_e$ applied to each differential volume element ensures that the total deformation gradient field is geometrically compatible (i.e., neighboring differential volume elements fit together without gaps or overlaps) and satisfies mechanical equilibrium in the current configuration $B(t)$

$$\boldsymbol{F} = \frac{\partial \boldsymbol{x}}{\partial \boldsymbol{X}}. \tag{1}$$

The set of material points B_0 is called the reference configuration, and we note that this configuration need not be stress-free in general. Herein, we assume without loss of generality that the reference configuration is always identical to the initial configuration, that is, $B_0 = B(t = 0)$. Differential volume elements $\mathrm{d}V$ in the reference configuration B_0 are deformed into volume elements

$$\mathrm{d}v = |\boldsymbol{F}|\mathrm{d}V \tag{2}$$

in the current configuration $B(t)$ where $|\boldsymbol{F}|$ is the determinant of $\boldsymbol{F}$. Herein, we model biological tissues as so-called constrained mixtures. That is, we assume that the material in each volume element is a mixture of n constituents. For the ith constituent, the deformation gradient can be split into an inelastic part $\boldsymbol{F}^i_{gr}$ and an elastic part $\boldsymbol{F}^i_e$ such that

$$\boldsymbol{F} = \boldsymbol{F}^i_e \boldsymbol{F}^i_{gr}. \tag{3}$$

Here, the inelastic part $\boldsymbol{F}^i_{gr}$ characterizes how the material of the ith constituent in a volume element in the reference configuration would deform if it were cut out from its surrounding continuum and additionally separated from the other constituents in the mixture and thus not subject to any loading or confinement any longer (cf. Fig. 2). $\boldsymbol{F}^i_{gr}$ captures inelastic changes of the stress-free configuration of the ith tissue constituent due to growth and remodeling (Rodriguez et al. 1994; Ambrosi and Guana 2007; Zöllner et al. 2012; Braeu et al. 2017; Grytsan et al. 2017; Kehl and Gee 2017; Truster and Masud 2017). The general idea to use an inelastic part of the deformation gradient to this end goes back to (Rodriguez et al. 1994), which introduced Eq. (3) for the simple special case $n=1$ so that only a single elastic and inelastic deformation tensor was required for the whole material. In general, the elastic state of the tissue material at each point is defined by $\boldsymbol{F}$ and $\boldsymbol{F}^i_{gr}$. In a given configuration, the elastic part of the deformation gradient $\boldsymbol{F}^i_e$ may be different among the individual constituents. However, we yet assume that all constituents deform together, that is, all experience the same deformation increments over time and thus form a constrained mixture.

Volumetric growth and remodeling in biological tissues happens slowly (typically on a time scale of hours, days, or months) and is thus modeled here as a quasi-static process so that the balance of linear momentum is

$$\mathrm{div}(\boldsymbol{P}) + \varrho_0 \boldsymbol{b}_0 = 0 \tag{4}$$

with the total referential mass density of the mixture

$$\varrho_0 = \sum_{i=1}^{n} \varrho_0^i, \tag{5}$$

the mass density per unit reference volume of the ith constituent ϱ_0^i, the body force vector $\boldsymbol{b}_0$ (per unit mass) and the first Piola-Kirchhoff stress tensor

$$\boldsymbol{P} = \frac{\partial \Psi}{\partial \boldsymbol{F}} \tag{6}$$

where

$$\Psi = \sum_{i=1}^{n} \varrho_0^i W^i \left(\boldsymbol{F}_e^i \right) + \Psi^{\#} \tag{7}$$

is the strain energy of the constrained mixture per unit volume. W^i is the strain energy of the ith constituent per unit mass, which is assumed to depend only on its elastic deformation, that is, on $\boldsymbol{F}_e^i$. The special strain energy $\Psi^{\#}$ (per unit volume) is accounting for excluded volume interactions between the individual mass increments and microstructural elements forming the constrained mixture. Such interactions are often assumed to ensure in practice a (nearly) constant spatial density ϱ of all the constituents together at any time. With Eq. (4.6) from (Holzapfel 2000), this assumption is equivalent to

$$dv = \frac{\varrho_0(\boldsymbol{X}, t)}{\varrho} \mathrm{dV} \tag{8}$$

or, using (2) in (8),

$$\varrho = \varrho_0 / |\boldsymbol{F}|. \tag{9}$$

Therefore, $\Psi^{\#}$ can be modeled by a penalty-type energy

$$\Psi^{\#}(t) = \frac{\varepsilon}{2} \left(|\boldsymbol{F}(t)| - \frac{\varrho_0(t)}{\varrho} \right)^2 \tag{10}$$

with some very large ε. We note that $\Psi^{\#}$ in (7) is an important difference between the approach introduced herein and most previous work. Below we will demonstrate that one of its nontrivial consequences is that it implicitly defines the anisotropy of the geometry changes resulting from volumetric growth, which has to be defined so far mainly on the basis of heuristic assumptions.

If ϱ_0^i and $\boldsymbol{F}_{gr}^i$ are known, the unknown current deformation field $\boldsymbol{x}$ can be computed immediately at any point in time using (1), (3) and (5)–(7) in (4) so that the balance of linear momentum (4) can be written completely in terms of the unknown deformation field $\boldsymbol{x}$, yielding in d dimensions for the d unknown components of $\boldsymbol{x}$ a system of d coupled differential equations. The crucial difficulty is thus determining $\boldsymbol{F}_{gr}^i$ and ϱ_0^i at each point in time.

To determine ϱ_0^i, one typically assumes a known initial value and an evolution equation of the type

$$\dot{\varrho}_0^i = \varrho_0^i \boldsymbol{k}_\sigma^i : \Delta \boldsymbol{G}^i. \tag{11}$$

Here, the overdot denotes a time derivative, $\Delta \boldsymbol{G}^i$ is a mass production stimulus, for example, the difference between the current stress or stretch and some homeostatic target value [cf. also Eq. (7) in (Cyron and Humphrey 2017)]. The colon in (11) denotes a double contraction product, and $\boldsymbol{k}_\sigma^i$ is a second-order gain tensor. In the literature, different choices for $\Delta \boldsymbol{G}^i$ and $\boldsymbol{k}_\sigma^i$ can be found. While the exact parameter values used for these quantities differ significantly, there is yet a high overall similarity at least between the functional forms used.

The situation is much more involved for $\boldsymbol{F}_{gr}^i$, for which even the general functional form of the evolution equations and $\boldsymbol{F}_{gr}^i$ itself remain highly controversial to date. Helping to overcome this controversy can be considered a primary objective of this paper.

Remark 1 The number of constituents n depends on the mathematical model of growth and remodeling. In the recently developed homogenized constrained mixture models (Cyron et al. 2016; Braeu et al. 2017) or also in the recruitment stretch models following (Watton et al. 2004; Eriksson et al. 2014; Grytsan et al. 2015), n can be understood as the number of structurally different constituents such as elastin, smooth muscle, and collagen (or also different collagen fiber families) that can be distinguished in a biological tissue. By contrast, when following the constrained mixture models based on multi-network theory, which were introduced by Humphrey and Rajagopal (2002) and further used, for example, by Wilson et al. (2012, 2013), n in Eq. (4) should rather be understood as the number of mass increments with different stress-free natural configurations present in each differential volume element. Recalling that constrained mixture models based on multi-network theory keep track of differential mass increments deposited during each differential time interval, n is for these models in theory infinite. In computational implementations where time is discretized by a finite number of points in time, also n is finite but in practice often very large. We note that the ideas developed herein can be applied to any of the above-mentioned models by simply incorporating in these models an interaction energy $\Psi^{\#}$ as in (7) and defining the evolution of $\boldsymbol{F}_{gr}^i$ according to the discussion below. Thereby, the exact form of $\Psi^{\#}$ is largely irrelevant as long as it ensures a constant spatial density of the material (cf. (9)) sufficiently accurately.

3 Physiological foundations

To overcome the controversy how to compute $\boldsymbol{F}_{gr}^i$, we first briefly recall some physiological foundations of growth and remodeling. Noting the partially inconsistent nomenclature used in the literature, we start with a few definitions.

In the following, the term remodeling refers to an inelastic reorganization of the microstructure of the tissue. On the microscale, this reorganization is accomplished by biological cells rearranging the tissue fibers and altering also the inter-molecular connections within and between these fibers.

The altered microstructure of the tissue will in general result in altered stress-free configurations of tissue material increments, that is, in an altered $\boldsymbol{F}^i_{gr}$ in Eq. (3). Tissue mass, however, is by definition not changed by remodeling.

In opposition to that, the term of growth refers in the following to the process of production or degradation of tissue mass as well as any elastic deformation of the tissue that is directly associated with this process. By definition, growth is understood in the following as a process during which the inter-molecular connections defining the stress-free configuration of tissue material remain unaltered. That is, growth is understood herein as a process not affecting $\boldsymbol{F}^i_{gr}$ in Eq. (3). It may rather be imagined as a kind of elastic swelling.

In practice, growth and remodeling, in the sense of the above definitions, may occur simultaneously. For example, cells may produce additional collagen fibers. The additional fiber volume deposited thereby within the tissue will in the first place induce an elastic distension of the extant tissue (i.e., a kind of swelling). The fiber production and the associated elastic distension together are referred to as *growth* herein. However, while or directly after the cells are producing new fibers, they may also alter the inter-molecular connections in the tissue, thereby changing the stress-free state of tissue material increments and thus *remodeling* the tissue. Obviously, growth and remodeling in the sense of the above definitions are physically per se independent processes and are thus to be treated separately also in mathematical modeling.

Relying on these definitions, this paper is based on two major hypotheses, which we first briefly introduce and then support by references to experimental observations reported in the literature.

Hypothesis 1 *Remodeling is driven by tensional homeostasis only*. We assume that cells remodel the surrounding tissue so as to maintain or achieve a preferred state of mechanical stress, which is called homeostatic state. Moreover, we assume that this mechanism, which is also called tensional homeostasis, is the only driver of remodeling.

Hypothesis 2 *The spatial mass density remains constant during growth*. We assume that the packing density of the fibers in the tissue does not change during growth, that is, it does not change when additional fibers are produced or extant fibers are degraded.

It is well known that cells such as fibroblasts or smooth muscle cells have a natural tendency to reorganize surrounding collagen tissues toward a preferred mechanical state. To date, it is not yet fully understood which mechanical quantity exactly (e.g., stress, stretch or stiffness) defines the target of this process. However, there is at least considerable evidence that it might be the stress in the tissue fibers or at least some closely related quantity (Brown et al. 1998; Ezra et al. 2010). The reorganization of the tissue due to tensional homeostasis is well known to imply also a reorganization of inter-molecular connections (Cyron and Humphrey 2017) and changes thereby the stress-free configuration of differential volume elements. While numerous papers have reported the phenomenon of tensional homeostasis, to the authors' best knowledge nobody has reported so far that deposition or degradation of tissue mass is directly associated with a specific kind of reorganization of inter-molecular connections in the tissue. Therefore, following Ockham's lex parsimoniae, we assume Hypothesis 1.

Cyron et al. (2016), Braeu et al. (2017), Cyron and Aydin (2017) demonstrated that remodeling due to tensional homeostasis can be captured by an evolution of the inelastic part $\boldsymbol{F}^i_{gr}$ of the deformation gradient following the equation

$$\left[\frac{\dot{\varrho}^i_0(t)}{\varrho^i_0(t)}+\frac{1}{T^i}\right]\left[\boldsymbol{S}^i-\boldsymbol{S}^i_{pre}\right]=\left[2\frac{\partial \boldsymbol{S}^i}{\partial \boldsymbol{C}^i_e}:\left(\boldsymbol{C}^i_e\boldsymbol{L}^i_{gr}\right)\right]_{\boldsymbol{F}=const}. \tag{12}$$

Therefore, Hypothesis 1 directly translates into the assumption that we can describe the evolution of $\boldsymbol{F}^i_{gr}$ in (3) by (12). In (12), $\boldsymbol{L}^i_{gr}=\dot{\boldsymbol{F}}^i_{gr}\boldsymbol{F}^{i-1}_{gr}$ is the velocity gradient of the inelastic deformation gradient. T^i is the average survival time of tissue fibers and structural connections during the microstructural reorganization driven by tensional homeostasis. $\boldsymbol{S}^i$ is the second Piola-Kirchhoff stress of the ith constituent, and $\boldsymbol{C}^i_e=\boldsymbol{F}^{iT}_e\boldsymbol{F}^i_e$ its elastic Cauchy–Green deformation tensor with $\boldsymbol{F}^i_e$ from (3). $\boldsymbol{S}^i_{pre}$ is the second Piola-Kirchhoff target stress of tensional homeostasis.

Hypothesis 2 was inspired by experimental observations reported, among others, by Wolinsky and Glagov (1967) and Matsumoto and Hayashi (1996). It was observed that the thickness of soft tissues such as arteries under increased load seems to adopt so as to maintain a certain preferred level of tissue stress. If, for example, blood pressure in an artery is increased, also its wall thickness increases until the original level of wall stress is restored. On the other hand, the observations reported by Flynn et al. (2010) suggest that fiber degradation in soft tissues strongly depends on the microscopic fiber stretch. This stretch can therefore also be expected to be restored by tensional homeostasis. However, tensional homeostasis can restore both fiber stress and fiber stretch at the same time only if fiber density in the tissue remains (approximately) constant during growth. This conclusion directly motivates Hypothesis 2. Mathematically, Hypothesis 2 means that (8) and (9) hold not only in the sense of an incompressibility condition during elastic deformation but also more generally during volumetric growth where they enforce a constant spatial mass density over time.

Remark 2 As discussed above, there is considerable experimental evidence supporting Hypothesis 1 and Hypothesis

2, which was the reason for choosing these two hypotheses as starting points for the theoretical discussion in this paper. Nevertheless, one should keep in mind that the amount of experimental observations shedding light on the physiological foundations of growth and remodeling in soft biological tissues is still very limited and so the hypotheses proposed and conclusions drawn in this paper certainly still require significant further examination in the future.

Remark 3 An essential feature of nearly all mathematical models of volumetric growth in soft biological tissues published so far (Rodriguez et al. 1994; Ambrosi and Guana 2007; Zöllner et al. 2012; Braeu et al. 2017; Grytsan et al. 2017; Kehl and Gee 2017; Truster and Masud 2017) is the assumption that growth itself is directly associated with some inelastic reorganization of the tissue microstructure, represented by some growth tensor (i.e., a growth-induced inelastic part of the deformation gradient). This leads to an ongoing controversy how to define this growth tensor. The growth model proposed herein bypasses the definition of any inelastic growth tensor. The only inelastic part of the deformation gradient to be defined is the one related to remodeling for whose definition one can resort to rather general observations made in vitro on the remodeling of fibroblast-seeded tissue equivalents.

Remark 4 Braeu et al. (2017) suggested to capture the inelastic deformation by growth and remodeling via a multiplicative split $\boldsymbol{F}^i_{gr} = \boldsymbol{F}^i_r \boldsymbol{F}^i_g$ with $\boldsymbol{F}^i_g$ capturing the inelastic deformation by growth and $\boldsymbol{F}^i_r$ capturing the inelastic deformation by remodeling. Mathematically, the approach introduced herein can be considered a special case of this concept with the particularly simple choice $\boldsymbol{F}^i_g = \boldsymbol{I}$, where $\boldsymbol{I}$ is the identity tensor.

Remark 5 The idea of treating growth and remodeling separately, which is essential in this paper, was, in some form, proposed already earlier by DiCarlo et al. (2006) for osseous tissue and subsequently also by Cyron et al. (2016), Braeu et al. (2017) for soft tissue.

4 Natural anisotropy of volumetric growth and remodeling

The constant spatial mass density assumed in Hypothesis 2 implies that growth is always associated with a change of tissue volume, a kind of elastic swelling of differential volume elements. At the same time, Hypothesis 1 implies that growth is not directly associated with any inelastic change of the tissue microstructure (i.e., any change of $\boldsymbol{F}^i_{gr}$). Therefore, Hypothesis 1 and Hypothesis 2 together imply that growth becomes in the first place a kind of elastic distension of differential volume elements in the tissue. This elastic distension changes the stress field in the tissue and thereby triggers remodeling (i.e., inelastic reorganization of the tissue) due to tensional homeostasis. In this section, we will demonstrate that this setting gives rise to a natural anisotropy of the geometry changes induced by volumetric growth, which is mainly governed by the anisotropy of the elastic stiffness of the tissue. We will focus thereby on an (isolated) differential volume element to exclude confounding effects from the surrounding continuum and boundary conditions. We will perform our analysis in two steps. In the first step, we will examine the elastic distension of the tissue directly associated with growth, in the second step the remodeling dynamics which it gives rise to.

Via (10), the amount of mass produced per differential volume element per unit time $\dot{\varrho}_0$ determines the ratio between the size of a differential volume element in current and reference configuration, that is, $|\boldsymbol{F}(t)|$. The dilatation of differential volume elements during volumetric growth is illustrated in Fig. 3. If new material is deposited in the tissue, the extant tissue will immediately dilate elastically in order to increase its volume and accommodate the additional material. The following discussion will demonstrate that this dilatation is naturally anisotropic. To see this, we first note that via (10) and (12) volumetric growth itself (without the remodeling it may give rise to in the long term) alters $|\boldsymbol{F}(t)|$ but leaves $\boldsymbol{F}^i_{gr}$ in (3) constant, which means that the change of $|\boldsymbol{F}(t)|$ must be associated with some change of $\boldsymbol{F}^i_e$. Next we resort to the concept of traction-free configurations. In a constrained mixture of n constituents as assumed above in (7), different constituents may have different individual stress-free configurations. That is, in general there exists no configuration in which all constituents in a differential volume element are stress-free at the same time. However, there always exists a so-called traction-free configuration in which the average stress of the different constituents weighted with their respective volume fractions ϱ^i_0/ϱ_0 is zero. The traction-free configuration can be imagined as the configuration of a differential volume element into which it would naturally deform when cut out from its surrounding continuum and not subjected to any external load. Herein, we denote the tensor mapping infinitesimal line elements from (the tangent space of) the reference configuration to (the tangent space of) the current traction-free configuration by $\boldsymbol{F}_G$. If a differential volume element is traction-free in a certain configuration, this holds also after any rigid body rotation. To render the notion of the traction-free configuration unique, we thus define without loss of generality that $\boldsymbol{F}_G$ does not imply any rotation compared to the reference configuration. That is, $\boldsymbol{F}_G$ is symmetric, and the rotation tensor resulting from its polar decomposition is simply the identity tensor. The evolution of the traction-free configuration in time can

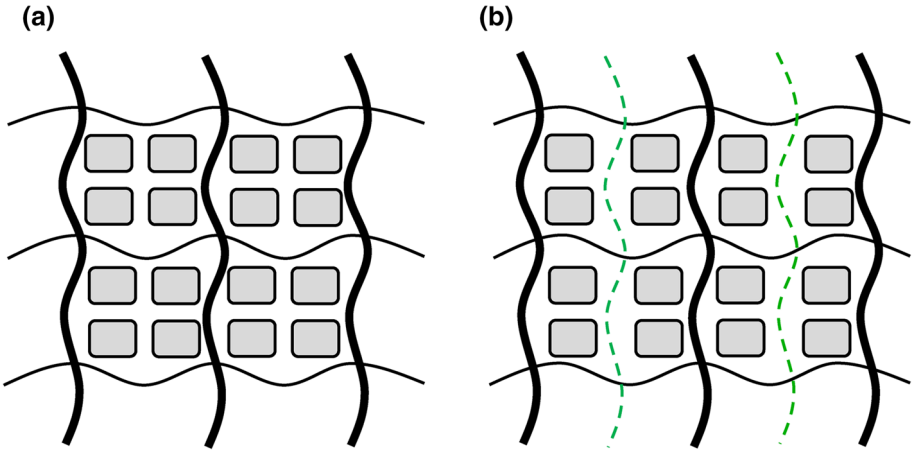

Fig. 3 Deposition of new material during growth directly induces an elastic distension of differential tissue volume elements that can be understood as a form of elastic swelling. This swelling will create the space that is required to accommodate the additional mass by expanding the volume element predominantly in the direction(s) of lowest stiffness. Because in the direction(s) of lowest stiffness the extant fibers will oppose the deformation of the volume element by swelling only minimally. **a** Differential volume element is illustrated whose stiffness in vertical direction is much higher than in horizontal direction (illustrated by much thicker load-bearing fibers in vertical direction). If in this volume element additional fibers are deposited, it will elastically dilate mainly in horizontal direction (**b**). This dilatation mainly in horizontal direction will trigger also remodeling (i.e., inelastic reorganization of the tissue) mainly in horizontal direction, leading finally to a long-term anisotropic inelastic deformation of the volume element mainly in horizontal direction

be described using the velocity gradient (Menzel and Kuhl 2012)

$$\boldsymbol{L}_G = \dot{\boldsymbol{F}}_{\boldsymbol{G}} \boldsymbol{F}_{\boldsymbol{G}}^{-1}. \tag{13}$$

The relative rate of change of the volume of the traction-free configuration of a differential volume element is

$$\mathrm{tr}(\boldsymbol{L}_G) = \frac{d\dot{v}_G}{dv_G} \tag{14}$$

with $\mathrm{tr}(\boldsymbol{L}_G)$ the trace of $\boldsymbol{L}_G$. As discussed above, we assume herein a constant spatial mass density ϱ in differential volume elements under any loading conditions and therefore also in their traction-free configuration. Therefore, the relative rate of change of the size of differential volume elements in the traction-free configuration must be equal to the relative rate of change of the mass in these volume elements, that is,

$$\frac{\dot{\varrho}_0}{\varrho_0} = \frac{d\dot{v}_G}{dv_G} = \mathrm{tr}(\boldsymbol{L}_{\boldsymbol{G}}). \tag{15}$$

$\dot{\boldsymbol{F}}_G$ is associated with an elastic distension of the extant material while new material is squeezed in. To quantify it, we consider an infinitesimal change $d\boldsymbol{F}_G$ of the traction-free configuration that results from the deposition of an additional mass increment dm. The traction-free configuration of the material that has been in the differential volume element already before deposition of the mass increment dm does not change during the deposition process (recalling that herein we assume that growth and remodeling are separate processes, see also Sect. 3). Let the elastic bulk stretch tensor of this material be $\boldsymbol{F}_E$. $\boldsymbol{F}_E$ maps between the traction-free configuration of the material existing before deposition of dm and its current traction-free configuration. By definition, before deposition of dm one has $\boldsymbol{F}_E = \boldsymbol{I}$. After deposition of dm and the associated change of the traction-free configuration by $d\boldsymbol{F}_G$, one has $\boldsymbol{F}_E = \boldsymbol{I} + d\boldsymbol{F}_E$ with

$$(\boldsymbol{I} + d\boldsymbol{F}_E)\boldsymbol{F}_G = \boldsymbol{F}_{\boldsymbol{G}} + d\boldsymbol{F}_{\boldsymbol{G}}, \tag{16}$$

giving

$$d\boldsymbol{F}_E = d\boldsymbol{F}_G \boldsymbol{F}_{\boldsymbol{G}}^{-1}. \tag{17}$$

Dividing (17) by the time increment dt over which the mass increment dm is deposited and using (13) yields

$$\dot{\boldsymbol{F}}_E = \boldsymbol{L}_G. \tag{18}$$

The rate of change of the elastic Cauchy–Green deformation tensor $\boldsymbol{C}_{\boldsymbol{E}} = \boldsymbol{F}_E^T \boldsymbol{F}_E$ of the extant material during the growth process is thus (in a given traction-free configuration where the extant material exhibits a bulk elastic stretch tensor $\boldsymbol{F}_E = \boldsymbol{I}$)

$$\dot{\boldsymbol{C}}_E = \dot{\boldsymbol{F}}_E^T \boldsymbol{F}_E + \boldsymbol{F}_E^T \dot{\boldsymbol{F}}_E = \dot{\boldsymbol{F}}_E^T + \dot{\boldsymbol{F}}_E = 2\boldsymbol{D}_G \tag{19}$$

with

$$\boldsymbol{D}_G = \frac{1}{2}\left(\boldsymbol{L}_G + \boldsymbol{L}_G^T\right) \tag{20}$$

the symmetric part of the velocity gradient $\boldsymbol{L}_G$. Strain energy of the extant material in the neighborhood of a given traction-free configuration (in which we have $\boldsymbol{C}_E = \boldsymbol{I}$ for the extant material) can be expressed via a Taylor expansion as

$$\Psi(\boldsymbol{C}_E = \boldsymbol{I} + d\boldsymbol{C}_E) = \Psi(\boldsymbol{C}_E = \boldsymbol{I}) + \frac{\partial \Psi}{\partial \boldsymbol{C}_E} : d\boldsymbol{C}_E + \frac{1}{2} d\boldsymbol{C}_E : \frac{\partial^2 \Psi}{\partial \boldsymbol{C}_E^2} : d\boldsymbol{C}_E + o(d\boldsymbol{C}_E : d\boldsymbol{C}_E) \tag{21}$$

with the Landau symbol $o(.)$ and colons denoting double contraction products between tensors. By definition in the traction-free configuration, $\partial \Psi / \partial \boldsymbol{C}_E = 0$. Then, from (19) and (21), we conclude that the elastic energy of the material in a differential volume element changes during mass deposition over a time interval of length dt by the increment

$$d\Psi = \frac{1}{2} d\boldsymbol{C}_E : \frac{\partial^2 \Psi}{\partial \boldsymbol{C}_E^2} : d\boldsymbol{C}_E = 2dt^2 \boldsymbol{D}_G : \frac{\partial^2 \Psi}{\partial \boldsymbol{C}_E^2} : \boldsymbol{D}_G. \tag{22}$$

As can be seen from (15), the mass production rate per unit reference volume $\dot{\varrho}_0$ determines the rate of relative volumetric expansion of the traction-free configuration. But it does not enforce any specific shape of the traction-free configuration. As a consequence of the principle of minimum energy, the shape of the traction-free configuration will thus evolve such that $d\Psi$ is minimal. Let $d\Psi$ be minimal for $\boldsymbol{D}_G = \boldsymbol{D}_G^*$. Then

$$\boldsymbol{D}_G^* = \underset{\boldsymbol{D}_G}{\operatorname{argmin}} \left\{ \boldsymbol{D}_G : \frac{\partial^2 \Psi}{\partial \boldsymbol{C}_E^2} : \boldsymbol{D}_G \right\}, \tag{23}$$

that is, $\boldsymbol{D}_G^*$ is the $\boldsymbol{D}_G$ which minimizes the term in the braces. Assuming a constant spatial mass density (as we do herein), using (15) and (20) in (23) leads to the constrained optimization problem

$$\boldsymbol{D}_G^* = \underset{\boldsymbol{D}_G : \operatorname{tr}(\boldsymbol{D}_G) = \dot{\varrho}_0 / \varrho_0}{\operatorname{argmin}} \left\{ \boldsymbol{D}_G : \frac{\partial^2 \bar{\Psi}}{\partial \boldsymbol{C}_E^2} : \boldsymbol{D}_G \right\} \tag{24}$$

where $\bar{\Psi} = \Psi - \Psi^*$ is the total strain energy minus the (isotropic) penalty energy Ψ^* modeling excluded volume interactions and ensuring constant spatial density. The fourth-order stiffness tensor $\partial^2 \bar{\Psi} / \partial \boldsymbol{C}_E^2$ is symmetric and assumed here to be positive definite. Its inverse is the compliance tensor $\bar{\mathbb{S}}$. As shown in "Appendix 1," the unique solution to (24) is

$$\boldsymbol{D}_G^* = \frac{\dot{\varrho}_0}{\operatorname{tr}\left(\bar{\mathbb{S}} : \boldsymbol{I}\right) \varrho_0} \bar{\mathbb{S}} : \boldsymbol{I}. \tag{25}$$

The symmetric part $\boldsymbol{D}_G$ of the velocity gradient $\boldsymbol{L}_G$ indicates how fast the traction-free configuration of a differential volume element dilates in different directions, cf. also Sect. 4.5.2 in (Gonzalez and Stuart 2008). For example, after a principal axis transformation the diagonal elements of $\boldsymbol{D}_G$ indicate the strain rate at which the traction-free configuration dilates along the principle axes. From (25), it is thus apparent that, as a rule of thumb, during volumetric growth differential volume elements will dilate elastically mainly in the direction(s) of maximal compliance, that is, of lowest stiffness. This can indeed be understood quite intuitively. The elastic dilatation associated directly with growth is a form of elastic swelling. The energetic cost for swelling, which implies a stretch of extant fibers, is obviously minimal in the direction(s) of lowest material stiffness of the extant material. This is also illustrated in Fig. 3.

So far we have discussed in this section in a first step only the immediate elastic dilatation of differential volume elements associated with growth. In a second step, we now examine the remodeling that results from this perturbation of the elastic stress field. The elastic dilatation by growth increases the elastic stress in fibers by an amount that is directly proportional to the elastic stretch induced in fiber direction by $\boldsymbol{D}_G^*$. As the latter elastic fiber stretch is in softer directions higher than in stiffer directions of the material, also the difference of fiber stress from the homeostatic target value due to growth will be. The higher this difference, the faster inelastic remodeling according to (12). Therefore, growth will not only result in an immediate elastic dilatation of differential volume elements predominantly in the softest material direction(s) but also to a long-term inelastic remodeling predominantly in these direction(s).

Remark 6 Note that the above derived natural anisotropy of volumetric growth and remodeling induced by the combination of anisotropic stiffness and tensional homeostasis can be captured only if the constant spatial mass density of the tissue is enforced by a penalty function such as $\Psi^{\#}$ in (7) rather than by a volumetric–deviatoric split of the deformation gradient as used in various previous articles about volumetric growth. The reason is that, when using a penalty function, dilatation of volume elements by deposition of mass automatically always affects the elastic stretch $\boldsymbol{F}_e^i$. Minimization of the associated strain energy ultimately yields (25) and thereby a growth anisotropy governed by the tissue stiffness.

The situation is completely different when using a volumetric–deviatoric split of the deformation gradient in order to model a constant spatial mass density of the tissue in a way similar to standard models of material incompressibility during elastic deformation. In this case, growth will not result in any elastic energy as long as it occurs isotropically and thus affects the volumetric part of the deformation gradient only (which does not appear in the strain energy function). Therefore, in this case, the argument of minimal strain energy put forward above would not induce any kind of growth anisotropy dependent on the stiffness anisotropy but

it would rather always lead to isotropic growth, which has indeed also been observed in computer simulations (Grytsan et al. 2015) but which is in contradiction to experimental observations in various tissues as discussed in more detail below.

Remark 7 Above only the symmetric part $\boldsymbol{D}_G$ of the velocity gradient $\boldsymbol{L}_G$ is examined. A discussion of the anti-symmetric part, which describes the rotation of the traction-free configuration, is skipped since it is not essential for understanding the aspects of growth dynamics on which we decided to focus herein.

Remark 8 In the theory developed herein, the evolution of the traction-free configuration of differential volume elements is governed by a minimum energy principle as revealed by (20). This establishes some link between the ideas introduced herein and the work of Gizzi et al. (2014) and Pandolfi et al. (2016) where electromechanical coupling in soft biological tissues is modeled by an inelastic part of the deformation gradient, which is also determined via the minimization of a potential.

5 Examples

The discussion from Sect. 4 can directly be applied to understand the experimentally observed volumetric growth and remodeling in a variety of different soft biological tissues in a very natural way as we will demonstrate in this section by several examples. The parameters used for the computational studies reported in the following subsections are all summarized in "Appendix 2."

5.1 Volumetric growth and remodeling in membrane-like tissues

In membrane-like tissues such as the bladder, the stomach, the small and large intestine, or blood vessels, the stiff, reinforcing collagen fibers are mainly oriented perpendicular to the wall thickness direction (Schriefl et al. 2012). The wall thickness direction is thus the by far most compliant direction. Our model thus predicts volumetric growth and remodeling mainly in wall thickness direction in such tissues, which is indeed in good agreement with experimental observations as discussed in the following subsections.

5.1.1 Vascular growth and remodeling in hypertension

In blood vessels, increased blood pressure is well known to stimulate volumetric growth via deposition of additional collagen fibers. This growth mainly increases wall thickness rather than length or diameter of blood vessels (Berry and Greenwald 1976; Matsumoto and Hayashi 1994). So far to the authors' best knowledge no explanation has been proposed why this is the case, whereas the discussion in Sect. 4 can explain this phenomenon in quite a natural way.

To underline the agreement between our theory and experiments, we present in this section the results of computer simulations based on our theory. Therein, the artery is modeled as a circular cylinder. Its wall is a constrained mixture of elastin, five collagen fiber families (circumferential, axial, diagonal, radial), and one circumferential smooth muscle fiber family. Geometry parameters, strain energy functions, and material parameters are taken from Sect. 4.3 of (Braeu et al. 2017) with just a few minor modifications. All the details of the computational model are given in "Appendix 2."

Remodeling of collagen and smooth muscle is captured by Eq. (12), which is equivalent to Eq. (17) in (Braeu et al. 2017). As in (Braeu et al. 2017), we assume also herein no remodeling of elastin. In the mass production Eq. (11), we choose both for collagen and smooth muscle fiber families

$$\boldsymbol{k}_\sigma^i = k_\sigma^i \boldsymbol{A}^{\boldsymbol{i}} \otimes \boldsymbol{A}^{\boldsymbol{i}} \tag{26}$$

with $\boldsymbol{A}^{\boldsymbol{i}}$ the unit direction vector of the respective fiber families in reference configuration and

$$\Delta \boldsymbol{G}^i = \boldsymbol{R}^T \boldsymbol{\sigma}^i \boldsymbol{R} - \boldsymbol{\sigma}_h^i. \tag{27}$$

Here, $\boldsymbol{\sigma}^i$ is the Cauchy stress of the ith constituent, $\boldsymbol{\sigma}_h^i$ some constant homeostatic target stress, and $\boldsymbol{R}$ the rotational part of the deformation gradient $\boldsymbol{F}$. This choice of $\boldsymbol{k}_\sigma^i$ and $\Delta \boldsymbol{G}^i$ is equivalent to the one in (Braeu et al. 2017).

In our simulations, we mimic the experiment of (Berry and Greenwald 1976) where at some point in time $t = 0$ the artery is subjected to a sudden increase in blood pressure p from 100 mmHg to 180 mmHg and the subsequent growth and remodeling is observed over several weeks.

The results of our computer simulations are presented in Fig. 4 with $T^i = 7$days in (12) and three different gain parameters $k_\sigma^i = 0.22/T^i$, $k_\sigma^i = 0.28/T^i$ and $k_\sigma^i = 0.34/T^i$ in (26). As expected from the discussion in Sect. 4, the volumetric growth induced by hypertension mainly leads to a thickening of the arterial wall because the wall thickness direction is by far the most compliant direction in the tissue. This is clearly visible by the relative change of the ratio between the mid-radius R_{mid}, the average between the inner and outer radius of the artery, and the wall thickness H over time, that is, by

$$\hat{H}(t) = \frac{R_{\text{mid}}(t)/H(t) - R_{\text{mid}}(t=0)/H(t=0)}{R_{\text{mid}}(t=0)/H(t=0)}. \tag{28}$$

As apparent from Fig. 4, for $k_\sigma^i = 0.28/T^i$ the ratio between wall thickening and radius dilation in the simulation

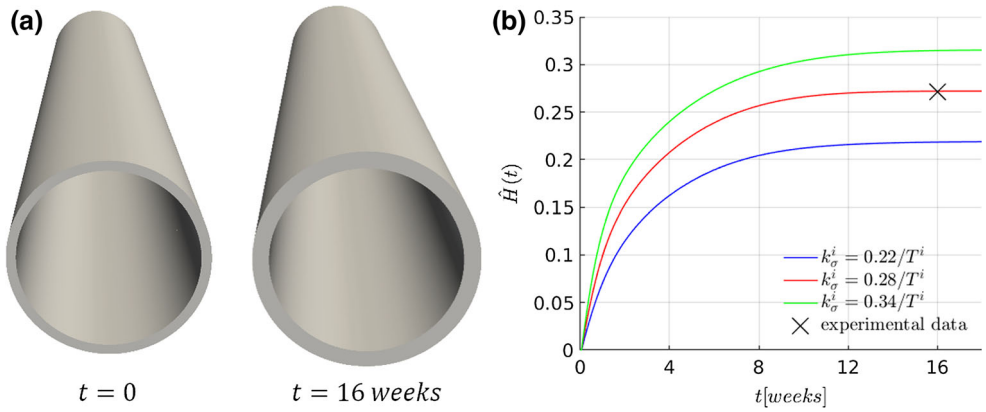

Fig. 4 Artery before (left) and after (right) increase in blood pressure from 100 mmHg to 180 mmHg subsequent to which both the diameter and the wall thickness increase by growth and remodeling. The relative change of the ratio $\hat{\boldsymbol{H}}$ between wall thickness and vessel mid-radius over time is plotted for different simulated gain parameters and compared to experimental data from (Berry and Greenwald 1976)

at $t = 16$weeks agrees well with the experimental observation reported by (Berry and Greenwald 1976). We thus note that the theory developed in this paper can-for an appropriate choice of parameters-excellently reproduce the kind of growth and remodeling observed in the vasculature without prescribing in any explicit way its specific anisotropy. In opposition to that, one can easily demonstrate that computational models where growth is prescribed to be an evolving isotropic inelastic deformation of differential volume elements, an approach that is frequently used in the literature, are in general unable to capture the growth and remodeling observed in arteries even qualitatively. The reason is that such models always produce a similar dilatation of the tissue in radial and circumferential direction, which is in clear contradiction to experimental observations.

5.1.2 Aneurysms

Aneurysms are local dilatations of the vascular wall. They typically enlarge over years and often finally rupture, which is one of the most common causes of death in industrialized countries. The initiation and enlargement of aneurysms remain poorly understood to date. Computer simulations are therefore increasingly used to study both. Here, we present the simulation of an enlarging aneurysm (Fig. 5) using the computational model described in Sect. 5.1.1 but with $k_\sigma^i = 0.05/T^i$ and $T^i = 101$ days. Moreover, in the simulation, we keep the blood pressure at the initial value of 100 mmHg and initiate the enlargement of the aneurysm by a damage to the elastin layer following Eq. (42) in "Appendix 2." This example demonstrates that our novel approach to volumetric growth and remodeling can capture volumetric growth and remodeling successfully not only in the mechanobiologically stable regime considered in Sect. 5.1.1 but also in the mechanobiologically unstable regime governing the enlargement of aneurysms (Cyron and Humphrey 2014; Cyron et al. 2014).

5.2 Volumetric growth in rope-like tissues

In rope-like tissues such as tendons or ligaments, volumetric growth by deposition of additional mass may occur, for example, due to inflammation, which induces deposition of ground matrix and swelling through attraction of water. This is well known to result in thickening, that is, an increase in cross section, rather than an increase in length or a substantial relaxation of axial tension (Bass 2012). Again, this phenomenon can be naturally explained from the discussion in Sect. 4. The much higher stiffness in axial than transverse direction makes tendons and ligaments expand during volumetric growth mainly in transverse direction. To illustrate the ability of our theory to capture this phenomenon, we model the geometry of the tendon as a rectangular prism with three collagen fiber families aligned with its edges. Computer simulations are performed with a simple orthotropic material resembling the situation in tendons and ligaments at least qualitatively. In our computational model, we used the strain energy

$$\Psi = \frac{\varrho_0^{gr}(t)}{\varrho_0^{gr}(t=0)} G\left[\mathrm{tr}\left(\bar{\boldsymbol{C}}\right) - 3\right] + \frac{1}{2}\sum_i \frac{\varrho_0^i(t)}{\varrho_0^i(t=0)} \varphi^i E\left[\left(\boldsymbol{A}_{gr}^i \otimes \boldsymbol{A}_{gr}^i : \boldsymbol{C}_e^i\right) - 1\right]^2 + \Psi^{\#}. \tag{29}$$

The isotropic Neo-Hookean energy which forms the first summand on the right-hand side of (29) represents the shear stiffness of the ground matrix (constituent superscript gr), which is assumed to be proportional to the tissue mass

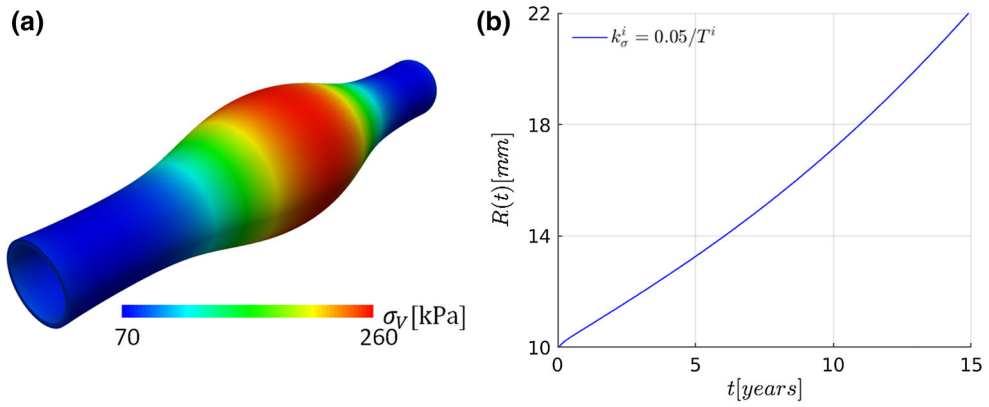

Fig. 5 **a** Von Mises stress in an idealized fusiform abdominal aortic aneurysm 15 years after initiation.**b** Maximal inner radius of the aneurysm over time

and be defined by the modulus $G = 13.85$MPa taken from Weiss et al. (1996). $\boldsymbol{C}$ is the Cauchy–Green deformation tensor and $\bar{\boldsymbol{C}}$ its isochoric counterpart. The sum of quadratic functions which forms the second summand on the right-hand side represents three families of collagen fibers oriented in axial ($i = co(ax)$) and in the two transverse directions ($i = co(0°), co(90°)$). These are aligned with the unit direction vectors $\boldsymbol{A}_0^i$ in reference configuration and the unit direction vectors $\boldsymbol{A}_{gr}^i = \boldsymbol{F}_{gr}^i \boldsymbol{A}_0^i / \left\| \boldsymbol{F}_{gr}^i \boldsymbol{A}_0^i \right\|$ in the inelastically deformed intermediate configuration. $\boldsymbol{C}_e^i$ is the elastic Cauchy–Green deformation tensor, $E = 125$MPa the elastic modulus of the collagen fibers taken from the one-dimensional model for ligaments proposed by Yu et al. (2001), and φ^i the fraction of collagen fibers forming a specific fiber family. The penalty function $\Psi^\#$ from (10) is used with $\varepsilon = 300$MPa. At time $t = 0$, the initial elastic stretch in fiber direction equals the respective homeostatic stretch which means that no mechano-regulated remodeling takes place at the start of the simulation. In general, remodeling in the ground matrix is assumed to be very slow, similar to the one of elastin in arteries, and thus neglected. By contrast, remodeling in the collagen fibers is much faster and therefore included in the simulation with a remodeling time constant $T^{co} = 24.5$ days in (12). We assume that at time $t = 0$ inflammatory processes start in the tissue, leading to deposition of additional mass, which is modeled herein as a special constituent of the constrained mixture with a referential mass density $\varrho_0^I(t)$ that increases from zero at time $t = 0$ to a value equal to the initial referential mass density of the healthy tissue at time $t = 6$ weeks. That is, within 6 weeks the total tissue mass is assumed to increase by a factor of two. Mass changes of the ground matrix and the collagen fibers happen on a very slow time scale compared to the mass changes due to inflammation and are therefore neglected in our simulation by choosing $\boldsymbol{k}_\sigma^i = 0$ for these constituents in (26). The additional mass deposited due to inflammation is assumed to be not load bearing and does thus not appear in (29). To mimic the boundary conditions in vivo, both ends of the idealized tendon are fixed in axial direction.

In Fig. 6a, we compare the initial geometry (opaque) with the geometry at time $t = 30$ weeks (transparent) when both mass deposition due to inflammation and the resulting remodeling of the collagen fibers are (largely) finished as apparent from Fig. 6b. Figure 6b shows the total collagen fiber stretch in axial and the two transverse directions compared to their inelastic counterparts $\lambda_{gr}^i = \sqrt{\boldsymbol{A}_0^i \otimes \boldsymbol{A}_0^i : \boldsymbol{C}_{gr}^i}$ with $\boldsymbol{C}_{gr}^i = \boldsymbol{F}_{gr}^{iT} \boldsymbol{F}_{gr}^i$.

Growth and remodeling illustrated in Fig. 6 can be understood as follows: Due to the elastic deformation induced by volumetric growth over the first six weeks, collagen fiber stress increases. Following Eq. (12), the associated elastic fiber stretch is converted by remodeling into an inelastic stretch λ_{gr}^i. This inelastic fiber relaxation continues until the original homeostatic stress level in each collagen fiber family is restored. In Fig. 6b, we can see that for the transverse collagen fiber families this is the case for t $\geq$ 20 weeks. Altogether the deposition of additional mass due to inflammation leads for $t \geq 20$ weeks to a state where the cross section of the tendon has significantly grown. At the same time, elastic stress in axial direction is on the same level as before. That is, the deposition of additional ground matrix has not induced a loss of axial tension in the tendon, which appears physiologically reasonable. We note that standard isotropic growth models are not able to reproduce this behavior. Rather in such models the growth of the tendon cross section would necessarily be associated with considerable loss of tension in axial direction for which, to the authors' best knowledge, so far no experimental evidence has been reported. While we have shown in this section that our growth model produces also for tendons results that appear physiologically reasonable, we also underline that we have not been able to support our computational results by a quantitative comparison with

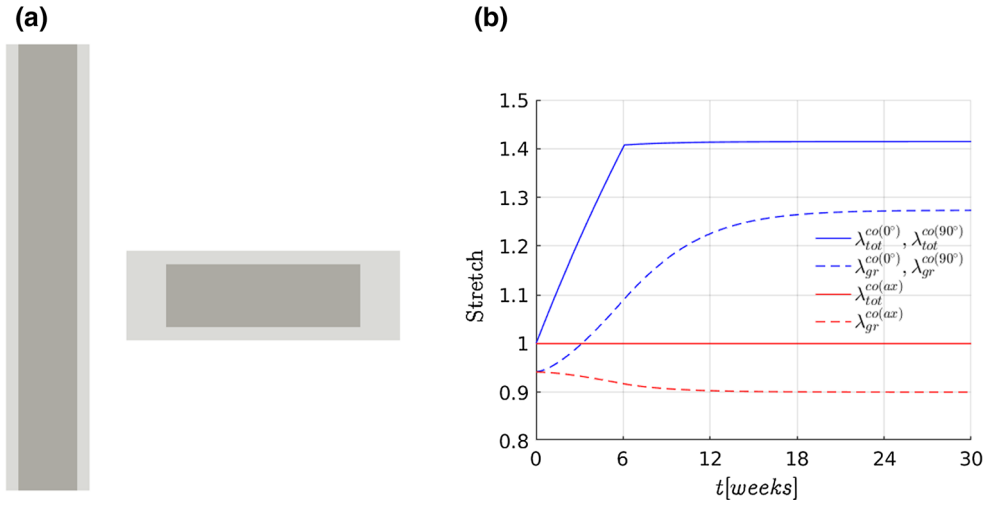

Fig. 6 **a** Axial section (left) and cross section (right) of initial geometry (opaque) versus geometry at time t = 30weeks after deposition of additional mass due to inflammation and remodeling of the collagen fibers (transparent). Volumetric growth and remodeling gives rise to an equal dilatation of the volume in both directions perpendicular to the axis of the tendon.**b** Total ($\lambda_{tot}^{co(0°)}$, $\lambda_{tot}^{co(90°)}$) and inelastic collagen fiber stretch ($\lambda_{gr}^{co(0°)}$, $\lambda_{gr}^{co(90°)}$) in the two main transverse directions and total ($\lambda_{tot}^{co(ax)}$) and inelastic ($\lambda_{gr}^{co(ax)}$) collagen fiber stretch in axial direction over time

experimental data due to a lack of such data in the literature. Performing such a quantitative comparison in collaboration with clinicians would be an important step to further evaluate the validity of the theory developed herein.

5.3 Volumetric growth in (nearly) isotropic tissues

In rope-like tissues such as tendons and ligaments, stiffness in axial direction is around two orders of magnitude higher than in transverse direction (Yin and Elliott 2004) . In membrane-like tissues such as blood vessels, stiffness in wall thickness direction is around two orders of magnitude lower than in the other directions (Wilson et al. 2013). In addition to these two categories, there are also soft tissues, which exhibit a nearly isotropic stiffness. For example, the stiffness of liver lobules exhibits only a mild anisotropy with one direction by just around a factor of two stiffer than the other two directions (Chui et al. 2007). In tissues with (nearly) isotropic stiffness we expect from the discussion in Sect. 4 (nearly) isotropic volumetric growth and remodeling. To demonstrate this, we performed computer simulations of volumetric growth with the following isotropic strain energy function:

$$\begin{aligned}\Psi = &\frac{\varrho_0^{gr}(t)}{\varrho_0^{gr}(t=0)} E^{gr}\left[\frac{1}{4(1+\nu^{gr})}(I_1 - 3 - 2\ln(|\boldsymbol{F}(t)|)) \right.\\ &\left. + \frac{\nu^{gr}}{2(1+\nu^{gr})(1-2\nu^{gr})}(|\boldsymbol{F}(t)|-1)^2\right]\\ &+ \frac{1}{2}\frac{\varrho_0^{co}(t)}{\varrho_0^{co}(t=0)} E^{co}\left[\left(\boldsymbol{M}_{iso}^{co} : \boldsymbol{C}_e^{co}\right) - 1\right]^2 + \Psi^{\#}. \end{aligned} \tag{30}$$

The first Neo-Hookean summand on the right-hand side represents the ground matrix (constituent superscript gr) with the elastic modulus $E^{gr} = 1$Pa and Poisson's ratio $\nu = 0.3$. The second quadratic summand on the right-hand side represents the collagen fibers (constituent superscript co) with the elastic modulus $E^{co} = 10$Pa and structural tensor $\boldsymbol{M}_{iso}^{co}$. By defining $\boldsymbol{M}_{iso}^{co}$ as a diagonal tensor with each term equal to $1/3$, the quadratic function in Eq. (30) represents an isotropic fiber distribution. Again the penalty function $\Psi^{\#}$ from (10) is used with a penalty parameter $\varepsilon = 1$kPa.

In such a tissue, we model a growth process similar to the one studied in Sect. 5.2. That is, we increase the total referential mass density $\varrho_0(t)$ by a factor of two over 10 weeks and assume that the newly deposited mass is not load bearing and does therefore not appear in the strain energy in Eq. (30). Additionally, we only consider remodeling of collagen fibers and neglect mass changes of the ground matrix and the collagen fibers, that is, $\boldsymbol{k}_\sigma^{gr} = \boldsymbol{k}_\sigma^{co} = 0$ in Eq. (11). We use a spheroidal initial geometry with radius R.

The result of the computer simulation of volumetric growth under these conditions is shown in Fig. 7. As expected for a material with isotropic stiffness, the initially spheroidal body grows isotropically (see Fig. 7a). Figure 7b shows that remodeling of the collagen fibers converts the elastic stretch induced by volumetric growth into an inelastic fiber stretch and after some time of adaptation a new homeostatic state is reached in which the collagen fiber stress largely equals the homeostatic value again after around 30 weeks.

The computational example in this section was motivated by the problem of volumetric growth and remodeling in the

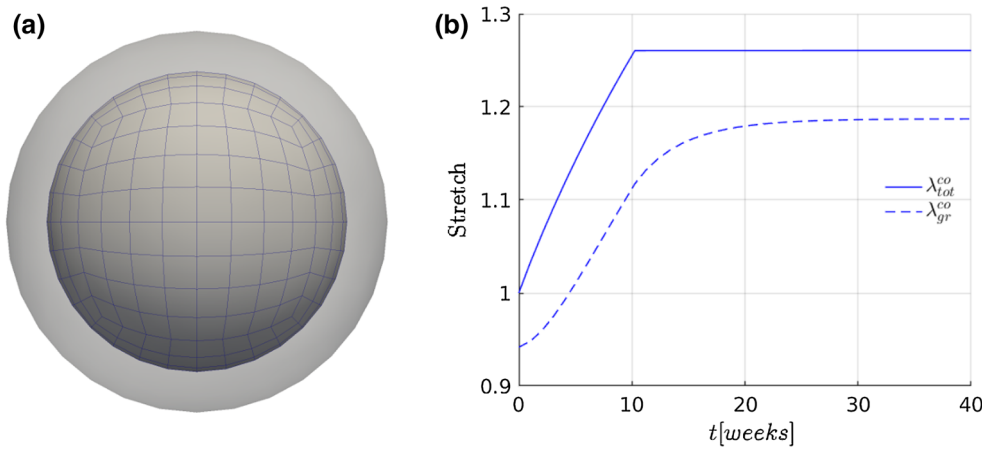

Fig. 7 **a** Volumetric growth in a spheroidal tissue with isotropic stiffness is isotropic, that is, it maps the initial geometry (opaque) on a dilated sphere (transparent).\break **b** Total stretch $\lambda_{tot}^{co} = R(t)/R(t=0)$ with radius $\boldsymbol{R}$ of the sphere and inelastic collagen fiber stretch $\boldsymbol{\lambda}_{gr}^{co}$ over time

liver or small tumors. Both kinds of tissue exhibit a nearly isotropic stiffness (Chui et al. 2007; Jain et al. 2014) and in both volumetric growth is frequently observed. In the liver, this volumetric growth is associated with the pathology of hepatic steatosis, where fat accumulates in the liver cells. Clinically, one observes that both during tumor growth and in hepatic steatosis the tissue volume typically expands in all spatial directions approximately equally. Interestingly, this is exactly what one would expect from (23) and the discussion in Sect. 4 for tissues with (nearly) isotropic stiffness. Saying this, we emphasize that we only point here at a surprising agreement between our theory and clinical observations in small tumors and the liver. We do, however, at this point not claim that the theory developed herein can fully explain volumetric growth and remodeling in small tumors or the liver. The reason for our caution is that the theory developed herein is crucially based on the assumption that microstructural reorganization (remodeling) is mainly governed by the principle of tensional homeostasis. While this idea is widely accepted for loadbearing soft tissues such as blood vessels, tendons or ligaments, it is so far unclear, to which extent (or whether at all) it is also applicable to tumor and liver tissue. At the same time, mass transport, the theory of porous media and some other more advanced aspects of modeling are neglected herein. These may, however, play important roles in the liver and tumors (Grillo et al. 2012; Mascheroni et al. 2018). Therefore, statements about the relation between the computational example in this section and growth and remodeling in the liver and small tumors should be made with great caution at this point. Hence, we limit our statement to simply pointing at the remarkable agreement between the results of our model and clinical observations made for liver or tumor growth.

6 Discussion

Most previous work tries to capture volumetric growth in soft biological tissues by way of an inelastic part of the deformation gradient often referred to as growth tensor. This always leads to the important question how to define such a tensor, in particular its anisotropy. Unfortunately, there is so far no satisfactory answer to this question, and thus, most work relies on heuristic ad hoc assumptions. To overcome this problem, we herein introduced a completely different approach. Our approach is based on two simple hypotheses. The first hypothesis is that during volumetric growth the total mass density of the tissue remains constant so that deposition of additional mass is automatically associated with an increase in tissue volume. The second hypothesis is that any reorganization of the elastic microstructure of the tissue, termed herein as remodeling, is governed by a single principle, the principle of tensional homeostasis. This principle has been identified over the last two decades by numerous studies as a key principle of soft tissue mechanobiology. It is therefore general rather than specific for a particular kind of soft tissue. In Sect. 4, we demonstrated that the above two simple hypotheses directly give rise to what one may consider a natural anisotropy of volumetric growth and remodeling. That is, in the absence of any additional confounding factors volumetric growth and remodeling will, as a rule of thumb, result in an expansion of differential tissue volume elements mainly in the direction(s) of lowest stiffness. In Sect. 5, we demonstrated that this natural anisotropy of volumetric growth and remodeling agrees very well with the anisotropy observed experimentally in a variety of different soft tissues ranging from blood vessels over tendons to tissues with a rather isotropic stiffness.

This means that the new approach introduced herein can explain the anisotropy of volumetric growth and remodeling observed experimentally in a host of different tissues from just two simple and general hypotheses, which are both supported by experimental observations and which are applicable to a large range of load-bearing collagenous soft biological tissues. In opposition to that, previous models of growth and remodeling based on the concept of an inelastic growth tensor had to come up for each specific kind of tissue with a tissue-specific definition of the growth tensor which was usually of a rather heuristic kind and not based on general or fundamental principles.

The growth theory developed herein has an interesting consequence regarding adaptation of living tissues to external loading. It is well known that fibers in living tissues have a natural tendency to rotate into the direction of mechanical loading. This naturally increases stiffness in loading direction. The theory developed herein then predicts that deposition of additional mass will automatically happen mainly in compliant tissue direction(s), that is, mainly perpendicular to the loading direction(s), which automatically increases the load-bearing cross section and thereby the strength of the tissue in the most efficient way.

The natural relation between stiffness and growth, which is the main result of this article, may help to understand better not only growth and remodeling during mechano-adaptation of adult tissues but also during morphogenesis. Especially during morphogenesis it remains hard to measure and also hard to model the complex and often anisotropic changes of the tissue geometry. The theory developed herein may offer a simple way to understand and predict these changes from stiffness, which is a quantity that can be measured and modeled often quite accurately. This means that further attempts to model the stiffness of biological tissues more accurately, following, for example (Gasser et al. 2006; Vasta et al. 2014; Gizzi et al. 2016, 2017; Niestrawska et al. 2016; Holzapfel and Ogden 2017), might in the future also be very helpful to understand better complex patterns of volumetric growth.

While the results shown in the examples section of this paper are promising, further studies are definitely required in order to decide to which extent the theory developed in this paper can capture the physiology of volumetric growth in different soft tissues realistically. Moreover, it might be an interesting avenue of future research to extend the theory developed herein such that it includes also the biochemical processes and transport processes that drive volumetric growth in biological tissues, for example along the lines of Grillo et al. (2012); Marino et al. (2017); Mascheroni et al. (2018).

Acknowledgements This work was supported by the Emmy Noether program of the German Research Foundation DFG (CY 75/2-1) and the International Graduate School for Science and Engineering (IGSSE) of Technical University of Munich. The authors thank D. Bigoni from University of Trento, Italy, for fruitful discussions.

Compliance with ethical standards

Conflict of interest The authors declare that they have no conflict of interest.

Appendix 1

In this appendix, we demonstrate how to solve the constrained minimization problem (24) analytically. To this end, we introduce a Lagrangian multiplier λ so that the constrained minimization problem can be reduced to an unconstrained minimization of the Lagrange functional

$$\mathcal{L}\left(\boldsymbol{D}_G^*, \lambda^*\right) = \boldsymbol{D}_G : \frac{\partial^2 \bar{\Psi}}{\partial \boldsymbol{C}_E^2} : \boldsymbol{D}_G + \lambda\left[tr(\boldsymbol{D}_G) - \frac{\dot{\varrho}_0}{\varrho_0}\right]. \quad (31)$$

Finding a minimum (or maximum) of (31) is equivalent to finding a stationary point of the Lagrange functional $\mathcal{L}$. Let at this stationary point $\boldsymbol{D}_G$ and λ take on the values $\boldsymbol{D}_G^*$ and λ^*, respectively. Then

$$\frac{\partial \mathcal{L}}{\partial \boldsymbol{D}_G}\left(\boldsymbol{D}_G^*, \lambda^*\right) = 2\frac{\partial^2 \bar{\Psi}}{\partial \boldsymbol{C}_E^2} : \boldsymbol{D}_G^* + \lambda^* \boldsymbol{I} = 0, \quad (32)$$

$$\frac{\partial \mathcal{L}}{\partial \lambda}\left(\boldsymbol{D}_G^*, \lambda^*\right) = \mathrm{tr}\left(\boldsymbol{D}_G^*\right) - \frac{\dot{\varrho}_0}{\varrho_0} = 0. \quad (33)$$

Eq. (32) yields

$$\boldsymbol{D}_G^* = -\frac{1}{2}\lambda^* \bar{\mathbb{S}} : \boldsymbol{I} \quad (34)$$

with the fourth-order compliance tensor

$$\bar{\mathbb{S}} = \left[\frac{\partial^2 \bar{\Psi}}{\partial \boldsymbol{C}_E^2}\right]^{-1}. \quad (35)$$

Using Eq. (34) in Eq. (33) gives

$$\lambda^* = -\frac{2\dot{\varrho}_0}{\mathrm{tr}\left(\bar{\mathbb{S}} : \boldsymbol{I}\right)\varrho_0}, \quad (36)$$

and using Eq. (36) in Eq. (34) yields

$$\boldsymbol{D}_G^* = \frac{\dot{\varrho}_0}{\mathrm{tr}\left(\bar{\mathbb{S}} : \boldsymbol{I}\right)\varrho_0}\bar{\mathbb{S}} : \boldsymbol{I}. \quad (37)$$

Note that $\boldsymbol{D}_G^*$ marks a minimum rather than a maximum of $\mathcal{L}$ and thereby of the elastic energy cost by volumetric growth due to the positive definiteness of the stiffness $\partial^2 \bar{\Psi} / \partial \boldsymbol{C}_E^2$ assumed herein.

Appendix 2

In this appendix, we summarize all relevant parameters and equations required to reproduce the simulations shown in the examples Sect. 5. In Sects. 5.1.1 and 5.1.2, we model the arterial wall as a constrained mixture of elastin, circumferential smooth muscle and, unlike Braeu et al. (2017), five collagen fiber families. Schriefl et al. (2012) showed that the orientation of collagen fibers is in general not perfectly aligned with the tangential plane of the aortic wall but rather may exhibit also a small radial component. To account for this phenomenon, we included in the constitutive model of the wall an additional collagen fiber family in wall thickness direction with a small reference mass density. In the following, the superscripts el, co, and sm are used for quantities referring to elastin, collagen, and smooth muscle, respectively. The total strain energy of elastin per unit mass is assumed to be given by the sum

$$W^{el} = W^{el}_{2D} + W^{el}_{3D} \tag{38}$$

with the isotropic two-dimensional Neo-Hookean strain energy function

$$W^{el}_{2D} = \frac{\mu^{el}_{2D}}{2}\left[\boldsymbol{C}^{el}_e : \boldsymbol{A}^{\parallel}_{gr} + \frac{1}{\left|\boldsymbol{A}^{\parallel}_{gr}\boldsymbol{C}^{el}_e\boldsymbol{A}^{\parallel}_{gr} + \boldsymbol{A}^{\perp}_{gr}\right|} - 3\right]. \tag{39}$$

Here, μ^{el}_{2D} is a stiffness parameter, $A^{rad}_{gr} = a^{rad}_{gr} \otimes a^{rad}_{gr}$ **is** the structural tensor in wall thickness direction with a^{rad}_{gr} the unit vector in wall thickness direction in the intermediate configuration of elastin, $A^{\parallel}_{gr} = I - a^{rad}_{gr} \otimes a^{rad}_{gr}$ is the structural tensor for the axial-circumferential plane in the vessel wall. The second strain energy contribution of elastin is the compressible isotropic three-dimensional Neo-Hookean strain energy

$$W^{el}_{3D} = \frac{E^{el}}{4\left(1+\nu^{el}\right)}\left(\mathrm{tr}\left(\boldsymbol{C}^{el}_e\right) - 3 - 2\ln\left(\left|\boldsymbol{F}^{el}_e\right|\right)\right) + \frac{E^{el}\nu^{el}}{2\left(1+\nu^{el}\right)\left(1-2\nu^{el}\right)}\left(\left|\boldsymbol{F}^{el}_e\right| - 1\right)^2 \tag{40}$$

with the specific elastic modulus E^{el} and Poisson's ratio ν^{el}. The strain energy per unit mass of each collagen fiber family is modeled with a Fung-type exponential function

$$W^{co} = \frac{k^{co}_1}{2k^{co}_2}\left(e^{k^{co}_2\left(I^{co}_a - 1\right)^2} - 1\right) \tag{41}$$

Table 1 Shared simulation parameters of the idealized cylindrical blood vessel studied in Sects. 5.1.1 and 5.1.2

Mesh		
Element type		8-noded hexahedral linear finite elements
Element technology		F-bar method to avoid locking (de Souza Neto et al. 1996)
Number of elements		165,888
Geometry/load		
Inner radius of cylinder	R	10 mm
Wall thickness of cylinder	H	1.41 mm
Length of cylinder	L	180 mm
Blood pressure on inner wall of cylinder	p	100 mmHg
Material parameters		
Elastin: 2D Neo-Hookean parameter	μ^{el}_{2D}	$\in$[71; 104] J/kg
Elastin: 3D Neo-Hookean elastic modulus	E^{el}	72 J/kg
Elastin: 3D Neo-Hookean Poisson's ratio	ν^{el}	0.3
Collagen: Fung exponential parameters	k^{co}_1	568 J/kg
	k^{co}_2	11.2
Smooth muscle: passive contribution	k^{sm}_1	7.6 J/kg
	k^{sm}_2	11.4
Smooth muscle: active contribution	σ^{sm}_{actm}	54 kPa
	λ^{sm}_0	0.8
	λ^{sm}_m	1.4
	λ^{sm}_{act}	1
Penalty parameter	ε	150 kPa
Initial reference mass densities		
Elastin	$\varrho^{el}_0(t=0)$	241.5 kg/m^3
Collagen: circumferential	$\varrho^{co(cir)}_0(t=0)$	61.845 kg/m^3
Collagen: axial	$\varrho^{co(ax)}_0(t=0)$	61.845 kg/m^3
Collagen: diagonal	$\varrho^{co(diag)}_0(t=0)$, $\varrho^{co(-diag)}_0(t=0)$	247.38 kg/m^3
Collagen: radial	$\varrho^{co(rad)}_0(t=0)$	32.55 kg/m^3
Smooth muscle	$\varrho^{sm}_0(t=0)$	157.5 kg/m^3
Total initial reference mass density	$\varrho_0(t=0)$	1050 kg/m^3

Table 1 continued

Growth and remodeling parameters		
Elastin: mean life time	T^{el}	101 years
Elastin: gain parameter	k_σ^{el}	0
Initial elastic stretch (equal to homeostatic stretch/deposition stretch for collagen and smooth muscle)		
Elastin: axial direction	$\lambda_e^{el(ax)}(t=0)$	1.25
Elastin: circumferential direction	$\lambda_e^{el(cir)}(t=0)$	1.34
Elastin: radial direction	$\lambda_e^{el(rad)}(t=0)$	$\in$[0.29; 0.51]
Collagen (in fiber direction)	$\lambda_e^{co}(t=0)$	1.062
Smooth muscle (in fiber direction)	$\lambda_e^{sm}(t=0)$	1.10

To distinguish between the different collagen fiber families, we use, when appropriate, superscripts *co(ax)*, *co(cir)*, *co(diag)*, *co(-diag)*, and *co(rad)* for circumferential, axial, diagonal, and radial collagen fibers. The homeostatic stretch in fiber direction of collagen and smooth muscle equals the elastic stretch in the initial configuration. To ensure mechanical and mechanobiological equilibrium in the initial configuration, the parameters μ_{2D}^{el} and $\lambda_e^{el(rad)}(t=0)$ are varied in the initial configuration in wall thickness direction according to the procedure described in "Appendix 1" of (Braeu et al. 2017)

Table 2 Additional simulation parameters for the idealized cylindrical blood vessel studied in Sect. 5.1.1

Simulation		
Time step size	Δt	0.34 days
Load		
Mean blood pressure jump	Δp	80 mmHg
Growth and remodeling parameters		
Collagen/Smooth muscle: turnover time	$T^{co} = T^{sm}$	7 days
Collagen/Smooth muscle: gain parameter	$k_\sigma^{co} = k_\sigma^{sm}$	[0.22, 0.28, 0.34]/T^{co}

with material parameters k_1^{co} and k_2^{co}, and I_a^{co} the square of the elastic stretch of the respective collagen fiber family. The strain energy of smooth muscle per unit mass is the sum

$$W^{sm} = W_{pas}^{sm} + W_{act}^{sm} \tag{42}$$

with a passive Fung-type part

$$W_{pas}^{sm} = \frac{k_1^{sm}}{2k_2^{sm}}\left(e^{k_2^{sm}(I_a^{sm}-1)^2} - 1\right) \tag{43}$$

Table 3 Additional simulation parameters for the idealized cylindrical blood vessel studied in Sect. 5.1.2

Simulation		
Time step size	Δt	5 days
Growth and remodeling parameters		
Collagen/smooth muscle: turnover time	$T^{co} = T^{sm}$	101 days
Collagen/smooth muscle: gain parameter	$k_\sigma^{co} = k_\sigma^{sm}$	0.05/T^{co}
Damage parameters in model aneurysm		
Damage spread in space	L_{dam}	10 mm
Damage spread in time	t_{dam}	40 days
Maximal damage	D_{max}	0.5

with material parameters k_1^{sm} and k_2^{sm}, and I_a^{sm} the square of the elastic stretch of the smooth muscle fiber family, and an active part

$$W_{act}^{sm} = \frac{\sigma_{actm}^{sm}}{\varrho_0(t=0)}\left(\lambda_{act}^{sm} + \frac{1}{3}\frac{\left(\lambda_m^{sm} - \lambda_{act}^{sm}\right)^3}{\left(\lambda_m^{sm} - \lambda_0^{sm}\right)^2}\right) \tag{44}$$

with λ_{act}^{sm} the active stretch in fiber direction, σ_{actm}^{sm} the maximal active Cauchy stress, and λ_m^{sm} and λ_0^{sm} the active stretches at maximum and zero active stress. Herein, we assume that $\partial\lambda_{act}^{sm}/\partial\lambda^{sm} = 1/\lambda^{sm}$ with λ^{sm} the total stretch of the smooth muscle fibers compared to the reference configuration, which is important to calculate the stress resulting from (44). Additionally, we add a penalty-type strain energy as given in Eq. (10) with the penalty parameter given in Table 1. In Sect. 5.1.2, the vessel is initially in equilibrium and all fibers are in a homeostatic state. At time $t = 0$, this homeostatic state is perturbed by spatially distributed damage to the elastin layer that progresses over time with the damage rate

$$\dot{D}^{el}(\boldsymbol{X}, t) = -\frac{1}{T^{el}}\varrho_0^{el}(\boldsymbol{X}, t) - \left[\frac{D_{max}}{t_{dam}}\exp\left[-0.5\left(\frac{X_3}{L_{dam}}\right)^2\right]\exp\left[-\frac{t}{t_{dam}}\right]\right]\varrho_0^{el}(\boldsymbol{X}, 0) \tag{45}$$

where a coordinate system is used with the origin in the center of the cylinder and the X_3-axis aligned with the symmetry axis of the cylinder. Table 1 summarizes the simulation parameters used both in Sects. 5.1.1 and 5.1.2. The parame-

Table 4 Simulation parameters of the simplified tendon model studied in Sect. 5.2

Simulation		
Time step size	Δt	3 days
Mesh		
Element type		8-noded hexahedral finite elements
Element technology		F-bar method to avoid locking (de Souza Neto et al. 1996)
Number of elements		384
Geometry		
Width	B	13.3 mm (Mello et al. 2006)
Thickness	H	4.3 mm (Aydin et al. 2014)
Length	L	100 mm
Reference mass densities		
Healthy tissue	$\varrho_0^H(t) = const$	1050 kg/m^3
Mass produced due to inflammation	$\varrho_0^I(t > 6weeks) = const$	1050 kg/m^3
Material parameters		
Ground matrix: Neo-Hookean shear parameter	G	13.85 MPa (Weiss et al. 1996)
Collagen: mass fraction in axial direction	$\varphi^{co(ax)}$	90%
Collagen: mass fraction in transverse directions	$\varphi^{co(0°)}, \varphi^{co(90°)}$	5%
Collagen: stiffness parameter	E	125 MPa
Penalty parameter	ε	300 MPa
Remodeling parameters		
Ground matrix: mean life time	T^m	101 years
Collagen: turnover time	T^{co}	24.5 days
Initial elastic stretch (equal to homeostatic stretch/deposition stretch)		
Collagen (in fiber direction)	$\lambda_e^{co}(t = 0)$	1.062

Table 5 Simulation parameters of the spheroidal tissue studied in Sect. 5.3

Simulation		
Time step size	Δt	7 days
Mesh		
Element type		8-noded hexahedral finite elements
Element technology		F-bar method to avoid locking (de Souza Neto et al. 1996)
Number of elements		2048
Geometry		
Initial radius	R	10 mm
Reference mass densities		
Healthy tissue	$\varrho_0^H(t) = const$	1050 kg/m^3
Newly deposited mass	$\varrho_0^D(t > 10weeks) = const$	1050 kg/m^3
Material parameters		
Ground matrix: elastic modulus	E	1 Pa
Ground matrix: Poisson's ratio	ν^{gr}	0.3
Collagen: stiffness parameter	E^{co}	10 Pa
Penalty-type function	ε	1 kPa
Remodeling parameters		
Ground matrix: mean life time	T^m	101 years
Collagen: turnover time	T^{co}	1 year (Decaris et al. 2015)
Initial elastic stretch (equal to homeostatic stretch/deposition stretch)		
Collagen (in fiber direction)	$\lambda_e^{co}(t = 0)$	1.062

ters that differ between Sects. 5.1.1 and 5.1.2 are presented separately in Tables 2 and 3.

In Sect. 5.2, we studied the growth of an idealized tendon due to inflammation. The size of the geometry was motivated by values reported in the literature for Achilles tendons. To model the elastic behavior of tendons at least qualitatively, we used the strain energy function from Eq. (27) and the simulation parameters summarized in Table 4.

In Sect. 5.3, we studied growth of a spheroidal tissue with the simulation parameters from Table 5.

References

Ambrosi D, Guana F (2007) Stress-modulated growth. Math Mech Solids 12(3):319–342

Ambrosi D, Ateshian GA, Arruda EM, Cowin SC, Dumais J, Goriely A, Holzapfel GA, Humphrey JD, Kemkemer R, Kuhl E, Olberding JE, Taber LA, Garikipati K (2011) Perspectives on biological growth and remodeling. J Mech Phys Solids 59(4):863–883

Aydın SZ, Filippucci E, Atagündüz P, Yavuz Ş, Grassi W, Direskeneli H (2014) Sonographic measurement of Achilles tendon thickness in seronegative spondyloarthropathies. Eur J Rheumatol 1(1):7–10

Bass E (2012) Tendinopathy: why the difference between tendinitis and tendinosis matters. Int J Therap Massage Bodyw 5(1):14

Berry CL, Greenwald SE (1976) Effects of hypertension on the static mechanical properties and chemical composition of the rat aorta1. Cardiovasc Res 10(4):437–451

Braeu FA, Seitz A, Aydin RC, Cyron CJ (2017) Homogenized constrained mixture models for anisotropic volumetric growth and remodeling. Biomech Model Mechanobiol 16(3):889–906

Brown RA, Prajapati R, McGrouther DA, Yannas IV, Eastwood M (1998) Tensional homeostasis in dermal fibroblasts: mechanical responses to mechanical loading in three-dimensional substrates. J Cell Physiol 175(3):323–332

Chui C, Kobayashi E, Chen X, Hisada T, Sakuma I (2007) Transversely isotropic properties of porcine liver tissue: experiments and constitutive modelling. Med Biol Eng Comput 45(1):99–106

Cyron C, Aydin R (2017) Mechanobiological free energy: a variational approach to tensional homeostasis in tissue equivalents. ZAMM-J Appl Math Mech 97(9):1011–1019

Cyron CJ, Humphrey JD (2014) Vascular homeostasis and the concept of mechanobiological stability. Int J Eng Sci 85:203–223

Cyron CJ, Humphrey JD (2017) Growth and remodeling of load-bearing biological soft tissues. Meccanica 52(3):645–664

Cyron CJ, Wilson JS, Humphrey JD (2014) Mechanobiological stability: a new paradigm to understand the enlargement of aneurysms? J R Soc Interface 11(100):20140680

Cyron CJ, Aydin RC, Humphrey JD (2016) A homogenized constrained mixture (and mechanical analog) model for growth and remodeling of soft tissue. Biomech Model Mechanobiol 15(6):1389–1403

de Souza Neto EA, Perić D, Dutko M, Owen DRJ (1996) Design of simple low order finite elements for large strain analysis of nearly incompressible solids. Int J Solids Struct 33(20):3277–3296

Decaris ML, Emson CL, Li K, Gatmaitan M, Luo F, Cattin J, Nakamura C, Holmes WE, Angel TE, Peters MG, Turner SM, Hellerstein MK (2015) Turnover rates of hepatic collagen and circulating collagen-associated proteins in humans with chronic liver disease. PLoS ONE 10(4):e0123311

DiCarlo A, Quiligotti S (2002) Growth and balance. Mech Res Commun 29(6):449–456

DiCarlo A, Naili S, Quiligotti S (2006) Sur le remodelage des tissus osseux anisotropes. Comptes Rendus Mécanique 334(11):651–661

Eriksson TSE, Watton PN, Luo XY, Ventikos Y (2014) Modelling volumetric growth in a thick walled fibre reinforced artery. J Mech Phys Solids 73:134–150

Ezra DG, Ellis JS, Beaconsfield M, Collin R, Bailly M (2010) Changes in fibroblast mechanostat set point and mechanosensitivity: an adaptive response to mechanical stress in floppy eyelid syndrome. Invest Ophthalmol Vis Sci 51(8):3853–3863

Flynn BP, Bhole AP, Saeidi N, Liles M, DiMarzio CA, Ruberti JW (2010) Mechanical strain stabilizes reconstituted collagen fibrils against enzymatic degradation by mammalian collagenase matrix metalloproteinase 8 (MMP-8). PLoS ONE 5(8):e12337

Gasser TC, Ogden RW, Holzapfel GA (2006) Hyperelastic modelling of arterial layers with distributed collagen fibre orientations. J R Soc Interface 3(6):15–35

Gizzi A, Cherubini C, Filippi S, Pandolfi A (2014) Theoretical and numerical modeling of nonlinear electromechanics with applications to biological active media. Commun Comput Phys 17(1):93–126

Gizzi A, Pandolfi A, Vasta M (2016) Statistical characterization of the anisotropic strain energy in soft materials with distributed fibers. Mech Mater 92(Supplement C):119–138

Gizzi A, Pandolfi A, Vasta M (2017) A generalized statistical approach for modeling fiber-reinforced materials. J Eng Math 109(1):211–226

Gonzalez O, Stuart AM (2008) A first course in continuum mechanics. Cambridge University Press, Cambridge

Goriely A, Vandiver R (2010) On the mechanical stability of growing arteries. IMA J Appl Math 75:549–570

Grillo A, Federico S, Wittum G (2012) Growth, mass transfer, and remodeling in fiber-reinforced, multiconstituent materials. Int J Non-Linear Mech 47(2):388–401

Grytsan A, Watton PN, Holzapfel GA (2015) A thick-walled fluid–solid-growth model of abdominal aortic aneurysm evolution: application to a patient-specific geometry. J Biomech Eng 137(3):031008

Grytsan A, Eriksson TSE, Watton PN, Gasser TC (2017) Growth description for vessel wall adaptation: a thick-walled mixture model of abdominal aortic aneurysm evolution. Materials 10(9):994

Grytz R, Meschke G, Jonas JB (2011) The collagen fibril architecture in the lamina cribrosa and peripapillary sclera predicted by a computational remodeling approach. Biomech Model Mechanobiol 10(3):371–382

Grytz R, Sigal IA, Ruberti JW, Meschke G, Downs JC (2012) Lamina cribrosa thickening in early glaucoma predicted by a microstructure motivated growth and remodeling approach. Mech Mater 44:99–109

Holzapfel G (2000) Nonlinear solid mechanics: a continuum approach for engineering. Wiley, New York

Holzapfel GA, Ogden RW (2017) Comparison of two model frameworks for fiber dispersion in the elasticity of soft biological tissues. Eur J Mech A/Solids 66(Supplement C):193–200

Humphrey JD, Rajagopal KR (2002) A constrained mixture model for growth and remodeling of soft tissues. Math Models Methods Appl Sci 12(03):407–430

Humphrey JD, Dufresne ER, Schwartz MA (2014) Mechanotransduction and extracellular matrix homeostasis. Nat Rev Mol Cell Biol 15(12):802–812

Jain RK, Martin JD, Stylianopoulos T (2014) The role of mechanical forces in tumor growth and therapy. Annu Rev Biomed Eng 16:321–346

Karšaj I, Sorić J, Humphrey JD (2010) A 3-D framework for arterial growth and remodeling in response to altered hemodynamics. Int J Eng Sci 48(11):1357–1372

Kehl S, Gee MW (2017) Calibration of parameters for cardiovascular models with application to arterial growth. Int J Numer Methods Biomed Eng 33(5):e2822

Lin WJ, Iafrati MD, Peattie RA, Dorfmann L (2017) Growth and remodeling with application to abdominal aortic aneurysms. J Eng Math 109(1):113–137

Lindquist Liljeqvist M, Hultgren R, Gasser TC, Roy J (2016) Volume growth of abdominal aortic aneurysms correlates with baseline volume and increasing finite element analysis-derived rupture risk. J Vasc Surg 63(6):1434–1442.e1433

Marino M, Pontrelli G, Vairo G, Wriggers P (2017) A chemo-mechano-biological formulation for the effects of biochemical alterations on arterial mechanics: the role of molecular transport and multiscale tissue remodelling. J R Soc Interface. https://doi.org/10.1098/rsif.2017.0615

Mascheroni P, Carfagna M, Grillo A, Boso D, Schrefler B (2018) An avascular tumor growth model based on porous media mechanics and evolving natural states. Math Mech Solids 23(4):686-712

Matsumoto T, Hayashi K (1994) Mechanical and dimensional adaptation of rat aorta to hypertension. J Biomech Eng 116(3):278–283

Matsumoto T, Hayashi K (1996) Response of arterial wall to hypertension and residual stress. In: Hayashi K, Kamiya A, Ono K (eds) Biomechanics. Springer, New York, pp 93–119

Mello RAF, Marchiori E, de Santos AASMD, Dos Torres Neto G (2006) Avaliação morfométrica do tendão de Aquiles por ultrasonografia. Radiol Bras 39(3):161–165. https://doi.org/10.1590/S0100-39842006000300003

Menzel A, Kuhl E (2012) Frontiers in growth and remodeling. Mech Res Commun 42:1–14

Niestrawska JA, Viertler C, Regitnig P, Cohnert TU, Sommer G, Holzapfel GA (2016) Microstructure and mechanics of healthy and aneurysmatic abdominal aortas: experimental analysis and modelling. J R Soc Interface. https://doi.org/10.1098/rsif.2016.0620

Pandolfi A, Gizzi A, Vasta M (2016) Coupled electro-mechanical models of fiber-distributed active tissues. J Biomech 49(12):2436–2444

Rodriguez EK, Hoger A, McCulloch AD (1994) Stress-dependent finite growth in soft elastic tissues. J Biomech 27(4):455–467

Sáez P, Peña E, Martínez MA, Kuhl E (2014) Computational modeling of hypertensive growth in the human carotid artery. Comput Mech 53(6):1183–1196

Schriefl AJ, Zeindlinger G, Pierce DM, Regitnig P, Holzapfel GA (2012) Determination of the layer-specific distributed collagen fibre orientations in human thoracic and abdominal aortas and common iliac arteries. J R Soc Interface 9(71):1275–1286

Skalak R, Farrow DA, Hoger A (1997) Kinematics of surface growth. J Math Biol 35(8):869–907

Soleimani M, Wriggers P, Rath H, Stiesch M (2016) Numerical simulation and experimental validation of biofilm in a multi-physics framework using an SPH based method. Comput Mech 58(4):619–633

Truster TJ, Masud A (2017) A unified mixture formulation for density and volumetric growth of multi-constituent solids in tissue engineering. Comput Methods Appl Mech Eng 314:222–268

Tsamis A, Cheng A, Nguyen TC, Langer F, Miller DC, Kuhl E (2012) Kinematics of cardiac growth: in vivo characterization of growth tensors and strains. J Mech Behav Biomed Mater 8:165–177

Valentín A, Humphrey J, Holzapfel GA (2013) A finite element-based constrained mixture implementation for arterial growth, remodeling, and adaptation: Theory and numerical verification. Int J Numer Methods Biomed Eng 29(8):822–849

Vasta M, Gizzi A, Pandolfi A (2014) On three- and two-dimensional fiber distributed models of biological tissues. Probab Eng Mech 37(Supplement C):170–179

Virag L, Wilson JS, Humphrey JD, Karsaj I (2017) Potential biomechanical roles of risk factors in the evolution of thrombus-laden abdominal aortic aneurysms. Int J Numer Method Biomed Eng 33:e2893. https://doi.org/10.1002/cnm.2893

Watton P, Hill N, Heil M (2004) A mathematical model for the growth of the abdominal aortic aneurysm. Biomech Model Mechanobiol 3(2):98–113

Weiss JA, Maker BN, Govindjee S (1996) Finite element implementation of incompressible, transversely isotropic hyperelasticity. Comput Methods Appl Mech Eng 135(1):107–128

Wilson JS, Baek S, Humphrey JD (2012) Importance of initial aortic properties on the evolving regional anisotropy, stiffness and wall thickness of human abdominal aortic aneurysms. J R Soc Interface 9(74):2047–2058

Wilson JS, Baek S, Humphrey JD (2013) Parametric study of effects of collagen turnover on the natural history of abdominal aortic aneurysms. Proc R Soc A 469(2150):20120556

Wolinsky H, Glagov S (1967) A lamellar unit of aortic medial structure and function in mammals. Circ Res 20(1):99–111

Yin L, Elliott DM (2004) A biphasic and transversely isotropic mechanical model for tendon: application to mouse tail fascicles in uniaxial tension. J Biomech 37(6):907–916

Yu C-H, Walker PS, Dewar ME (2001) The effect of design variables of condylar total knees on the joint forces in step climbing based on a computer model. J Biomech 34(8):1011–1021

Zöllner AM, Abilez OJ, Böl M, Kuhl E (2012) Stretching skeletal muscle: chronic muscle lengthening through sarcomerogenesis. PLoS ONE 7(10):e45661

Publisher's Note Springer Nature remains neutral with regard to jurisdictional claims in published maps and institutional affiliations.

Verzeichnis der betreuten Studienarbeiten

Im Rahmen dieser Dissertation entstanden am Lehrstuhl für Numerische Mechanik (LNM) in den Jahren von 2015 bis 2019 unter wesentlicher wissenschaftlicher, fachlicher und inhaltlicher Anleitung des Autors die im Folgenden aufgeführten studentischen Arbeiten. Der Autor dankt allen Studierenden für Ihr Engagement bei der Unterstützung dieser wissenschaftlichen Arbeit.

Studierende(r)	**Studienarbeit**
Sebastian Fuchs	*Implementation of a Nonlinear Membrane Finite Element*, Semesterarbeit, 2015
Sebastian Fuchs	*A Growth and Remodeling Formulation for a Membrane Finite Element*, Masterarbeit, 2016
Sebastian Kaltenbach	*An Updated Lagrangian Finite Element Formulation for Adaptive Mesh Smoothing in Aneurysm Growth*, Masterarbeit, 2017
Christoph Fraundorfer	*Automatization of a Remeshing Procedure for Finite Element Methods with Gmsh*, Semesterarbeit, 2018
Dingzhi Zhang	*Entwicklung und Validierung eines realistischen Materialmodells für ein abdominales Aortenaneurysma*, Semesterarbeit, 2018
Philipp Schäfer	*Development of a framework to apply prestrain to constrained mixture materials*, Masterarbeit, 2018
Amadeus Gebauer	*Growth and Remodeling for Cardiac Mechanics Simulations*, Masterarbeit, 2019